

Aus der Radiologischen Klinik
Abteilung Radioonkologie und Strahlentherapie des
Universitätsklinikums Heidelberg
(Ärztlicher Direktor: Prof. Dr. med. Dr. rer. nat. Jürgen Debus)
In Zusammenarbeit mit dem Deutschen Krebsforschungszentrum (DKFZ)

**Evaluation of photon, proton, helium, and carbon ion irradiation in
prototypic NSCLC and HNSCC preclinical xenograft models**

Inauguraldissertation
zur Erlangung des Doktorgrades scientiarum humanarum (Dr. sc. hum.)

an der
Medizinischen Fakultät Heidelberg

der
Ruprecht-Karls-Universität

vorgelegt von

Mahdi Akbarpour

aus dem

Oroumieh, Iran

2022

Dekan: Herr Prof. Dr. med. Dr. h. c. Hans-Georg Kräusslich

Doktorvater: Herr Prof. Dr. med. Dr. rer. nat. Jürgen Debus

Table of contents

Table of contents	3
Abbreviations	6
1. Introduction	11
1.1 Preface	11
1.2 Radiotherapy	11
1.2.1 Radiotherapy in cancer treatment.....	11
1.2.2 Particle beam therapy.....	12
1.3 Lung Cancer	13
1.3.1 Epidemiology	13
1.3.2 Histology and staging	14
1.3.3 Preclinical A549 model of NSCLC	17
1.4 Head and neck cancer	17
1.4.1 Epidemiology	17
1.4.2 HPV status	18
1.4.3 Preclinical FaDu model of HNSCC	19
1.5 Functional genomics.....	20
1.5.1 RNA interference	20
1.5.2 CRISPR/Cas9 genome editing	21
1.6 CRISPR/Cas9 genetic screens.....	22
1.6.1 <i>In-vitro</i> genetic screens	23
1.6.2 <i>In-vivo</i> genetic screens.....	23
1.7 CRISPR/Cas9 screening libraries.....	25
1.7.1 GeCKO and GeCKO v2 libraries	25
1.7.2 Brunello library.....	26
1.7.3 TKO library	26
Aim of this dissertation	27
2. Materials and methods	29
2.1 Materials	29
2.1.1 Cell lines.....	29
2.1.2 Chemical materials	29
2.1.3 Non-chemical materials	30
2.1.4 Kits	30
2.1.5 Animals and anesthesia	30
2.1.6 Laboratory devices	31

2.1.7	Software	31
2.2	Methods.....	31
2.2.1	Basic cell culture procedures.....	31
2.2.2	Cell lines used	32
2.2.3	Generating Cas9-expressing single cell clones	32
2.2.4	Plating efficiency.....	33
2.2.5	Clonogenic survival assay	33
2.2.6	T7 Endonuclease I assay	33
2.2.7	Whole genome CRISPR/Cas9 screen in <i>in-vivo</i> models	35
2.2.8	Determination of infection condition for pooled screens	35
2.2.9	Subcutaneous xenograft mouse models	35
2.2.10	Photon irradiation	36
2.2.11	Charged particle Irradiation	36
2.2.12	Genomic DNA and total RNA extraction from tumors.....	37
2.2.13	Library preparation and sequencing.....	37
2.2.14	Sequencing read count processing	39
2.2.15	Statistical analysis and gRNA abundance analysis.....	40
3.	Results	41
3.1	<i>In-vitro</i> characterization of single cell clones	41
3.2	<i>In-vitro</i> and <i>in-vivo</i> representation of GeCKO A and Brunello libraries	42
3.3	Correlation between tumor growth kinetics <i>in-vivo</i> and library representation	43
3.4	Effect of fractionated conventional photon irradiation on <i>in-vivo</i> growth of FaDu and A549 tumors.....	44
3.5	Tumor growth in particle irradiated FaDu and A549 models.....	46
3.6	Library complexity decreases as a function of irradiation	49
3.7	UMAP representation of gene expression for different irradiation qualities	50
3.8	Photon irradiation induced transcriptional regulations	52
3.9	Linear Energy Transfer (LET) dependent alterations of gene expression	55
3.10	Guide RNA abundance analyses.....	57
3.11	UMAP representation of gRNA data in FaDu and A549	58
3.12	Genes with higher gRNA abundance in photon irradiated vs. control FaDu tumors.....	59
3.13	Genes with higher gRNA abundance in photon irradiated vs. control A549 tumors.....	62
3.14	Genes showing relative guide abundance association with LET in FaDu model.....	64

3.15	Genes showing relative guide abundance association with LET in A549 model.....	66
3.16	Guide abundance differences between control and treated tumors and regulation on gene expression level	68
4.	Discussion.....	70
4.1	Changes in library complexity.....	73
4.1.1	Library representation decreases between <i>in-vitro</i> and <i>in-vivo</i> conditions	73
4.1.2	Library complexity decreases over time	74
4.1.3	Tumor growth kinetics correlates with library complexity and radiation treatment	74
4.2	Transcriptome profiling and gene expression differences after irradiation.....	75
4.2.1	Gene expression differences in FaDu model.....	75
4.2.2	Gene expression differences in A549 model	77
4.3	KEGG pathway analysis	78
4.4	gRNA analysis	78
4.4.1	gRNA abundance differences in FaDu model	79
4.4.2	gRNA abundance differences in A549 model.....	79
4.5	Correlation between RNA expression and gRNA abundance genes	81
5.	Summary.....	82
6.	Zusammenfassung.....	84
7.	References.....	86
	Thesis related publications	100
	Acknowledgments	101
	Eidesstattliche Versicherung	102

Abbreviations

α PD-1	Programmed cell death protein
AAV	Adeno-associated virus
ABC transporters	ATP-binding cassette transporters
ADAR	Adenosine deaminase RNA specific
AJCC	American Joint Committee on Cancer
AKT	Protein kinase B
ALK	Anaplastic lymphoma kinase
ARID2	AT-rich interaction domain 2
BAD	BCL2 associated agonist of cell death
BMF	Bcl2 modifying factor
BMP8A	Bone morphogenetic protein 8A
BNIP3	BCL2 interacting protein 3
Bonf	Bonferroni correction
Bp	Base pair
BRAF	B-Raf proto-oncogene, serine/threonine kinase
C ¹² -ions	Carbon ions
CACNA2D3	Calcium voltage-gated channel auxiliary subunit alpha2 delta3
CDKN2A	Cyclin dependent kinase inhibitor 2A
CAFs	Cancer-associated fibroblasts
CT	Chemotherapy
CRISPR	Clustered regularly interspaced short palindromic repeats
CXCL14	C-X-C motif chemokine ligand 14
DAMPs	Danger associated molecular patterns
DNA	Deoxyribonucleic acid
DMEM	Dulbecco's Modified Eagle Medium
DMSO	Dimethylsulfoxid
DPBS	Dulbecco's phosphate-buffered saline
DSB	Double strand break
EDTA	Ethylenediamine tetraacetic acid

EGFR	Epidermal growth factor receptor
EML4	Echinoderm microtubule associated-protein-like 4
ErbB	Erythroblastic oncogenic B
FANCM	Fanconi anemia complementation group M
FAT1	FAT atypical cadherin 1
FCS	Fetal calf serum
FDR	False discovery rate
FGF2	Fibroblast growth factor 2
FGFR	Fibroblast growth factor receptor
Foxn1	Fork head box N1
FPKM	Fragments per kilo base of transcript per million mapped fragments
FUBP1	Far upstream element binding protein 1
FUT6	Fucosyltransferase 6
gRNA	Guide RNA
GTPase	Guanosine triphosphatase
Gy	Gray
H ⁺	Proton ions
H3K4	Histone H3 lysine K4
He ⁴ -ions	Helium ions
HHEX	Haematopoietically expressed homeobox
HNSCC	Head and neck squamous cell carcinoma
HPV	Human papilloma virus
HDR	Homology-directed repair
HIT	Heidelberg Ion-Beam Therapy Center
IL32	Interleukin 32
IMDM	Iscove's Modified Dulbecco's Medium
Indel	Insertion / deletion
KDM5C	Lysine demethylase 5C
KEAP1	Kelch-like ECH associated protein 1
KEGG	Kyoto Encyclopedia of Genes and Genomes
KeV/μm	Kilo electron volt per micrometer
KMT2D	Lysine Methyltransferase 2D

KRAS	Kirsten rat sarcoma viral oncogene homolog
LET	Linear energy transfer
LUM	Lumican
LQM	Linear quadratic model
MACC1	Metastasis-associated in colon cancer-1
MaGECK	Model-based Analysis of Genome-wide CRISPR/Cas9 Knockout
MAPK	Mitogen-activated protein kinase
MDH2	Mitochondrial malate dehydrogenase 2
MEM	Minimum Essential Medium
MET	MET proto-oncogene, receptor tyrosine kinase
MHCI	Histocompatibility complex I
MMEJ	Microhomology-mediated end joining
MMP19	Matrix metalloproteinase 19
MOI	Multiplicity of infection
mRNA	Messenger ribonucleic acid
mTOR	Mammalian target of rapamycin
NF- κ B	Nuclear factor κ -light-chain-enhancer of activated B cells
NGS	Next generation sequencing
NOTCH1	Neurogenic locus notch homolog protein 1
NHEJ	Non-homologous end joining
NSCLC	Non-small cell lung cancer
O ¹⁶ -ions	Oxygen ions
OLS	Ordinary least squares
P2RX7	Purinergic receptor P2X 7
P53	Tumor protein p53
PAM	Protospacer adjacent motif
PC	Principal component
PCR	Polymerase chain reaction
PDPN	Podoplanin
PGLYRP4	Peptidoglycan recognition protein 4
PIK3CA	Phosphatidylinositol-4,5-bisphosphate 3-kinase catalytic subunit alpha

PKIB	cAMP-dependent protein kinase inhibitor- β
PMMA	Poly methyl methacrylate
Ras	Rat sarcoma virus
RBE	Radiobiological effectiveness
RCHT	Radiochemotherapy
RP11	Retinitis pigmentosa 11
RNA	Ribonucleic acid
RNAi	RNA interference
RNAseq	RNA sequencing
RNAse III	Ribonuclease III
Rpm	Rounds per minute
RUNX1	RUNX family transcription factor 1
RT	Radiotherapy
S100A 12	S100 calcium binding protein A12
SABR	Stereotactic ablative radiotherapy
Sccl	Single cell clone
SD	Standard deviation
SEMA3B	Semaphorin 3B
SEM	Standard error of mean
SMARCA2	SWI/SNF related matrix associated actin dependent regulator of chromatin subfamily member 2
SMARCA4	SWI/SNF related matrix associated actin dependent regulator of chromatin subfamily member 4
SERPINB11	Serpin family B member 11
shRNA	Short hairpin RNA
SOBP	Spread-out Bragg peak
SPRK1	Serine/Arginine-Rich splicing factor Kinase 1
STAT1	Signal transducer and activator of transcription 1
STAT3	Signal transducer and activator of transcription 3
STK11	Serine/threonine kinase 11
SYNE1	Synaptic nuclear envelope protein 1
SYT12	Synaptotagmin 12
T7 E1	T7 endonuclease 1

TCA	Tricarboxylic acid cycle
TGF- β	Transforming growth factor β
TGFBR1	Transforming growth factor beta receptor 1
TGFBR2	Transforming growth factor beta receptor 2
TKO	Toronto KnockOut
TLRs	Toll like receptors
TME	Tumor microenvironment
TNC	Tenascin-C
TNM	Tumor, Node, and Metastasis
TP53	Tumor protein 53
TRAP1	Tumor necrosis factor receptor associated protein1
tracrRNA	Trans-activating CRISPR RNA
TSC1	TSC complex subunit 1
TSPAN1	Tetraspanin 1
TSPAN8	Tetraspanin 8
UMAP	Uniform Manifold Approximation and Projection
VEGF	Vascular endothelial growth factor A
VST	Variance stabilizing transformation
WDR5	WD repeat domain 5
XAF1	X-linked inhibitor of apoptosis (XIAP)-associated factor 1

1. Introduction

1.1 Preface

Radiotherapy is a cornerstone of cancer therapy. More than 50% of cancer patients undergo radiotherapy in their course of disease. Non-small cell lung cancer (NSCLC) and head and neck squamous cell carcinoma (HNSCC) constitute two example cancer entities where improvement in radiotherapy has substantially contributed to improved outcomes over the past decades. Particle therapy with protons and heavier ions have been postulated to elicit superior biophysical properties and are therefore candidate new modalities for high precision cancer therapy. Using prototypic NSCLC and HNSCC *in-vivo* tumor models combined with functional genomics (CRISPR-Cas9), this dissertation aims to systematically characterize the radiobiological effect of these new particle therapy modalities.

1.2 Radiotherapy

1.2.1 Radiotherapy in cancer treatment

In clinical practice, radiotherapy (RT) seeks to simultaneously deliver the maximal dose required to kill malignant cells and the minimal damaging dose to the surrounding normal tissue (Baskar et al., 2012). Over half of cancer patients will receive RT in the course of their treatment (Delaney et al., 2005). RT can be administered either alone, in a definitive setting, in combination with chemotherapy or following surgery as an adjuvant setting. RT is capable of curing >40% of all cancer patients (Ringborg et al., 2003). Additionally, it is indicated for selected benign diseases and in disease palliation, in case of pain, obstruction (for example, an occluding bronchial mass), in stabilization of weight-bearing joints in case of bony metastases and in urgent treatment of intracranial pressure caused by brain metastases and prevention of paralysis in the case of spinal cord compression (Christian et al., 2008).

The relevant damage induced by RT can be classified into indirect and direct DNA damage (Baskar et al., 2012). Indirect damage occurs when radiation beams generate oxygen free radicals inside the cell (through ionization of the water components),

resulting in double-strand breaks (DSBs) (Rockwell et al., 2009). Direct damage occurs when high energy particles induce DSBs along their traversal through tissue (Kozubek & Krasavin, 1984).

The contribution of direct vs. indirect DNA damage depends on the type of ionizing radiation used. Photon radiotherapy is the most routinely used modality to treat tumors. Photon beams (also known as X-rays and Gamma-radiation depending on RT source) are sparsely ionizing beams (Zhang et al., 2021). Likewise electron and protons are applied as charged beams with a low linear energy transfer (LET) (Baskar et al., 2012) and induce cell death at lower doses predominantly via indirect DNA damage. The main disadvantage of photon RT is that its energy scatters and decreases along the path of tissue penetration (depth). This result in the deposition of radiation in the surrounding normal tissue, which leads to side effects of treatment. To minimize normal tissue complications RT is administered in a fractionated manner over a series of daily fractions typically given over several weeks. For example, a typical fractionation regimen would be the administration of 54-72 Gy in fractions of 2 Gy each (Thames et al., 1990). Fractionation schemes exploit the fact that normal tissue cells are able to repair DNA damage more efficiently than cancer cells (Baskar et al., 2012).

1.2.2 Particle beam therapy

Particle beams with charged ions like carbon ions are more densely ionizing radiation, thus creating more complex direct DNA damage along their tracks (Mohamad et al., 2017). That is why particle RT with helium, carbon, oxygen ion utilized in this thesis is postulated to have a higher relative biological effectiveness (RBE) compared to photon and low-LET proton irradiation. RBE is the iso-effective dose at which different radiation modalities can generate the same biological effect (Sorensen et al., 2021; Zhou et al., 2019). For example, carbon ions have an RBE of ~2-3 compared to photons for different endpoints like neurologic side effects and tumor cell killing, respectively (Bendinger et al., 2021).

Linear energy transfer (LET) is defined as “the amount of energy transferred by an ionizing particle per unit distance” in keV/ μm (Antonovic et al., 2014). Photons are considered as low LET irradiation. However, particle beams have mixed LET, meaning they possess a lower LET in the entrance/plateau area traversing through normal

tissue and a high LET in the Bragg Peak at tumor site (Jakel et al., 2003; Karger & Peschke, 2017). This means that particle beams using carbon ions are more advantageous in their dose deposition than photon beams and release their energy at the “Bragg peak region” (Figure 1) within deeper layers of the tissue. Technological advancements such as raster scanning techniques allow particle therapy to be deposited in a “spread-out Bragg Peak” (SOBP), which is effectively a cumulative overlaying of several individual Bragg peaks. This results in the delivery of a high local dose to the tumor while the normal tissue around it remains spared (Zhou et al., 2019).

Clinically this means that there is not only a difference in dose deposition but also in radiation quality between entrance low-LET and dose leading to less damage and sparing of normal tissue while tumor is irradiated with a steep dose gradient *i.e.*, higher dose, LET and consequently RBE (Durante & Debus, 2018; Schaub et al., 2020; Weber & Kraft, 2009).

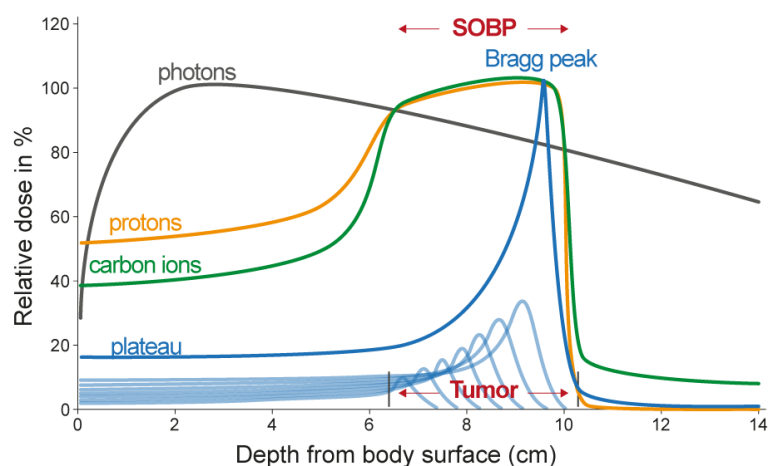


Figure 1. Depth-Dose profile of photons, Bragg peaks, single pristine Bragg and SOBP protons and carbon ions. To cover the entire tumor volume the Bragg peak is widened using a set of overlapping beams with different energies to form SOBP. Figure prepared by Dr. Katrin Rein.

1.3 Lung Cancer

1.3.1 Epidemiology

Lung cancer is the most common cause of cancer-related deaths worldwide (Bray et al., 2018). An estimated 1.4 million lung cancer-related deaths occur yearly (de Groot et al., 2018). Non-small cell lung cancer (NSCLC) is the most prevalent histological

subtype accounting for ~84% of cases (Siegel et al., 2018) with tobacco smoking being the most important risk factor (de Groot et al., 2018). In non-smokers, risk factors include environmental exposure, second-hand smoking and occupational carcinogens (de Groot et al., 2018). Following decades of public health prevention campaigns and tobacco control policies, incidence rates for men have begun to decrease in the United States and the European Union (Barta et al., 2019). Worldwide, the incidence of lung cancer continues to rise, for instance in Asia where air pollution and occupational exposure play an important role (Barta et al., 2019). After adjusting for gender, NSCLC is the second most common cancer in men (14% of incident cases) and women (13%) (de Groot et al., 2018). The rates of female lung cancer are also on the rise (de Groot et al., 2018). With improvements in screening and treatment techniques, the five-year survival of NSCLC was 26.4% in 2017 (Ganti et al., 2021). Prognosis is chiefly impacted by the extent of disease at presentation (categorized by the Tumor, Node, and Metastasis (TNM) stage). The best outcomes are achieved for patients with early-stage disease (>73% for stage IA). By contrast, patients with metastatic disease have poor outcomes (<10% OS at 5 years) (Woodard et al., 2016).

1.3.2 Histology and staging

NSCLC can be further classified into distinct histopathological classes, each class having characteristic molecular and genetic alterations that impact the choice of treatment. Adenocarcinoma is the most common subtype, implicated in 50% of cases (Groot et al. 2018). Adenocarcinomas may exhibit characteristic activating mutations in epidermal growth factor receptor (EGFR) in roughly 15% of cases, which can be targeted using third generation EGFR tyrosine kinase inhibitors such as Osimertinib (Soria et al., 2018; Wu et al., 2020). Roughly 30% of adenocarcinomas have KRAS (Kirsten rat sarcoma viral oncogene homolog) proto-oncogene mutations. KRAS protein is GTPase which cycles between active and non-active forms in response to extracellular stimuli. Hyperactivating mutations decrease its intrinsic GTPase activity, leading to higher amount of an active GTP-bound population and result in tumor initiation and progression and is associated with poor prognosis (Prior et al., 2012; Skoulidis & Heymach, 2019). KRAS mutations are seen in both early-stage and metastatic adenocarcinomas (Jordan et al., 2017) and the mutations are associated with poor response against EGFR inhibitors (Eberhard et al., 2005). In ~4% of cases,

a fusion of the echinoderm microtubule associated-protein-like 4 (EML4) gene and the Anaplastic lymphoma kinase (ALK) gene will result in constitutively activated tyrosine kinase activity and can be targeted using ALK inhibitors (Griffin & Ramirez, 2017). Other targetable mutations include ROS1, BRAF or MET (Skoulidis & Heymach, 2019). Squamous cell carcinoma is the second most common subtype, arising frequently in the proximal portion of the bronchi (Kallini et al., 2015). The most common druggable targets in squamous cell carcinoma include PIK3CA, FGFR1, MET, DDR2 and BRAF (Drilon et al., 2012; Kim, 2013). The recognition of targetable gene alterations has changed the management of lung cancer and personalized therapy and has led to remarkable responses in selected patients (Herbst et al., 2018).

Staging of lung cancer follows the TNM system from the American Joint Committee on Cancer (AJCC) (Table 1 and 2).

Table 1. Staging of NSCLC (8th AJCC edition)

Tx: Tumor in sputum/bronchial washings but not assessed on imaging or bronchoscopy T0: No evidence of tumor Tis: Carcinoma in Situ
T1: ≤3 cm surrounded by lung/visceral pleura, not involving the main bronchus T1a(mi): minimally invasive T1a: ≤1cm T1b: >1 but ≤2cm T1c: >2 but ≤3cm
T2: >3 but ≤5cm or a tumor involving the main bronchus without carina, regardless of the distance, or a tumor invading the visceral pleura, or presence of atelectasis or post obstructive pneumonitis extending to hilum T2a: >3 but ≤4cm T2b: >4 but ≤5cm
T3: >5 but ≤7cm or a tumor that involves the chest wall, pericardium, phrenic nerve or satellite nodules in the same lobe
T4: >7 cm or a tumor invading the mediastinum, diaphragm, heart and/or great vessels
N1: ipsilateral peribronchial or hilar nodes and intrapulmonary nodes

N2: Ipsilateral mediastinal and/or subcarinal nodes
N3: contralateral mediastinal or hilar; ipsilateral/contralateral scalene/supraclavicular
M: distant metastasis
M1a: in contralateral lung, pleura/pericardial nodule, malignant effusion
M1b: single extrathoracic metastasis
M1c: multiple extrathoracic metastases in one or more organs

Table 2. (Continued) Staging of NSCLC (8th AJCC)

	N0	N1	N2	N3
T1	IA	IIB	IIIA	IIIB
T2a	IB	IIB	IIIA	IIIB
T2b	IIA	IIB	IIIA	IIIB
T3	IIB	IIIA	IIIB	IIIC
T4	IIIA	IIIA	IIIB	IIIC
M1a	IVA	IVA	IVA	IVA
M1b	IVA	IVA	IVA	IVA
M1c	IVB	IVB	IVB	IVB

Prognosis is largely dependent on the extent of the disease at presentation. Patients with early resectable disease have the best cure rate (Goldstraw et al., 2016). Surgical resection is the standard of care (Shirvani et al., 2014). Nevertheless, advances in radiotherapy (RT) technique have also revolutionized treatment of early-stage I-II disease, whereby patients who may not be candidates for surgical resection can receive stereotactic ablative radiotherapy (SABR) (Shirvani et al., 2014). SABR is a technique whereby a much higher radiotherapy dose can be applied in a short period of time (typically over the course of days) while sparing nearby normal tissue structure (Chang, 2015). Stage II/IIIA patients are treated by surgery followed by adjuvant chemotherapy or immunotherapy. In the case where the patient is not a candidate for surgical resection, radiation therapy is offered (Burdett et al., 2015). Treatment of stage IIIB tumors depends on the patient's health as well as extent of disease involvement and is dominated by radiochemotherapy (RCHT) (Baas et al., 2011). In the metastatic Stage IV setting, beyond immunotherapy and chemotherapy schedules, patients with driver mutations are eligible to receive targeted therapy and often receive radiotherapy

for control of critical metastatic sites like e.g., frequently present brain and bone metastases (Hsu et al., 2017).

1.3.3 Preclinical A549 model of NSCLC

Adenocarcinoma is the most common subtype of NSCLC (Groot et al. 2018). A549 is lung adenocarcinoma epithelial cell line, derived in 1972 from a 58-year-old Caucasian male by removing and culturing pulmonary carcinoma tissue (Giard et al., 1973). The doubling time of A549 is 22 hours and *in-vitro*, these cells grow as a monolayer. A549 cell line carries KRAS G12S mutation, other altered driver genes for A549 model are summarized on Figure 2.



Figure 2. Altered cancer driver genes lung adenocarcinoma. Font size indicates the frequency of the mutation. Mutations are indicated in red (gain of function), blue (loss of function) and grey (ambiguous). Copy number alterations are indicated in purple (amplification) and green (deletion). Figure adapted from (cellmodelpassports.sanger.ac.uk).

1.4 Head and neck cancer

1.4.1 Epidemiology

Head and neck squamous cell carcinomas (HNSCCs) are the sixth most common cancers worldwide (Alsaifi et al., 2019). These cancers develop from the mucosal

epithelium in the oral cavity, pharynx and larynx. The prognosis and therapeutic options of HNSCC depend on anatomical location, epidemiologic factors, and cancer stage. Oral cavity and larynx cancers have been correlated with exposure to tobacco-derived carcinogens and/or excessive alcohol consumption (Rettig & D'Souza, 2015).

1.4.2 HPV status

Oropharynx cancers are increasingly attributed to infection with human papillomavirus (HPV) (Noone et al. 2018). Rates of oropharyngeal cancer are on the rise and it has superseded cervical cancer as the most frequent HPV driven cancer in the United States (Brennan et al., 2021). In comparison to other head and neck tumors, HPV driven oropharyngeal cancer is associated with a better prognosis and survival outcome. Patients with HPV driven tumors who receive the same treatment have 58% lower risks of death and 51% lower risks of developing a recurrence (Ang et al., 2010). The precise mechanism behind the improved sensitivity towards treatment is not completely elucidated (Bol & Gregoire, 2014). Nevertheless, survivorship is high in this patient group, spurring the design of clinical trials considering de-escalation of treatment (Mirghani & Blanchard, 2018) (Tawk et al., 2022).

By contrast, HPV negative HNSCC are challenging to treat. Patients are often older and sicker than patients with HPV driven tumors. Treatment strategies depend on the anatomical site of origin, TNM status and the patient's overall health (Johnson et al., 2020). In early-stage disease, cure can be achieved through surgical resection followed by adjuvant chemotherapy or RT if risk factors are present, or primary RCHT (Johnson et al., 2020). In advanced stages, treatment schemes are generally multimodal and consisting of surgical eradication followed by RCHT or definitive RCHT (Pignon et al., 2009). For patients with metastatic disease, treatment options include further targeted agents or immunotherapy (Ferris et al., 2016). Due to "field cancerization" of the upper aerodigestive tract following a sustained exposure to carcinogens patients are prone to develop tumor recurrences (Braakhuis et al., 2003; Califano et al., 1996) . Local recurrences are associated with poor prognosis. Some risk factors for local recurrence include the presence of tumor at surgical margins after resection and extracapsular extension of the tumor at the site of affected lymph nodes (Bernier et al., 2005). These patients benefit from adding chemotherapy to radiotherapy in the postoperative setting. In patients with locally advanced cancer that

is not amenable to surgery, the first line treatment is a combination of RT with cisplatin-based chemotherapy (Pignon et al., 2009). The toxicity of treatment increases when more than one modality is used. Surgery is associated with increased bleeding risk, pain and eating difficulties (dysphagia) and use of gastrostomy feeding tubes (Hay et al., 2017). RT is associated acutely with mucositis, dysphagia, nausea/vomiting, skin changes (dermatitis) and necessity of using feeding tubes (Adelstein et al., 2003; Rosenthal et al., 2014). Long-term side-effects include fibrosis, dysphagia, dryness of the mouth (xerostomia) and second primary cancers (Eisbruch et al., 2004; Garden et al., 2008; Langendijk et al., 2008; Machtay et al., 2008). The addition of chemotherapy to RT synergizes these side-effects and increases the rate of toxicities during treatment from 51% to 85% (Adelstein et al., 2003). Therefore, for patients with HPV negative HNSCC, it is necessary to find the balanced treatment that is capable of achieving cure and maintaining a sufficient quality of life for the patient (Tawk et al., 2022). To develop versatile new treatment strategies, including personalized therapy, there is an urgent need for identifying genetic biomarkers of radioresistance and to understand how genes are regulated in response to RT (Tawk et al., 2021).

1.4.3 Preclinical FaDu model of HNSCC

FaDu is hypopharyngeal squamous cell carcinoma cell line, established in 1968 from a punch biopsy from a 56-year-old male patient with squamous cell carcinoma. The cell line was named FaDu for the patient from whom the tissue was removed. It has epithelial morphology and grows as a monolayer with the doubling time around 50 hours (Rangan, 1972). Alterations in both tumor suppressor TP53 and CDKN2A genes, similar to those observed in primary tumors, are present in FaDu cell line (Figure 3) (Nichols et al., 2012).

RNA is treated by the RNase III-like enzyme Dicer to form small interfering RNAs (siRNAs) to accomplish RNA silencing (Cowley et al., 2014). However, there are several limitations in RNAi approach, such as the extent and duration of mRNA cleavage, resulting in transient gene knockdown; and off-target effects, resulting an unintended gene knock-down due to sequence similarity with the intended target.

1.5.2 CRISPR/Cas9 genome editing

The CRISPR/Cas system was first recognized and explored as repetitive DNA sequences in prokaryotes (Jansen et al., 2002). The system which revolutionized the targeted genome editing-based explorations is the *Streptococcus pyogenes* type II CRISPR/Cas9 system (Doudna & Charpentier, 2014). It is an adaptive defense mechanism that uses a small RNA targeting sequence, enabling endonuclease Cas9 to bind DNA sequences upstream of a protospacer adjacent motif (PAM) and cause a DSB (Jinek et al., 2013). In bacteria and archaea, CRISPR locus contains unique spacer sequences acquired from invading genetic elements (protospacers) (Sorek et al., 2013). Protospacers are flanked by PAM sequence, which serves as a binding signal for Cas9 (Sternberg et al., 2014). Targeting and cleavage need a presence of RNA duplex consisting of CRISPR RNA (crRNA) and a transactivating crRNA (tracrRNA) (Deltcheva et al., 2011). Any DNA sequence that is flanked by PAM can be targeted. PAM in *Streptococcus pyogenes* is 5'-NGG-3', where "N" is any nucleobase followed by two guanines "G" (Jinek et al., 2012). In the engineered CRISPR/Cas9, crRNA and tracrRNA is substituted with the single guide RNA (gRNA) which is a fusion transcript and guides the Cas9 protein to the desired location (Jinek et al., 2012). By using an appropriate delivery system (such as lentiviral vehicles) the gRNA and Cas9 protein are delivered into the cells and combine to form the gRNA-Cas9 complex. DSB is induced when the nuclease activity of the Cas9 domains cleaves the target DNA sequence after the third nucleotide base upstream of the PAM after binding to the target site (Anders et al., 2014).

There are two major pathways that repair DSBs: non-homologous end joining (NHEJ) and homology-directed repair (HDR) (Chapman et al., 2012; Lieber, 2010; San Filippo et al., 2008). HDR, which uses an undamaged homologous sequence, normally from the sister chromatid, as a template, is considered highly accurate. NHEJ, on the other hand, is active throughout the cell cycle and religates the broken DNA ends, sometimes

in an error-prone manner. This can cause insertion or deletion mutations (Indels) that can result in frame-shift mutations and gene knockout. When standard repair pathways fail, alternative DSB repair pathways such as microhomology-mediated end joining (MMEJ) can activate (McVey & Lee, 2008) which may result in deletions or chromosome translocations. Finally, the precision of the HDR repair pathway can be used to insert the exact desired sequence into the target genomic region by providing a homologous donor template (Sander & Joung, 2014; Stracker & Petrini, 2011; Zhang et al., 2017) (Figure 4).

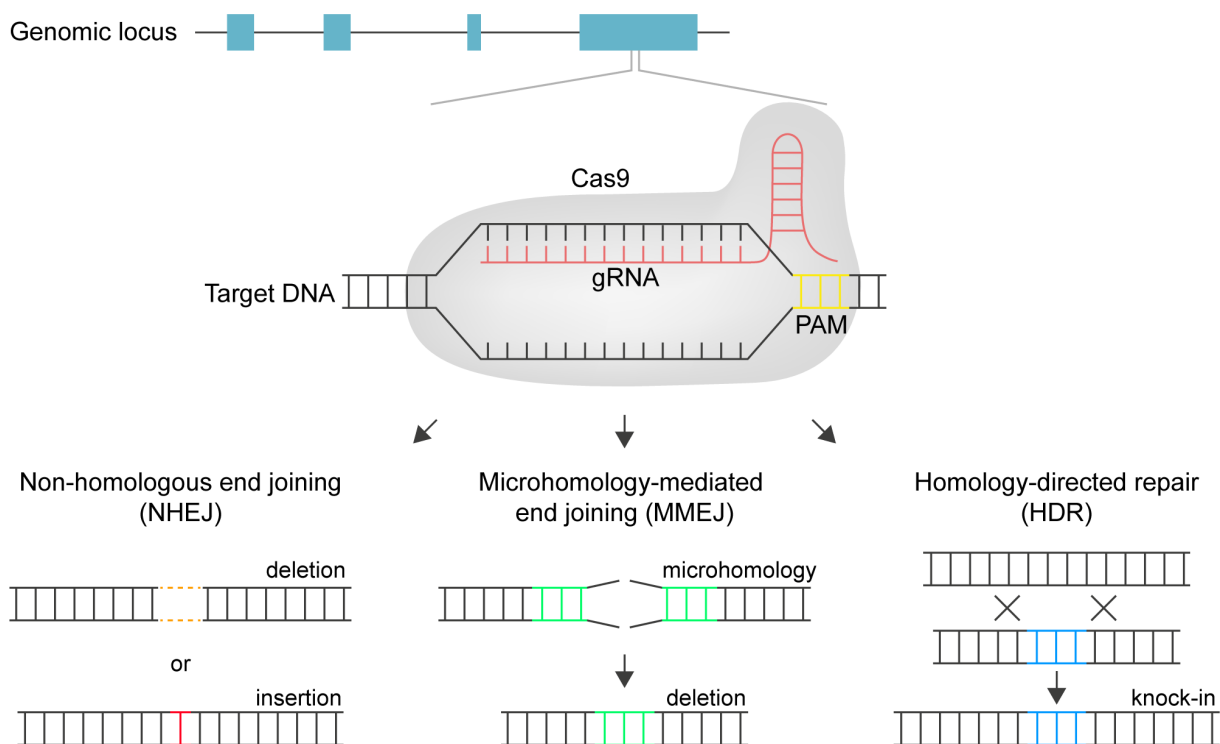


Figure 4. CRISPR/Cas9-mediated genome editing. Recruitment of Cas9 to the target DNA is mediated by gRNA, containing PAM. Cas9-induced DSBs are repaired either by NHEJ or MMEJ, which can result in insertions or deletions, or by HDR by using a donor DNA template, enabling desired sequence changes. Figure prepared by Dr. Katrin Rein.

1.6 CRISPR/Cas9 genetic screens

CRISPR/Cas based genome editing has become a robust tool in cancer biology owing to its easy planning and adaptability (Hsu et al., 2014). Genetic screening links genotype with phenotype in a process in which the expression of multiple genes in cell lines or animal models are systematically modulated and the cellular phenotypes of interest (e.g., proliferation) are selected (Grimm, 2004).

1.6.1 *In-vitro* genetic screens

A typical CRISPR *in-vitro* screen starts by viral transduction of desired cell type (e.g., tumor cell line) with gRNA library to integrate gRNAs into the genome of the target cells. Low multiplicity of infection (MOI) is used, which results, with high probability, in one perturbation per cell. Cellular pool with the desired phenotype is then selected, and the readout typically measures depletion or enrichment of gRNAs in this pool (e.g., cell death or proliferation, respectively). Sequencing of the DNA containing the gRNAs before and after phenotype selection reveals changes in gRNA representation and thereby selects candidate genes for further experiments (Figure 5 a) (Chow & Chen, 2018; Kuhn et al., 2021).

CRISPR screens were first developed by using pooled gRNA libraries which target all annotated genes in the human genome at once (Shalem et al., 2014). The feasibility, efficiency and availability of gRNA libraries has made CRISPR knock-out pooled screens a widely used method for interrogating gene function in cancer (Katti et al., 2022). CRISPR screens have played an important role to identify genes involved in multiple processes, including regulators of drug resistance (Sanjana et al., 2016), synergistic and synthetic lethal interactions (Han et al., 2017), and essential genes (Hart et al., 2015), among others.

1.6.2 *In-vivo* genetic screens

While *in-vitro* screens are highly valuable for identifying properties of cancer cells and potential therapeutics, they do not take into account complex cellular interactions at the tumor microenvironment, e.g. innate or adaptive immune response, the degree of tissue remodeling and extracellular matrix deposition, and tissue architecture that can all influence the phenotypes (Quail & Joyce, 2013). Advances in cancer research highlighted that tumor cells heavily crosstalk with their microenvironment with a multitude of consequences for tumor biology (Abdollahi & Folkman, 2010; Hanahan & Folkman, 1996; Hanahan & Weinberg, 2011). This is considered in *in-vivo* screens, which for example were indeed revealing cancer dependencies in tumor microenvironment that *in-vitro* screens failed to identify (Miller et al., 2017).

In direct *in-vivo* screens, delivery, and expression of genetic modification reagents directly *in-vivo* is commonly achieved by using lentiviruses or plasmids for local delivery, and adeno-associated virus (AAV) for systemic delivery. However, delivering and expressing enough reagents is challenging, therefore plasmids or AAV can be combined with effector proteins (i.e., integrase, recombinase, or transposase) that facilitate integration (Xue et al., 2014). Cas9, coupled with sgRNA, promoters, and other elements exceed the packaging capacity of viral vectors for *in-vivo* applications (Wu et al., 2010). Therefore, transgenic animal models in which Cas9 is integrated into the genome, reduce delivery burden, and provide more efficient platform for *in-vivo* screens (Platt et al., 2014). Cellular coverage can be limiting especially if genome-wide libraries are used. This requires scaling up considerably and using cells or DNA from multiple animals per replicate, and therefore limiting the library size to target a certain class of proteins. The readout of *in-vivo* screen is similar to the one of *in-vitro* screen, where gRNA representation is compared between control and experimental condition (Figure 5 b) (Kuhn et al., 2021).

To overcome difficulties of direct delivery of gene editing reagents, indirect *in-vivo* screens can be an effective approach. In indirect *in-vivo* screens, the target cell line is first transduced *in-vitro* and subsequently transplanted into model animal to assess phenotypes *in-vivo* (Figure 5 c). While being highly effective, the limitations include specific cell types that allow transplantation, and in case human cell lines are used, the requirement of immunocompromised animals (Chow & Chen, 2018; Kuhn et al., 2021). The identification of mutations associated with tumor growth and metastasis was one of the first examples of CRISPR/Cas9 applications for indirect *in-vivo* functional genetic screens (Chen et al., 2015). *In-vivo* CRISPR screens have among others identified tumor suppressors (Katigbak et al., 2016), oncogenes (Braun et al., 2016), synthetically lethal genes (Yau et al., 2017) and regulators of cancer immunotherapy (Patel et al., 2017).

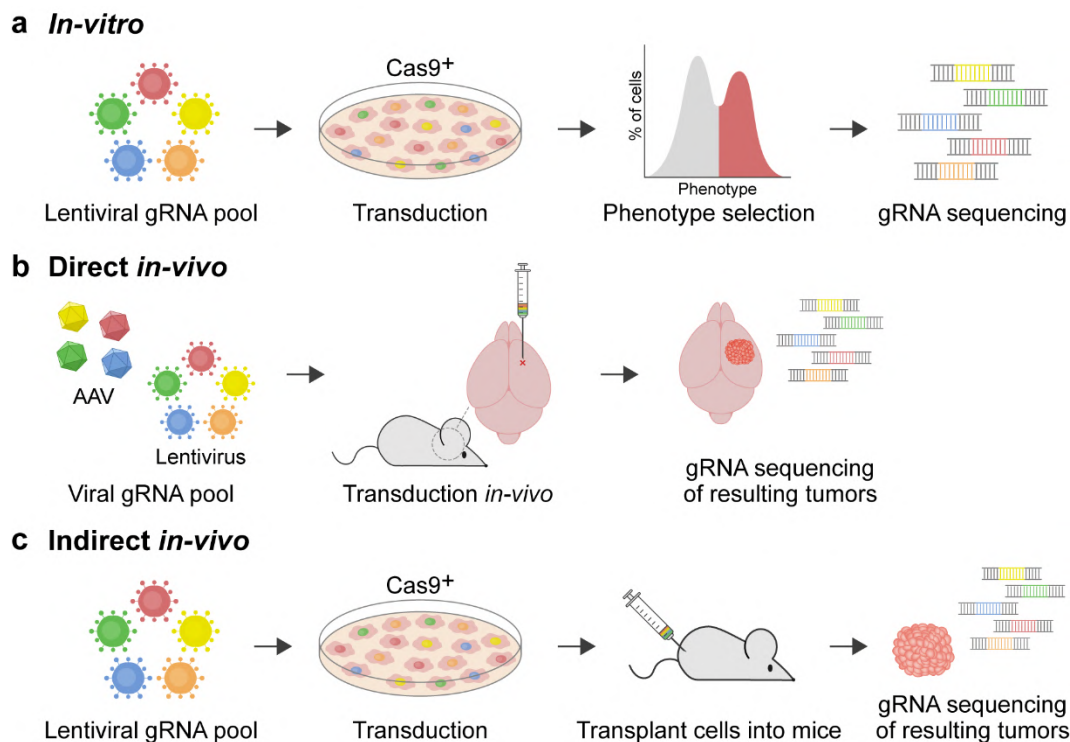


Figure 5. *In-vitro* and *in-vivo* CRISPR screen example workflows. a) In *in-vitro* screen, gRNA library is introduced into a desired cell line and cells are collected before and after a certain phenotype (e.g., proliferation) selection. gRNA cassettes are then amplified from genomic DNA and sequenced. b) In a direct *in-vivo* screen, gRNA library is delivered directly into the target cells by using, for example, lentivirus or AAV. Intracranial viral injection, for example, can drive tumorigenesis. The gRNA representation of resulting tumors is compared with control condition. c) In an indirect *in-vivo* screen, gRNA library is first introduced into a cell line of interest, followed by transplantation (e.g., subcutaneous injection). In the case of a tumorigenesis screen, the resulting tumor is harvested, and gRNAs sequenced. Figure prepared by Dr. Katrin Rein.

1.7 CRISPR/Cas9 screening libraries

1.7.1 GeCKO and GeCKO v2 libraries

First widely used whole genome screening library was lentiviral genome-scale CRISPR-Cas9 knockout (GeCKO) library targeting 18,080 genes with 64,751 unique guide sequences (Shalem et al., 2014) and was used to identify genes essential for cell viability in cancer and pluripotent stem cells. The original library was improved by both the lentiviral packaging and choice of guide sequences, resulting an increase in functional viral titer (GeCKO v2). The GeCKO v2 libraries consist of over 100,000 unique gRNAs sequences for gene knock-out in the human genome. This library is available as two half-libraries (A and B). When used together, the A and B half-libraries contain 6 sgRNAs per gene (3 sgRNAs in each library). Both A and B half-libraries

contain 1000 control sgRNAs each designed not to target in the genome. The A library also targets 1,864 miRNAs (4 sgRNAs per miRNA). This library is available in one vector (lentiCRISPRv2) or two vector (lentiCas9-Blast and lentiGuide-Puro) formats (Sanjana et al., 2014) (Table 3).

1.7.2 Brunello library

The human CRISPR Brunello lentiviral pooled library was developed to minimize the impact of off-target activity on screening results and to improve on-target activity of gRNAs. It is available in either one vector (lentiCRISPRv2 backbone) or two vector (lentiGuide-Puro backbone) system. The Brunello CRISPR knockout pooled library has 76,441 gRNAs to make edits across 19,114 genes in the human genome. It contains 4 sgRNAs per gene and 1000 control sgRNAs designed not to target the genome (Doench et al., 2016) (Table 3).

1.7.3 TKO library

The Toronto KnockOut (TKO) Library was developed to expand the catalog of human core and context-dependent fitness genes (Hart et al., 2015) and further optimized for editing efficiency, resulting in TKO v3 Library that contains 70,948 gRNAs targeting 18,053 protein coding genes with 142 control gRNAs targeting EGFP, LacZ, and luciferase. The optimized library size of TKO v3 offers the benefit of improved accuracy, efficiency and scalability for CRISPR screens, as it small enough to perform genome-wide screens and sensitive enough to minimize false negatives (Hart et al., 2017) (Table 3).

Table 3. List of genome-wide CRISPR libraries

Library	gRNAs	Genes	miRNAs	gRNAs/gene	control gRNAs
GeCKO v2	123411	19050	1,864	6	2000
A+B	65,383 (A) 58,028 (B)			3 (A) 3 (B)	1000 (A) 1000 (B)
Brunello	76441	19114	0	4	1000
TKO v3	70948	18053	0	4	142

Aim of this dissertation

The aim of this thesis was to systematically characterize novel radiation qualities i.e., particle irradiation with protons, helium, carbon, and oxygen ions available at Heidelberg Ion-Beam Therapy Center (HIT) in HNSCC and NSCLC *in-vivo* preclinical xenograft models. To dissect the molecular underlying of tumor response to these radiation modalities transcriptome and functional genomic analysis was conducted.

The objectives of this work were:

1. Establish the FaDu HNSCC and A549 NSCLC xenograft models and the radiotherapy setup for conventional photon irradiation as well as irradiation with the four particle qualities at HIT.
2. Generate Cas9 stable A549 and FaDu clones and integrate genome-wide lentiviral CRISPR/Cas9 based libraries using two different platforms, i.e., GeCKO and Brunello libraries, respectively.
3. Perform quality control and characterization of the GeCKO A and Brunello libraries under standard *in-vitro* vs. more complex *in-vivo* constraints considering tumor microenvironment (TME) selection pressure.
4. Study the effect of fractionated conventional irradiation with photons/x-ray *in-vivo*.
5. Study the effect of fractionated proton irradiation as a clinical standard particle therapy modality with assumed fixed RBE of 1.1 vs. irradiation with a gradual increase of LET using heavier i.e., helium, carbon, and oxygen ions.
6. Decipher the tumor transcriptome response to different radiation qualities via RNA-seq analysis.

7. Dissect tumor evolutionary dynamic with and without radiotherapy selection pressures, considering the additional effect of single gene knock-out on top of the inherent genetic background of the two tumor models.
8. Identify novel regulators of radiosensitivity of HNSCC and NSCLC for the development of biomarkers and novel drug targets.

2. Materials and methods

2.1 Materials

2.1.1 Cell lines

Name (species; tissue origin)	Supplier
A549 (human lung adenocarcinoma)	DSMZ, Germany
FaDu (human hypopharyngeal carcinoma)	Jochen Hess, Germany
293T (human embryonic kidney)	SBI System, Bioscience, Germany

2.1.2 Chemical materials

Acetic Acid>99.8%	Sigma-Aldrich, Germany
Agarose (11404.05)	SERVA, Germany
Ampicillin (A051-B)	G-Biosciences, USA
Crystal Violet (C0775)	Sigma-Aldrich, Germany
DMEM (FG0415)	Biochrom, Germany
DMSO (P60-36720100)	PAN Biotech, Germany
DPBS (14190-094)	Thermo Fisher, USA
FCS (S0615)	Biochrom, Germany
Isopropanol	Sigma-Aldrich, Germany
Lipofectamine 2000 (11668-27)	Invitrogen, USA
IMDM (12440053)	Thermo Fisher, USA
LB-Agar (X965.1)	Roth, Germany
LB-Medium (X964.1)	Roth, Germany
MEM (31095-029)	Biochrom, Germany
Methanol (32213)	Sigma-Aldrich, Germany
1x NEBuffer 2	New England Biolabs, Germany
10x Taq Buffer	Genaxxon bioscience, Germany
6x DNA Loading Dye	Thermo Scientific, USA
Opti-MEM Reduced Serum Medium	Gibco Invitrogen, USA
PAXgene Tissue FIX	PreAnalytix GmbH, Germany

Penicillin/Streptomycin	Gibco Invitrogen, USA
Puromycin	Gibco Invitrogen, USA
PLUS™ Reagent	Thermo Scientific, USA
RNase-free Water	Sigma-Aldrich, Germany
S.O.C Medium	Fisher BioReagents, Germany
T7 Endonuclease 1	New England Biolabs, Germany
Trypan Blue	Sigma-Aldrich, Germany
Trypsin/EDTA	PAN Biotech, Germany

2.1.3 Non-chemical materials

Greiner 96-well plate	Greiner bio-one, Germany
Greiner 24-well plate	Greiner bio-one, Germany
Greiner 12-well plate	Greiner bio-one, Germany
Greiner 6-well plate	Greiner bio-one, Germany
Tissue culture flask T-75	SARSTEDT, Germany
Tissue culture flask T-175	SARSTEDT, Germany
Cellstar falcon tubes	Greiner bio-one, Germany
29G Injection needle	BD Microlance, Germany
Disposable syringe	BD Microlance, Germany
Cryo tubes	Thermo Scientific, USA

2.1.4 Kits

NucleoBond® DNA-kit	MACHEREY-NAGEL, Germany
RNeasy® Mini Kit	QIAGEN, Germany
DNA Chips	Agilent Technologies, USA
RNA Nano Chips	Agilent Technologies, USA
EnGen® Mutation Detection Kit	New England Biolabs, Germany

2.1.5 Animals and anesthesia

NMRI-Foxn1 ^{nu/nu} nude mice	JANVIER labs, France
---------------------------------------	----------------------

Isoflurane

Bayer Vital GmbH, Germany

2.1.6 Laboratory devices

DNA Engine Thermal Cycler

Bio-Rad, USA

Agilent 2100 Bio-analyzer

Agilent Technologies, Germany

AccuJet Pro automatic pipette

Brand, Germany

Biowizard cell culture hood

KOJAIR, Finland

ChemiDoc system

Bio-Rad, USA

200R Mikro centrifuge

Hettich Zentrifugen, Germany

460R Rotanta centrifuge

Hettich Zentrifugen, Germany

-80°C deep freezer

Sanyo, Germany

Nanodrop 1000 spectrophotometer

NanoDrop, USA

Vortexer

IKA Janke&Kunkel, Germany

Water bath

Huber, Germany

2.1.7 Software

CS-Cal

<http://angiogenesis.dkfz.de/oncoexpress/software/>

ImageJ7Fiji

<http://imagej.nih.gov/ij/>

SUMO

<http://angiogenesis.dkfz.de/oncoexpress/software/>

TableButler

<http://angiogenesis.dkfz.de/oncoexpress/software/>

SeedScan

<http://angiogenesis.dkfz.de/oncoexpress/software/>

GraphPad Software

www.graphpad.com

2.2 Methods

2.2.1 Basic cell culture procedures

FaDu cells were cultured in MEM medium supplemented with 10% fetal calf serum (FCS) and 1% Penicillin/Streptomycin. A549 cells were cultured in DMEM medium complemented with 10% FCS and 1% Penicillin/Streptomycin. Media with mentioned

supplements are referred to as complete medium. For cell passaging, cells were washed with DPBS once and incubated with Trypsin/EDTA for 5 minutes at 37°C. Complete medium was added to stop Trypsin activity. The cell suspension was centrifuged at 1000 rpm for 5 minutes. The supernatant was discarded, and the cells were dispersed at a dilution of 1/5 in new medium.

2.2.2 Cell lines used

FaDu is human squamous cell carcinoma line with epithelial morphology which obtained from hypopharyngeal tumor; its doubling time is 30 hours and they adherent to the culturing flask. In nude mice they grow as an undifferentiated carcinoma (Hessel et al., 2003).

A549 is human lung adenocarcinoma and developed through the removal of cancerous lung tissue, it grows as a monolayer and attaching to the culture flasks. It is KRAS mutant, EGFR and TP53 wild type. This line used for testing of novel drugs *in-vitro* and *in-vivo* in the field of cancer. The A549 cell line derived xenograft (CDX) is one of the most used xenograft lung cancer models (Balis et al., 1984).

2.2.3 Generating Cas9-expressing single cell clones

Genetic heterogeneity which exists in cancer cell lines increases the likelihood of false positive hits in functional genomic screens. To minimize these effects for the performance of our functional screens in *in-vivo*, clonal FaDu (HNSCC) and A549 (NSCLC) cell lines were derived that express Cas9.

To generate Cas9 expressing lines, FaDu and A549 cells were transduced using lentiviral particles produced in 293T cells using pSpCas9(BB)-2A-Puro (PX459) V2.0 plasmid (Addgene #62988). Following determination of optimal dose of blasticidin as selective antibiotic, DMEM medium was mixed with polybrene to achieve 10µg/ml concentration. In the next step lentiviral aliquot was thawed at 37°C and lentivirus dilution in DMEM-polybrene were prepared. 5×10^4 cells were transduced in 6-well plates by adding 0.5ml of virus solution and incubated for 48 hours. Transduced cells were selected using complete DMEM medium containing blasticidin. Confluent well of a 6-well plate was expanded into a 10cm dish. To generate single cell clones, cells

were seeded in 96-well plates in limiting dilutions: 1×10^5 cells were suspended in 5 ml of medium and 500 μ l of prepared cell suspension was added to 4.5ml of medium. In the next step cells were diluted 1:10 ratio and 100 μ l of suspension was seeded in each well of 96-well plates. The cells were cultured in incubator at 37°C for two weeks, while monitoring the formation of colonies. Wells with only one clone were selected for further expansion into larger plates. Derived single cell clones were passaged and stock frozen in liquid nitrogen for future use.

2.2.4 Plating efficiency

Single cell clones were selected to compare their plating efficiency with the wild type cells. 500 cells of wild type and selected single clones were seeded in 6-well plates in triplicate and were incubated at 37°C to form clones. After 2 weeks of culturing, number of clones which were formed were counted and divided by initial seeding number and their percent of plating efficacy was calculated.

2.2.5 Clonogenic survival assay

The response to irradiation of single cell clones and the parental cell lines was evaluated by performing clonogenic survival assay. 500cells/well of 6-well plate were seeded for non-irradiated control plates, cells seeding densities increased up to 4000 cells for higher radiation doses. Cells were seeded in triplicates. Plates were incubated overnight at 37°C and were irradiated with 1Gy as the lowest and 8Gy as the highest dose with 2Gy increasing intervals on a Siemens Artiste (6MV) linear accelerator at the Department of Medical Physics in Radiation Therapy (DKFZ). After irradiation, plates were incubated for two weeks to form colonies. When colonies were observed by eye, they were stained with crystal violet. For image acquisition, plates were exposed for 0.03 sec with trans-illumination white light by using ChemiDoc system (Bio-Rad). Colonies were counted automatically by using image processing software ImageJ. Survival fractions were computed using the in-house software CS-Cal.

2.2.6 T7 Endonuclease I assay

To evaluate the cleavage efficiency in clonally derived FaDu and A549 lines, CRISPR/Cas9-mediated double strand break (DSB) in the SYNE1 gene was induced

by transducing each cell line with lentiviral vectors expressing gRNA sequence specific for the Synaptic nuclear envelope protein 1 (SYNE1) locus (vectors were cloned by Dr. Maximillian Knoll and Dr. Ali Nowrouzi). For lentivirus transduction, FaDu-Cas9 and A549-Cas9 cells were seeded in 12-well plates with the seeding density of 5×10^4 cells/well and incubated at 37°C. The following day, cells were transduced with 500 μ l of the lentivirus solutions. Successfully transduced cells were selected with 2 μ g/ml (FaDu-Cas9 cells) or 4 μ g/ml (A549-Cas9 cells) of puromycin selection. One of the wells containing non-transduced FaDu-Cas9 and A549-Cas9 cells was treated also with puromycin to serve as positive control. The genomic region in which the DSB was induced was amplified by PCR (Table 4) and purified using QIAquick PCR purification Kit according to the manufacturer's protocol. To perform T7 Endonuclease I (T7EI) assay, 200ng of purified PCR product was mixed with 2 μ l of 1xNEBuffer 2 and exposed to high temperature (denaturation) followed by a cooling down step to form heteroduplexes (Table 5). After the formation of heteroduplexes, the solution was treated with 1 μ l of T7EI to cleave DNA fragments. Cleavage products were detected by agarose gel electrophoresis.

Table 4. PCR program for amplifying DSB induced region

Description	Temperature	Time	Replications
Initial denaturation	95°C	2 minutes	1 Cycle
Denaturation	95°C	45 seconds	30 Cycles
Annealing	58°C	45 seconds	30 Cycles
Elongation	72°C	1 minute	30 Cycles
Final elongation	72°C	5 minutes	1 Cycle

Table 5. T7 Endonuclease 1 heteroduplex formation program

Description	Temperature	Time / Rate
Initial denaturation	95°C	5 minutes
Annealing	95°C to 85°C	2°C/s
Annealing	85°C to 25°C	0.1°C/s

2.2.7 Whole genome CRISPR/Cas9 screen in *in-vivo* models

For performing the functional screens *in-vivo*, the FaDu-Cas9 and A549-Cas9 single cell clones were selected and transduced with the genome-wide Brunello library (Addgene Catalog # 73178). GeCKO library A (Addgene Catalog # 1000000049) was previously integrated in the team in FaDu-Cas9 and A549-Cas9 single cell clones.

2.2.8 Determination of infection condition for pooled screens

In order to have one vector copy per cell that would be equivalent with one gene knockout per cell, multiplicity of infection (MOI) of 0.3 was used. To find optimal virus volumes for achieving the desired MOI, FaDu and A549 cells were seeded at 1×10^6 cells/ml in each well of a 12-well plate. The next day, wells were transduced at 1:10, 1:50, 1:100, and 1:200 dilutions with or without Brunello library virus. Plates were incubated for additional 24 hours and after that cells were transferred in duplicates into 6-well plates in 1:1 ratio. One replicate was treated with and the other without puromycin. As soon as non-transduced control cells treated with puromycin were not viable, the percentage of transduction rate was calculated by counting the puromycin treated cells divided by cell count without puromycin multiplied by 100. Virus titer per ml was calculated as the number of seeded cells multiplied with transduction efficiency divided by the dilution factor multiplied by 100.

2.2.9 Subcutaneous xenograft mouse models

All *in-vivo* experiments were conducted in accordance with the German Cancer Research Center (DKFZ) institutional animal welfare rules approved by the federal animal welfare authorities of Regierungspräsidium Karlsruhe. NMRI-Foxn1^{nu/nu} female mice from Janvier Labs (France) that were 4-6 weeks old were allowed to acclimatize in the animal facility for 1-2 weeks after arrival before starting experiments. 3×10^6 FaDu and A549 cells in 100 μ l PBS were injected subcutaneously into the right hind limb of the mice. The size of tumors was measured every second day with a caliper and when their volume reached $150 \pm 50 \text{mm}^3$ they were randomized to non-irradiated and irradiated groups. The mice were sacrificed when the volume of primary/recurrent tumor reached 1500mm^3 or one side of tumor reached to 15mm.

2.2.10 Photon irradiation

For photon irradiation, anesthetized mice (n=10) for each model were placed on a horizontal plate and tumors were irradiated with a vertical photon beam using Siemens Artiste (6MV) linear accelerator at the Department of Medical Physics in Radiation Therapy (DKFZ). The tumors were placed into the radiation field while the body was shielded and irradiated with 13 fractions of 3Gy daily to a total physical dose of 39Gy.

2.2.11 Charged particle Irradiation

Particles were administrated at the Heidelberg Ion-Beam Therapy Center (HIT). The irradiation plan was developed by Dr. Stephan Brons. For irradiation, anesthetized mice (n=10) of each particle were placed on a holder which was designed to place tumors into the radiation field (Figure 6 a,b). The tumors were irradiated daily with 8 fractions at a physical dose of 3Gy protons (Beam energy: 127.5-136.3 MeV/u, LET 4.5keV/ μ m (range 3.3-8.5 keV/ μ m)), carbon ions (Beam energy: 245.4-261.6 MeV/u, LET 80 keV/ μ m (range 55-175 keV/ μ m)), helium ions (Beam energy : 128.4-136.1 MeV/u, LET \approx 18 keV/ μ m) and oxygen ions (Beam energy: 291.8-311.2 MeV/u, LET 120 keV/ μ m (range 70-225 keV/ μ m)), within a SOBP of 15x15x15 mm at a water equivalent depth of 124 ± 10 mm behind a 100mm Poly methyl methacrylate (PMMA) (Figure 6 c,d).

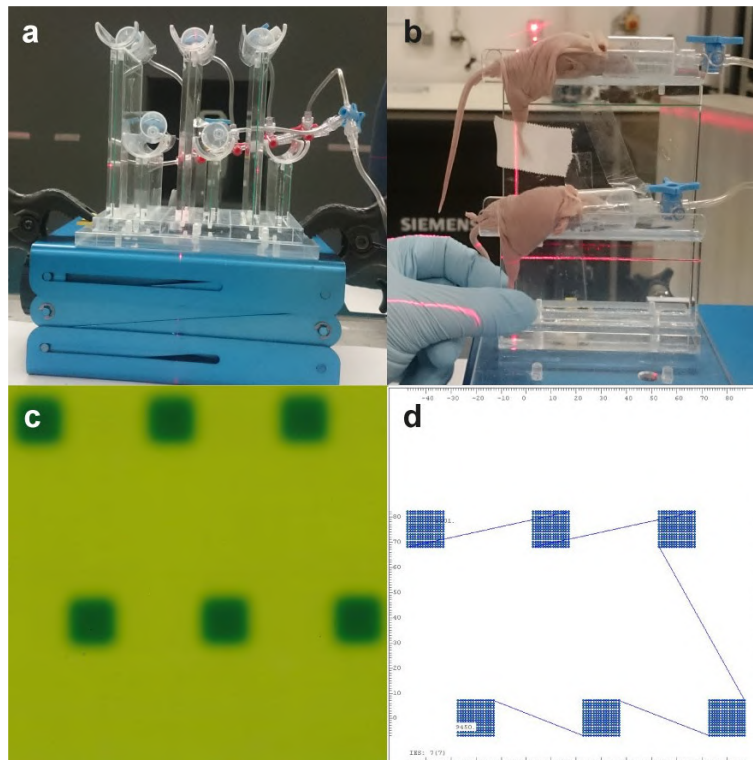


Figure 6. Radiation field description. a) Holder to place tumor into the irradiation field. b) Anesthetized mice with tumors were placed in holder. c) Irradiated film to confirm irradiation with beam. d) Irradiation geometry to reach height and width of 15 mm.

2.2.12 Genomic DNA and total RNA extraction from tumors

When mice were sacrificed, tumors were excised, and genomic DNA was isolated from tumor tissues according to the protocol for NucleoBond DNA extraction Kit (Macherey-Nagel). Total RNA was isolated from snap frozen tumor tissues according to the protocol for RNA extraction in the RNeasy RNA Mini kit (Qiagen).

2.2.13 Library preparation and sequencing

For each sample, two PCR cycles were performed (Figure 7). First PCR (Table 6) was to amplify the whole genomic region and contained in total of 24 μ g of isolated gDNA. For each sample, eight PCR reactions were performed and pooled together. The second PCR was a nested PCR to improve sensitivity/specificity and contained 2.5 μ l of first PCR pooled product. PCR conditions were the same as for the first PCR. Each sample from the second PCR was pooled together and was purified with AMPure beads (Beckman) in 1:1 ratio according to manufacturer's instructions. Concentrations

of purified samples were measured via Nanodrop spectrophotometer and 500ng of each sample was used in a pooled lane. In the next step the pooled lane product was run in Bioanalyzer Agilent 2100 and pooled lane concentration was measured using Qubit Fluorometric Quantification (Invitrogen), the average size of library (bp) and its concentration was used for calculating the amount of needed library to run NovaSeq 6000 (Illumina) sequencing (Figure 7). Sequencing was performed at the DKFZ Genomics and Proteomics Core Facility, and results were provided in FastQ files.

Table 6. PCR program for library preparation

Description	Temperature	Time	Replications
Initial denaturation	98°C	10 seconds	1 Cycle
Denaturation	98°C	1 seconds	15 Cycles
Annealing	60°C	5 seconds	15 Cycles
Elongation	72°C	10 seconds	15 Cycles
Final elongation	72°C	1 minutes	1 Cycle

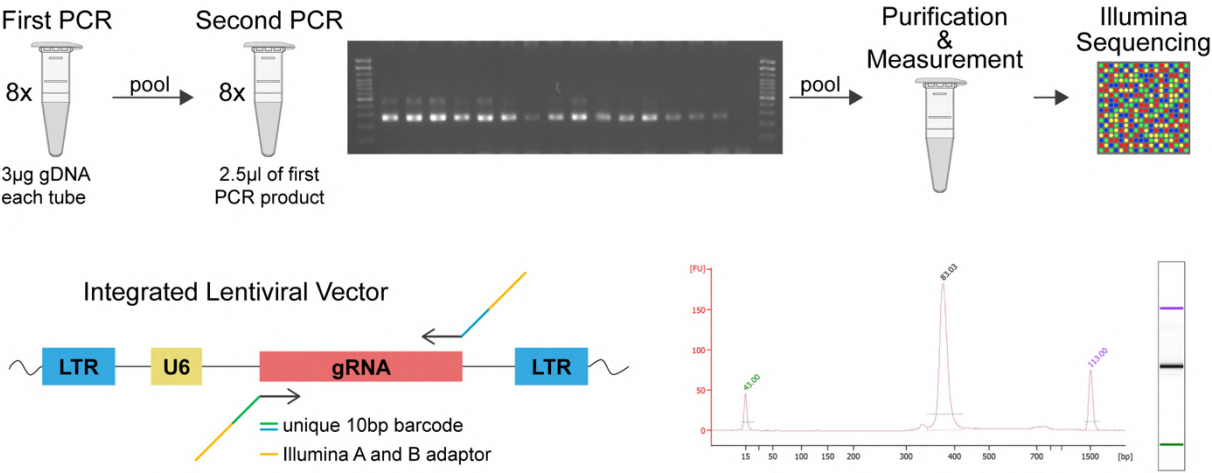


Figure 7. Library preparation and multiplexing for NGS

The experimental setup of the screens is described in the following schematics:

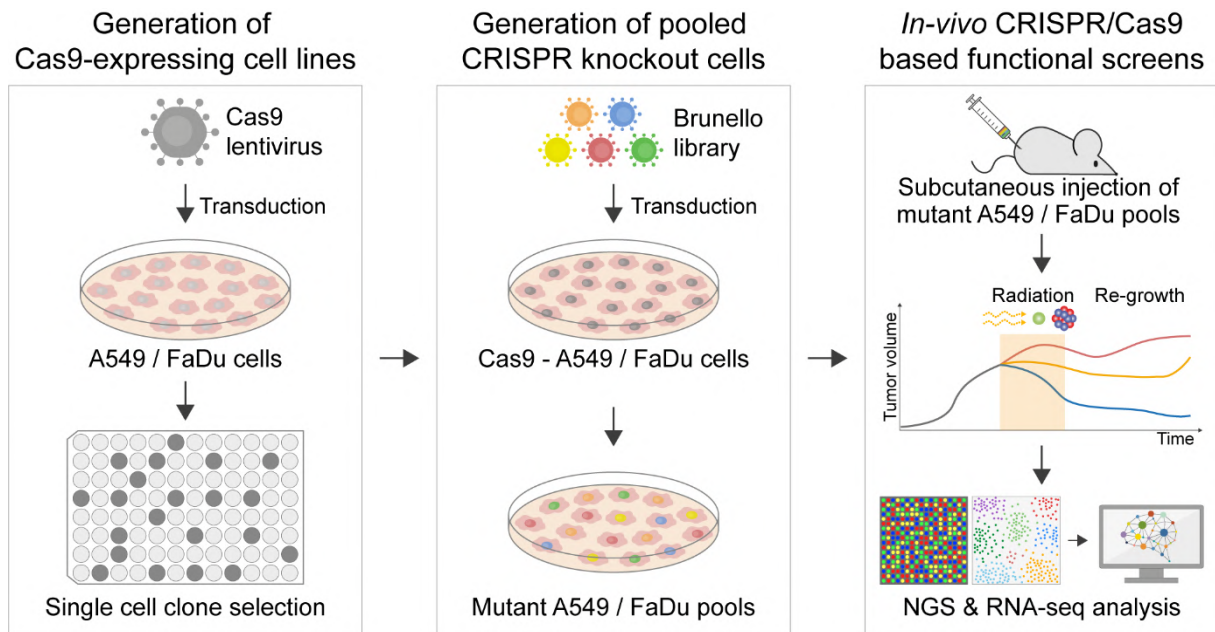


Figure 8. Experimental setup of the screens

2.2.14 Sequencing read count processing

SeedScan in-house software was used for pre-processing of NGS FastQ files. In order to identify a sample, first specific barcode pairs which were used for each sample (forward/reverse) were detected. Reads which did not match the barcodes were rejected. Later, library guides sequence was searched, and matched targets were counted and normalized to a million reads. For identification of guides sample's sequences were matched against the guide library allowing 1 error (base exchange/insertion/deletion), +/- 2bp-shift against expected position in the construct (i.e. up to 2 insertion/deletion upstream the guide sequence).

FastQ files of NovaSeq6000 sequencing of RNA libraries (100bp, PE) were preprocessed as follows: raw reads were aligned against a merged human/mouse reference genome (human: GRCh39.p13, mouse: GRCm39.p6) by applying TopHat v2.1.1/Bowtie 2. For removing duplicate reads, deduplication step was applied by using Picard Tools. Cufflinks v2.1.1 was used to quantify gene expression count using the human reference genome (GRCh39.p13) annotations, mouse read counts were ignored. Counts are reported as Fragments Per Kilobase transcript length per Millions reads analyzed (FPKM). Gene counts were prepared as an expression matrix and used for further analysis.

2.2.15 Statistical analysis and gRNA abundance analysis

Survival fractions from clonogenic survival assay were computed using the in-house software CS-Cal (v1.01b, by c.schwager@dkfz.de). GraphPad Prism 7 was used to plot tumor growth, survival curves and bar charts. Means of data were presented with standard deviation (SD) or standard error of mean (SEM). Student's t-Test was used to determine statistical significances. For RNA expression analysis, raw data was transformed using the variance stabilizing transformation (vst) function from the DeSeq2 package (Love et al., 2014), and mean aggregated per gene. Non complete cases (NA, Inf) were removed. As unwanted variability was present in the analyzed samples, principal component analysis was performed, and information contained in the first principal component was removed. gRNA abundance and its relation with treatments were analyzed as following: gRNA count matrixes were aggregated over targeted genes per sample (maximum value); genes were then ranked per sample (highest observed value: highest rank), non-detected genes were set to NA. Next, genes were aggregated over treatment groups (control, photon, etc.) by using the respective maximum rank. Only genes being detected in any carbon ion and oxygen ion treated samples were retained. This resulted in 1331 genes for further analysis in FaDu model and 18686 genes in A549 model (out of 19113 genes in total). Imputed data (van Buuren & Groothuis-Oudshoorn, 2011) matrixes (not aggregated per group) were used for analyses of associations with LET, and differences between control and photon irradiated tumors. Kyoto Encyclopedia of Genes and Genomes (KEGG) pathway enrichment analyses were performed with the enrichR package (Jawaid, 2021). Gene set enrichment analyses were performed with the tmod package, using the tmodUtest function (Weiner 3rd J, Domaszewska T. 2016). All above mentioned analyses were performed in R software (R Core Team, 2018) with help of the internal bioinformatic subgroup.

3. Results

3.1 *In-vitro* characterization of single cell clones

Genetic heterogeneity which exists in cancer cell lines increases the chance of false positive hits in functional genomic screens. In order to minimize these effects and to have similar Cas9 cutting efficacy for our functional screens *in-vivo*, clonal FaDu (HNSCC) and A549 (NSCLC) lines expressing Cas9 were generated.

Three single cell clones (Scc) of A549 were selected to compare their plating efficiency with the wild type cell line (Figure 9 a). Clones #1 and #2 showed significant differences in comparison with wild type ($p=0.03$ and $p=0.04$, respectively). There was no significant difference between clone #3 and wild type ($p=0.06$).

To evaluate whether single cell clones respond similarly to the pool of parental wild type cells to irradiation, clonogenic survival assay was performed (Figure 9 b). A two-tailed Mann Whitney test was performed to evaluate statistically significant differences in the clone numbers (survival reduction) was obtained after 4, 6 and 8 Gy radiation doses of all three clonal cell lines. No statistical difference was observed between wild type and the clonal cell lines, $p=0.7$, $p=0.9$ and $p>0.9$ in Scc #1, #2, and #3 respectively.

To evaluate the cleavage efficiency in clonally derived cell lines, double strand breaks (DSBs) were induced by transducing each line with lentiviral vectors expressing gRNA sequence specific for the Synaptic nuclear envelope protein 1 (SYNE1) locus. T7 Endonuclease I (T7 E1) assay was performed to evaluate gene editing efficiency (Figure 9 c). The cleavage percent of A549 clone #1 with 63.38% was the lowest cleavage percentage in comparison to other tested clones. The higher cleavage percentages were observed in clones #2 and #3 with 93.16% and 94.3% respectively.

Based on the plating efficacy, and T7 E1 assay results, clone #3 was selected for transduction with Brunello library.

FaDu single cell clone was previously cloned in the lab and used for the further experiments.

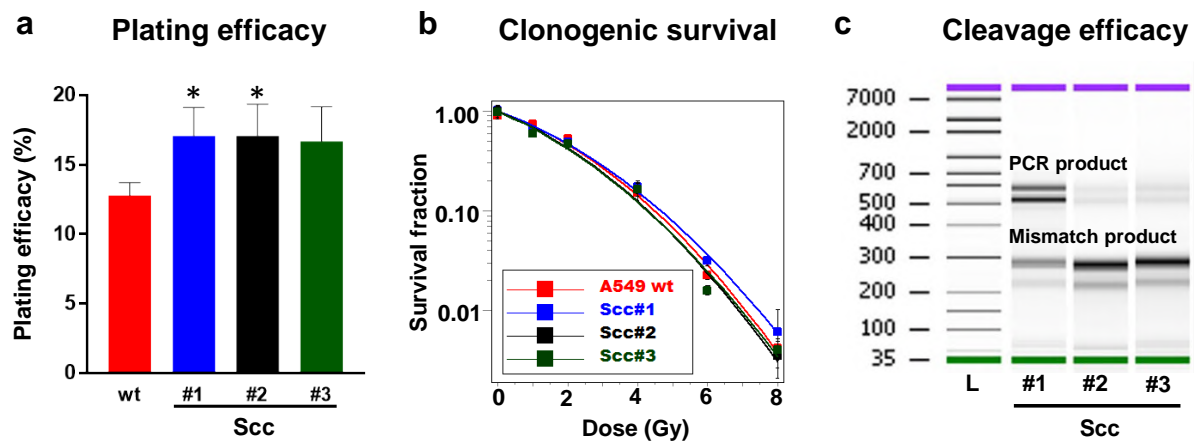


Figure 9. In-vitro characterization of single cell clones. a) Plating efficacy of A549 single cell clones (Scc) in comparison to wild type cell line. Data represents mean \pm SEM; #1 n=3 p=0.03, #2 n=3 p=0.04 and #3 n=3 p=0.06. b) Clonogenic survival of single cell clones after photon irradiation in comparison to A549 wild type cell line, data were fitted to a linear quadratic model (LQM). Data represents mean \pm SD. c) Cleavage efficacy quantification of single cell clones. T7 Endonuclease 1 assay was performed on purified PCR products and samples were run in Bioanalyzer. Pseudogel plot shows cleaved mismatch and intact PCR fragments.

3.2 In-vitro and in-vivo representation of GeCKO A and Brunello libraries

First, we assessed library representation between in *in-vitro* and in non-irradiated control mice (*in-vivo*). The representation of the *in-vitro* FaDu-GeCKO A library was 91.4%, the average representation of non-irradiated control tumors *in-vivo* was $27.42 \pm 4.12\%$ (Figure 10 a). The average representation of the FaDu-Brunello library was $92.8 \pm 0.53\%$ and the average representation of non-irradiated control tumors *in-vivo* was $40.9 \pm 5.03\%$ (Figure 10 b).

The average representation of two technical replicates in A549-Brunello library in the *in-vitro* samples was $94.8 \pm 0.60\%$ and the average representation in non-irradiated control tumors *in-vivo* was $35.3 \pm 2.76\%$ (Figure 10 c). These results indicate that library representations are reduced *in-vivo* mice and show variation between mice.

Distributions of detected guides of log₁₀ transformed read counts are shown in Figure 10 d,e,f. Both *in-vivo* and *in-vitro* distributions are highly similar between replicates within each model, as are *in-vitro* distributions between models. *In-vivo* gRNA distributions are skewed, with the mode being between 10 and 100 whereas mode for *in-vitro* is between 100 and 1000 reads. However, *in-vivo* guide distributions show higher fractions of gRNAs with higher numbers of reads (>1000) as compared to *in-vitro* samples.

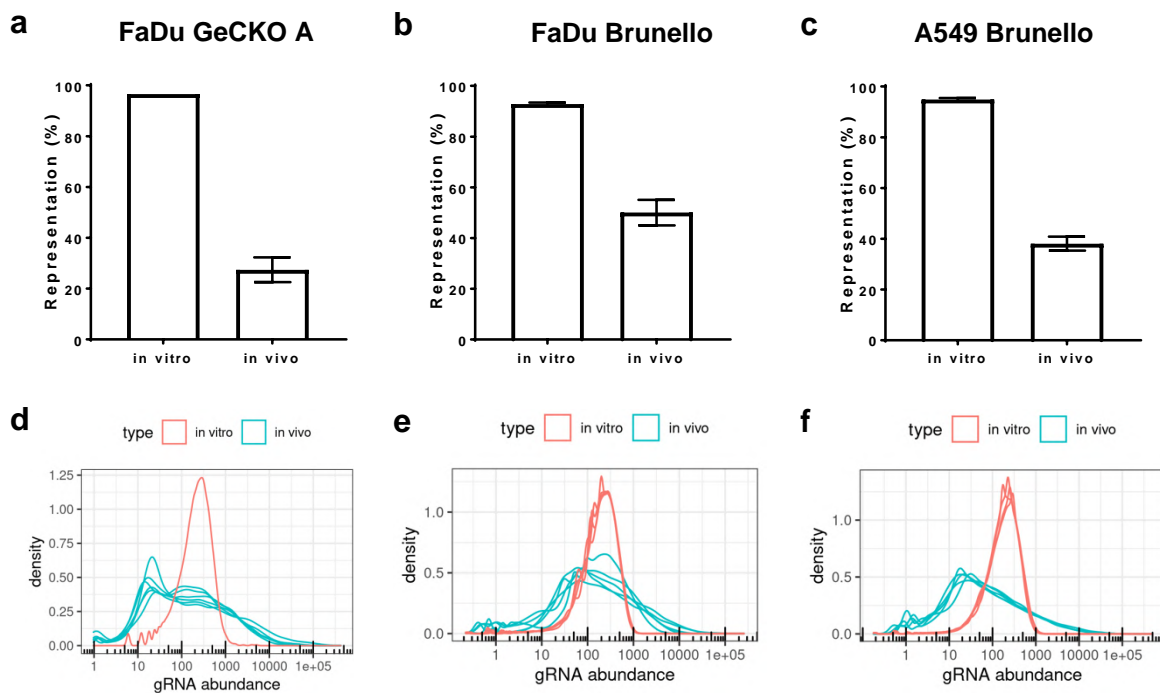


Figure 10. *In-vitro* and *In-vivo* representation of GeCKO A and Brunello libraries. *In-vitro* representation of a) FaDu GeCKO A library (n=1). b,c) Brunello library in FaDu (n=4) and A549 (n=4) respectively. The representation of guides in both libraries was above 92% *in-vitro*. Representation of tumor xenografts *in-vivo* (n=5) showed variances between individual mice and reduction of the representation of guides in comparison to *in-vitro* representation in both libraries. Data represents mean \pm SEM. d,e,f) Distribution of gRNA abundance in *in-vitro* and *in-vivo*.

3.3 Correlation between tumor growth kinetics *in-vivo* and library representation

Transduced FaDu and A549 cells with GeCKO A or Brunello library were implanted subcutaneously into nude mice. Representation of libraries is shown in Figure 11. Representation is shown as the percentage of detected gRNAs (>0 reads) from the full library complexity (65383 and 76441 unique gRNAs in GeCKO A and Brunello,

respectively). A negative linear association between library complexity and survival time (days to sacrifice) was found in all models (Figure 11 a,b,c).

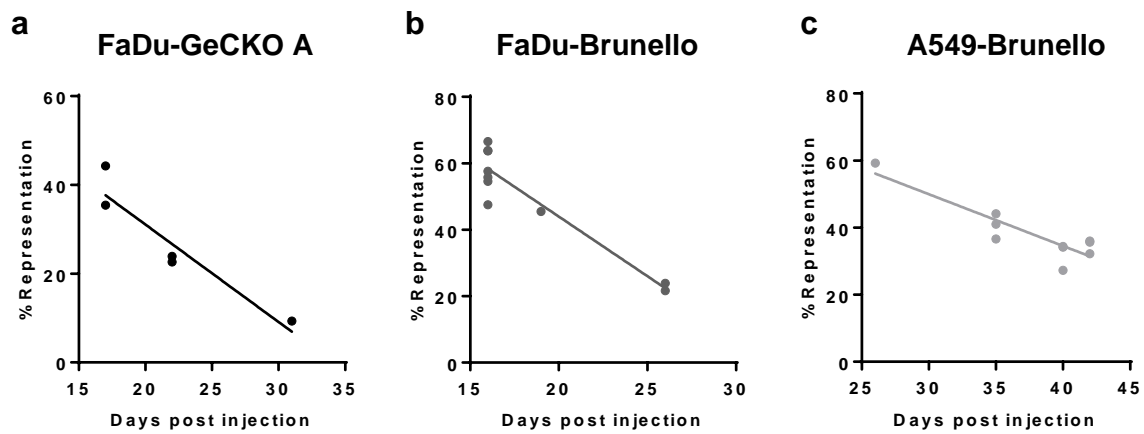


Figure 11. Library representation decreases as tumor growth increases. Percent of detected (>0 reads) unique gRNAs vs. the entire library complexity. X-axis: days of tumor take out and termination, after tumor cell injection. Linear regression fits are shown.

3.4 Effect of fractionated conventional photon irradiation on *in-vivo* growth of FaDu and A549 tumors

These experiments were performed using FaDu and A549 Brunello libraries. To test whether photon irradiation can inhibit or delay tumor growth, a group of tumors bearing mice (n=10) were irradiated with 13 consecutive fractions of 3 Gy using a vertical photon beam on a clinical linear accelerator (Linac, Siemens Artiste, 6MV). Cumulative dose was 39Gy (Figure 12 a).

A delay in tumor growth could be seen starting 6 days post therapy (FaDu) and after 16 days post therapy (A549). At day 8, average tumor volume of control and photon mice was $1037.16 \pm 218.11 \text{ mm}^3$ and $484.51 \pm 80.21 \text{ mm}^3$ in FaDu model ($p=0.001$). At day 20, average tumor volume of control and photon was $792.98 \pm 327.37 \text{ mm}^3$ and $251 \pm 66.71 \text{ mm}^3$ in A549 model ($p<0.0001$) (Figure 12 b,d).

Median survival of 8 days in non-irradiated mice in FaDu model was increased to 37 days in irradiated mice, in A549 model median survival of control mice was 24 days which was prolonged to 42 days post irradiation. Overall survival increased significantly in both models ($p<0.0001$) (Figure 12 c,e).

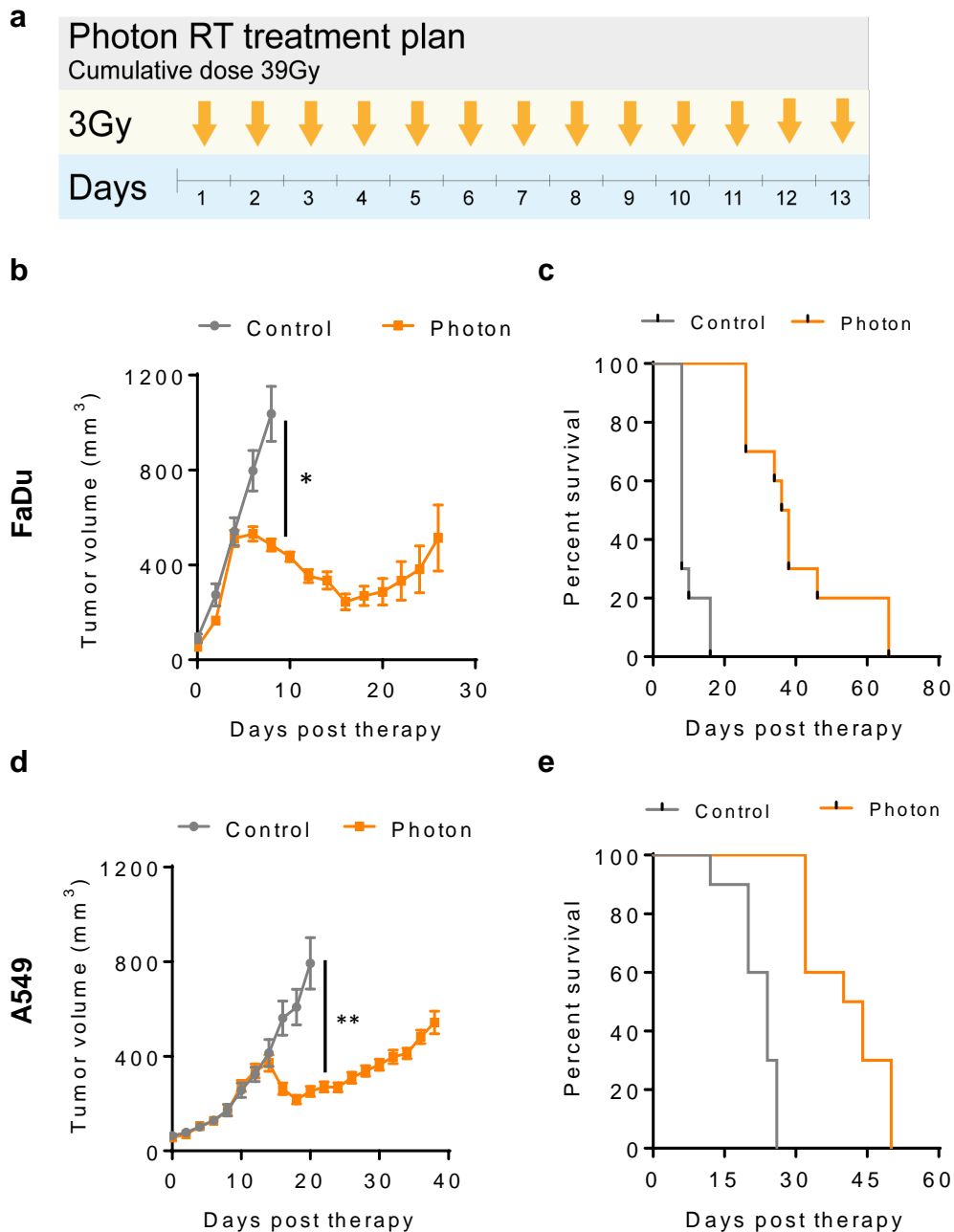


Figure 12. Tumor kinetics in control vs. photon irradiated mice in FaDu and A549 models. a) Photon RT treatment scheme for both models. b,d) Average tumor volumes of control and irradiated FaDu (b) and A549 (d) cohorts over the observation period. Data represents mean \pm SEM, $p=0.001$ (FaDu) and $p<0.0001$ (A549) (t-test). c,e) Kaplan-Meier survival curves for FaDu (c) and A549 (e) cohorts. Median survival in photon irradiated mice was 37 and 42 days in FaDu and A549, respectively. For both, FaDu and A549 tumor models, overall survival was significantly increased in photon irradiated mice compared to non-treated controls, $p<0.0001$ (Log-Rank Mantel-Cox test).

3.5 Tumor growth in particle irradiated FaDu and A549 models

Subsequent experiments examined the effect of novel radiation qualities with gradual increase of LET i.e., irradiation with helium, carbon, and oxygen ions vs. particle therapy reference irradiation with protons. Tumor growth curves representing mean volume of tumors across each group are shown in Figure 13. Tumor growth curves of each individual tumor/mouse are shown in Figure 14. A physical dose of 3 Gy of proton, helium, carbon and oxygen irradiation was applied in 8 consecutive fractions (Figure 13 a).

Average tumor volumes after particle irradiation are shown in Figure 13 b and d up to day 37 (FaDu) and 44 (A549) after therapy where intergroup comparison was meaningful. In both models, the slowest tumor growth was observed in carbon/oxygen groups, followed by helium and proton group. In A549, oxygen treatment led to a stabilization of average tumor volume, whereas for carbon treatment, tumor started re-growing after 30 days, helium and oxygen only showed a transient delay of tumor growth between day 10 and 20. In FaDu, tumor regression following carbon and oxygen RT was observed, whereas a stabilization (days 6-14) followed by increase in tumor size was observed after helium and proton irradiations. Comparison of irradiated mice in FaDu showed significant difference of proton vs. carbon and oxygen ion group, $p < 0.0002$. There were also significant differences between proton and carbon and oxygen ions in A549 model, $p = 0.002$ and $p = 0.0007$ respectively. A trend for enhanced growth delay after helium vs. proton was observed in both models.

Median survival for FaDu model after irradiation with proton and helium was 29 and 33.5 days, respectively. In contrast, a median survival was not reached in mice treated with carbon and oxygen ions, due to the high tumor control rates (>75%). In A549 model, median survival after proton, helium, carbon ion treatment was 42.5, 51 and 94 days respectively. >65% of A549 bearing mice that received oxygen ion treatment were controlled, hence, the median survival was not reached in this group (Figure 13 c,e).

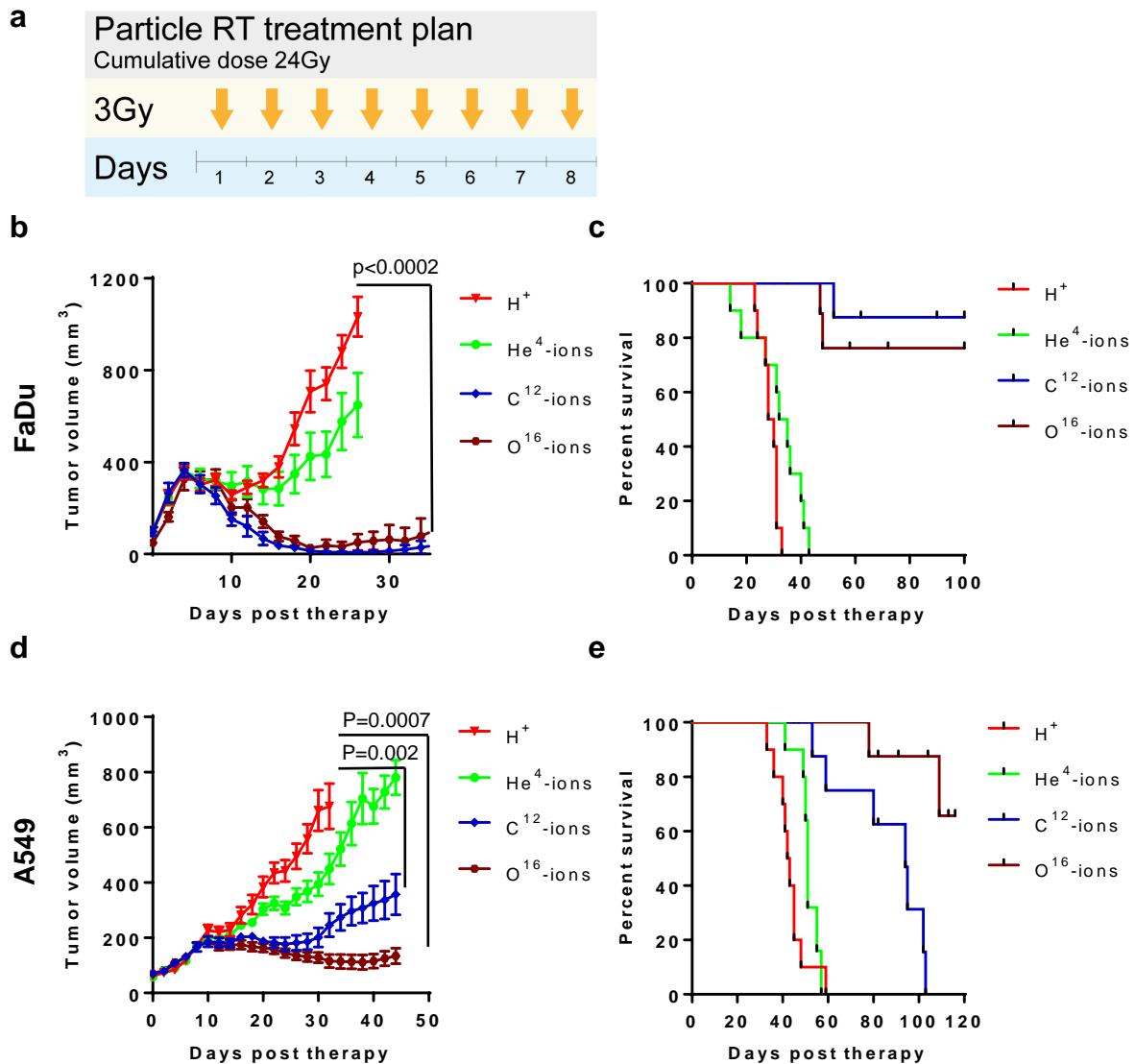


Figure 13. Tumor growth kinetics following particle irradiation in FaDu and A549 models. a) Particle RT application scheme for both models. b,d) Tumor growth kinetics in FaDu (b) and A549 (d) cohorts (average tumor volumes +SEM) after injection are presented. Comparison between irradiated mice in FaDu model show significant differences between proton and carbon ion and oxygen ion, $p=0.0001$. In A549 model there was significant difference between proton and carbon $p=0.002$ and oxygen $p=0.0007$ ion treatments. c,e) Kaplan-Meier survival curves for FaDu (c) and A549 (e) cohorts. Median survival for FaDu model in proton and helium groups was 29 and 33.5 days, respectively, and was not reached in carbon and oxygen ion groups. In A549 model median survival after proton, helium, carbon ion treatment was 42.5, 51, 94 days respectively and was not reached in oxygen group.

To better explore the heterogeneity in tumor growth kinetics over the entire observation period, spaghetti plots are presented. Figure 14 depicts tumor growth fate of each individual mouse after particle RT in FaDu (a) and A549 model (b).

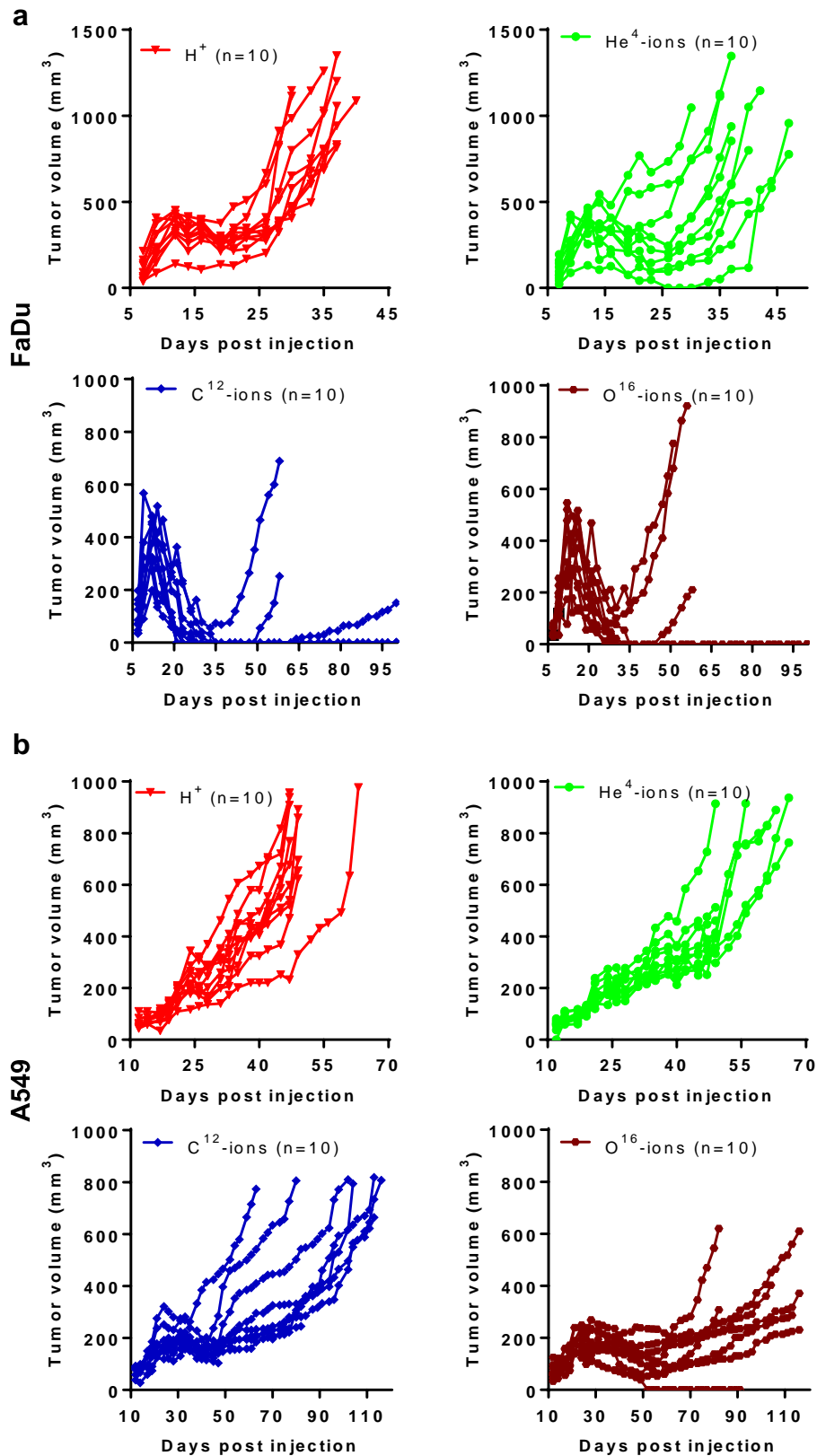


Figure 14. Individual tumor growth kinetics of particle irradiated mice in FaDu and A549 models. Tumor growth of each mouse after irradiation with particles is presented in a) FaDu and b) A549.

3.6 Library complexity decreases as a function of irradiation

It was shown in Figure 11 that the total library complexity in both models decrease with gradual increase of the time to progression (tumor take out) in non-treated control tumors. In addition to time dependent reduction of library complexity, it was aimed to determine the effect of irradiation on library complexity. Both conventional photon irradiation as well as particle irradiation markedly decreased the library complexity (Figure 15).

In FaDu model, tumors irradiated with photons, reduction of library complexity reached 11.3% compared to 50.05% in non-irradiated tumors (t-Test, $p=0.0001$, Figure 15 a). In A549 model, complexity in photon irradiated tumors was 28.6%, whereas non-irradiated control mice showed 38.07% (t-Test, $p=0.07$, Figure 15 b).

The average library complexity in FaDu tumors irradiated with protons was 16.2% and 11% after treatment with helium ions. A trend was observed between these two radiation qualities in terms of library complexity reduction, $p=0.05$ (Figure 15 c). The average library complexity after treatment with carbon ions was 1.27%, and 1.84% after treatment with oxygen ions. This reduction differed significantly in comparison to mice that received proton treatment, $p=0.0007$ and $p=0.002$ respectively (Figure 15 c). A significant gradual decrease of complexity with LET was observed ($p<0.001$, linear model analysis).

The average library complexity in A549 tumors irradiated with protons was 34.22% and 26.1% after treatment with helium ions. There was a trend between these two radiation qualities in terms of library complexity reduction, $p=0.08$ (Figure 15 d). The average library complexity after treatment with carbon ions was 15.2% and 16.01% after treatment with oxygen ions. Comparisons of proton with carbon ions and oxygen ions showed significant differences, $p=0.0004$ and $p=0.0009$ respectively (Figure 15 d). Again a significant gradual decrease of complexity with LET was observed ($p=0.045$, linear model analysis).

Complexity in treated tumors in A549 model was reduced to lesser extent compared to FaDu tumors. This observation is in line with differential tumor growth kinetics in these two tumors in response to the radiation qualities.

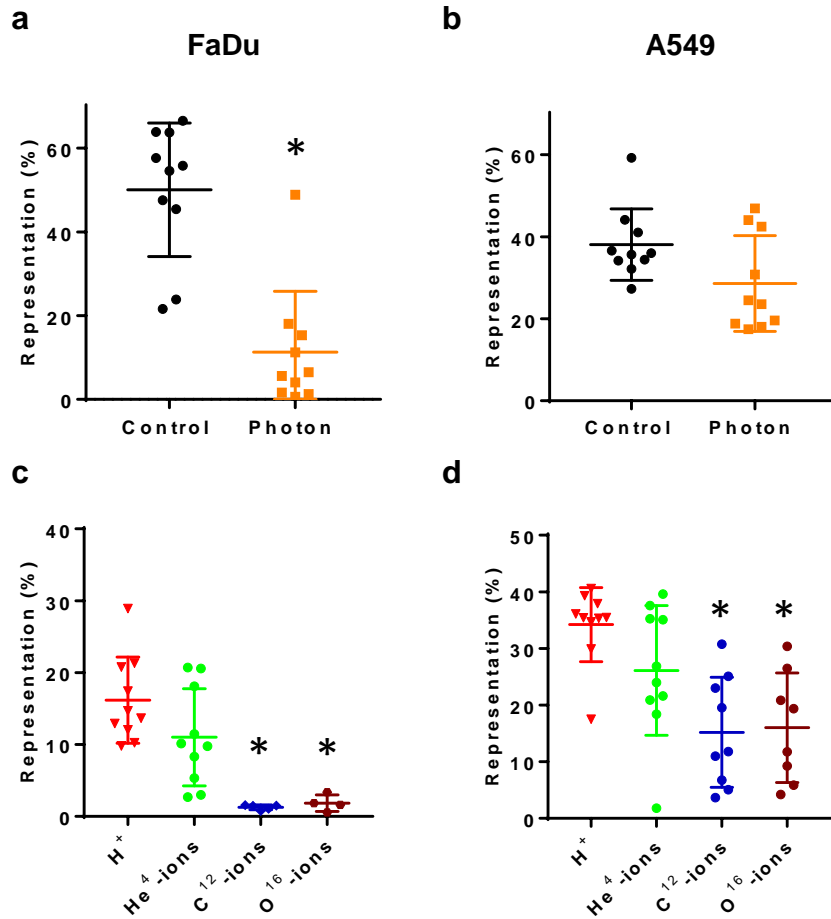


Figure 15. Reduced tumor library complexity after irradiation. a,b) Reduced complexity of FaDu (a) and A549 (b) libraries in mice irradiated with photon irradiation (n=10, per group). It was significantly different in FaDu model (*, p=0.0001) and showed a trend in A549 model (p=0.07). c,d) Gradual decrease of the tumor library complexity in FaDu (c) and A549 (d) libraries, as a function of increased LET of particle irradiation *, p <0.01 for significant reduction in carbon and oxygen irradiated tumors vs. proton (as internal low-LET reference).

3.7 UMAP representation of gene expression for different irradiation qualities

To identify differences in genes and pathways affected by irradiation, transcriptomes of irradiated and non-irradiated tumors using RNA-seq data were analyzed. RNA was extracted from tumors following irradiation with 39Gy (photons) and 24Gy (particles) when tumors reached the sacrifice size.

To examine differential transcriptional perturbations as a function of radiation quality, calculated 2-d UMAPs are presented (Figure 16). Control and photon irradiated samples showed a clear separation in both FaDu and A549 models (Figure 16 a,c).

In FaDu model, the median of proton, helium and oxygen ions treated samples demonstrated a gradual decrease in both dimensions, while carbon ion treated samples showed a stronger distance in the dimension 2 to the rest of the centroids (Figure 16 b). In A549 model, helium treated tumors demonstrated a larger distance compared to the rest of the centroids in UMAP-2 dimension, while UMAP-1 dimension gradually separated proton, helium and the two higher LET carbon and oxygen treated samples (Figure 16 d).

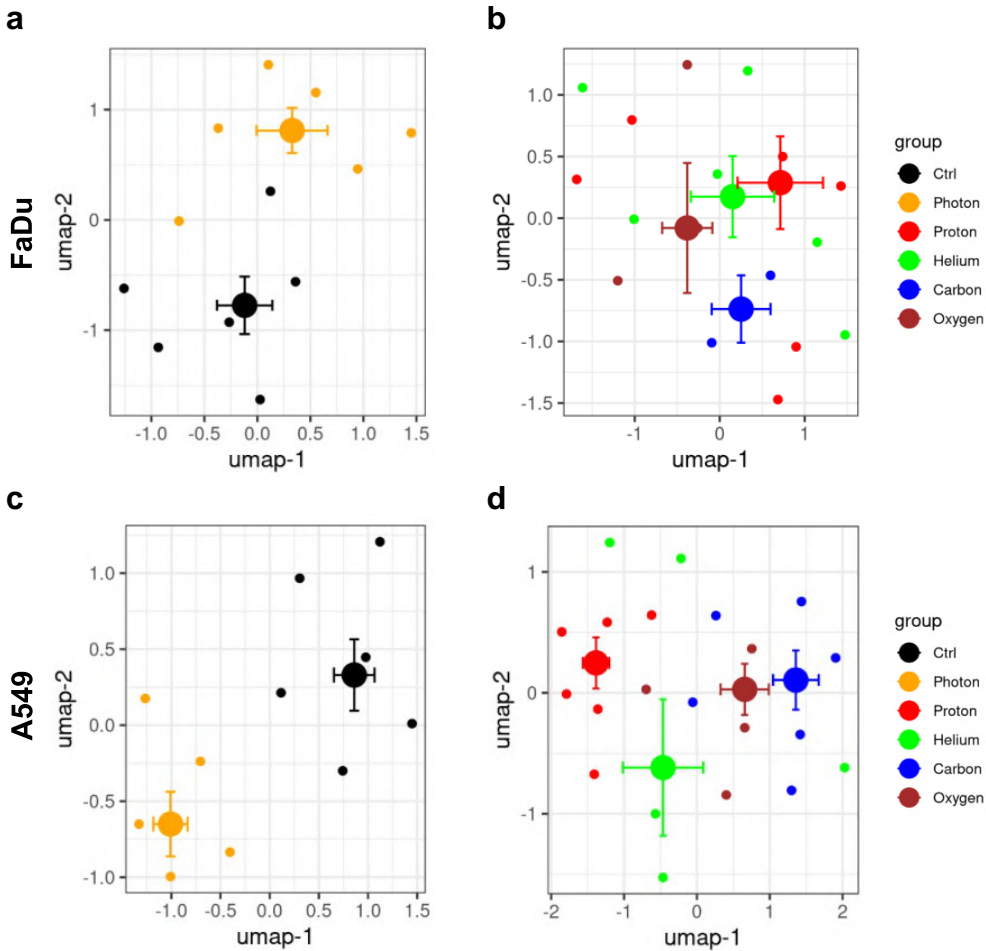


Figure 16. UMAP representation of transcriptional clusters for different radiation qualities in FaDu and A549 tumors. a,b) Comparison of radiation qualities in FaDu model. c,d) Comparison of radiation qualities in A549 model. Calculated per sample set and cell line, the thick dots visualize treatments median and SE for treatment.

3.8 Photon irradiation induced transcriptional regulations

To investigate possible mechanisms leading to resistance after photon therapy, gene expression differences between control and photon irradiation were analyzed with linear model and results were shown as coefficients of photon versus control and Wald-type p-value. Figure 17 a,b shows differences between photon and control samples in FaDu and A549 models, respectively. The labeling of samples in x-axis indicates gene up- or downregulations (black or blue labels, respectively) in photon treated samples versus control. Overall, the number of differentially expressed genes was higher in A549 model: 3848 genes (non-adjusted $p < 0.05$) and 236 genes (Benjamini-Hochberg, $FDR < 0.05$). In FaDu model, the number of differentially expressed genes was 3451 (non-adjusted $p < 0.05$) and 34 (Benjamini-Hochberg, $FDR < 0.05$). No overlaps between both models were detected for gene candidates selected with p value adjustment (Benjamini-Hochberg, $FDR < 0.05$).

In FaDu model, examples of upregulated genes after photon radiation include several genes modulating immune response e.g., Peptidoglycan Recognition Protein 4 (PGLYRP4), S100 Calcium Binding Protein A12 (S100A12), C-X-C motif chemokine ligand 14 (CXCL14) and Purinergic Receptor P2X 7 (P2RX7). Other upregulated genes included Interleukin 32 (IL32), which has been shown to modulate tumor microenvironment (Yan et al., 2018), peptidase inhibitor Serpin family B member 11 (SERPINB11), chromatin remodeling component SWI/SNF related matrix associated actin dependent regulator of chromatin subfamily member 2 (SMARCA2) and Podoplanin (PDPN), which has been shown to have diverse roles in the malignant progression of tumors (Kato et al., 2022).

Proposed negative prognostic biomarker for HNSCC (Feng et al., 2021), RUNX Family Transcription Factor 1 (RUNX1), DNA damage repair component Fanconi anemia complementation group M (FANCM) and a proposed tumor suppressor Semaphorin 3B (SEMA3B) were downregulated after photon radiation.

In A549 model, several upregulated genes with the roles in tumor growth and proliferation were found, such as Fucosyltransferase 6 (FUT6), Lumican (LUM), Metastasis-associated in colon cancer-1 (MACC1), Tetraspanin 1 and 8 (TSPAN1 and TSPAN8) and cAMP-dependent protein kinase inhibitor- β (PKIB). Calcium Voltage-

Gated Channel Auxiliary Subunit Alpha2delta3 (CACNA2D3) and Bcl2 Modifying Factor (BMF) genes, both of which are associated with apoptosis (Nie et al., 2019; Pinon et al., 2008), were downregulated in photon irradiated tumors.

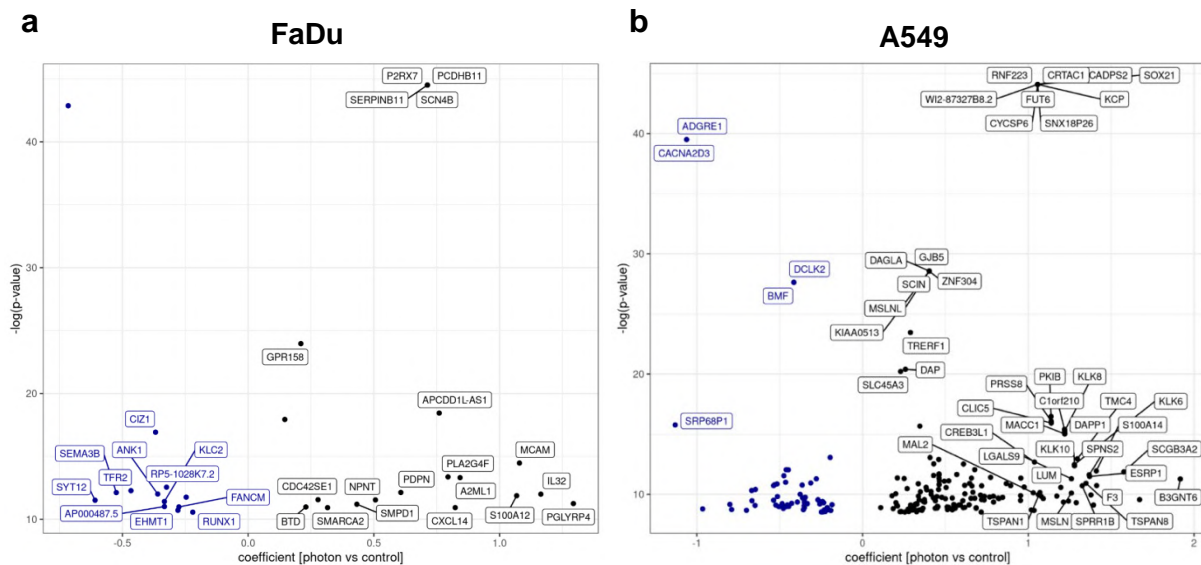


Figure 17. Differential gene-expression in photon irradiated vs. control tumors. Black labeled dots (right side), correspond to radiation upregulated vs. blue labeled dots (left side) correspond to radiation downregulated genes compared to control. To avoid gene-name overlap not all dots are labeled with gene-names. Only significantly regulated genes with FDR < 0.05 are shown in these volcano plots. FaDu (a) and A549 (b) models.

In order to functionally annotate the differentially regulated genes between photon and control samples, KEGG pathway analysis (Figure 18) was performed in both models. First, genes from differential gene expression (photon vs ctrl, linear model analysis, non-adjusted p-value < 0.05), in A549, in FaDu, and genes differentially regulated in both model (intersect), were analyzed in KEGG Pathway per geneset (A549, FaDu, intersect), separately for up- and downregulated genes. Significantly enriched pathways (non-adjusted p-value < 0.05) were selected and identified genes were displayed in Venn Diagram (Figure 18 a,c). Corresponding heatmaps (Figure 18 b,d) (completelinkage, Euclidean distance) show genes detected in all KEGG enrichment analyses.

Different DNA repair pathways as nucleotide excision repair, base excision repair and Fanconi anemia pathway were identified (downregulated after photon irradiation), as well as immune pathways, such as antigen processing and presentation, Graft-vs-host disease and Allograft rejection pathways (upregulated after photon irradiation).

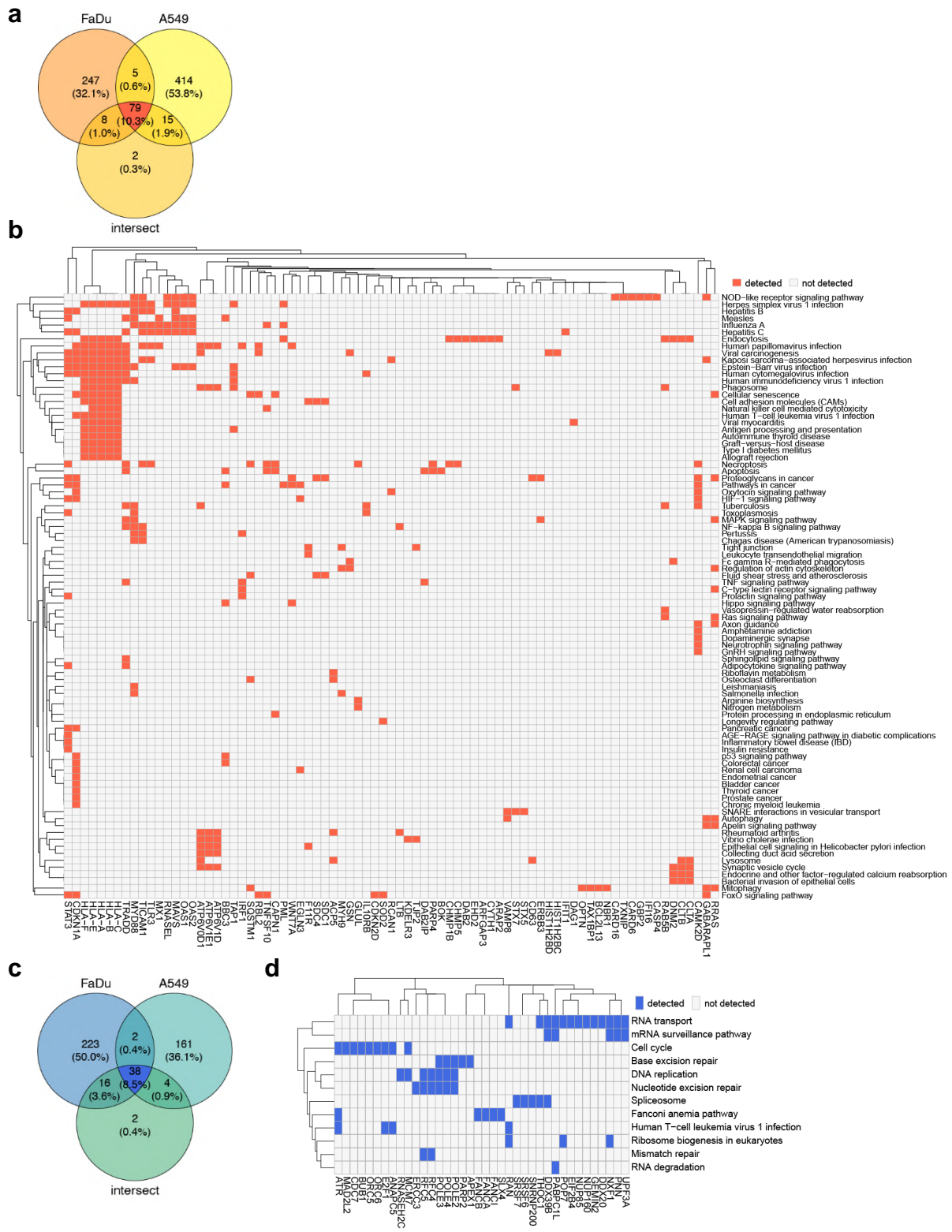


Figure 18. Pathway enrichment for common differentially regulated genes in both tumor models. a) Genes identified from enriched KEGG pathway analysis upregulated after photon irradiation vs. ctrl in both tumor models, intersect genes (n=79) are labeled in red color. b) Heatmap of n=79 intersect genes shows clusters of genes associated with immune activation pathways (left side, pathways related to viral infections, antigen presentation and immune processes). Enriched KEGG pathways are shown, non-adjusted p-value < 0.05. c) Genes identified from enriched KEGG pathway analysis downregulated in photon vs. ctrl treated

samples, intersect genes (n=38) are labeled in blue color. d) Heatmap of n=38 intersect genes and identified KEGG pathways, non-adjusted p-value < 0.05. Genes associated with DNA-Damage Response pathways are clustering together.

3.9 Linear Energy Transfer (LET) dependent alterations of gene expression

After analyzing differences between photon irradiation and control samples in section 3.8, particle treated samples were evaluated by performing gene expression associations with LET, using ordinary least squares (OLS) linear model analysis. Four particle irradiation qualities were used for treatment of tumors with the dose average LETd of ~4.5, 18, 80 and 120 keV/μm for proton, helium, carbon, and oxygen ions, respectively (see also materials and methods). In A549, 98 genes were identified after Bonferroni p-value adjustment (p<0.05) (Table 7). In A549 and FaDu, 1016 and 2 genes, respectively, were identified with FDR<0.05 (Benjamini-Hochberg). There were 303 common genes between two models with non-adjusted p<0.05.

The stringently selected 98 genes associated with LET in A549 model showed a gradual expression trend from proton to helium, carbon and oxygen (Figure 19 a). KEGG pathway analysis of these 98 genes (Figure 19 b) identified immune associated pathways and Nuclear factor kappa B (NF-κB) signaling to be significantly enriched in irradiated A549 model as a function of LET. Gene set enrichment analysis confirmed the LET dependent regulation of these genes also in FaDu model (Figure 19 c).

Table 7. Association of gene expression with LET in A549 and FaDu

Selection	A549	FaDu	Intersect
pBonf < 0.05	N=98	N=0	
FDR < 0.05	N=1016	N=2	
p < 0.05	N=4551	N=1892	N=303

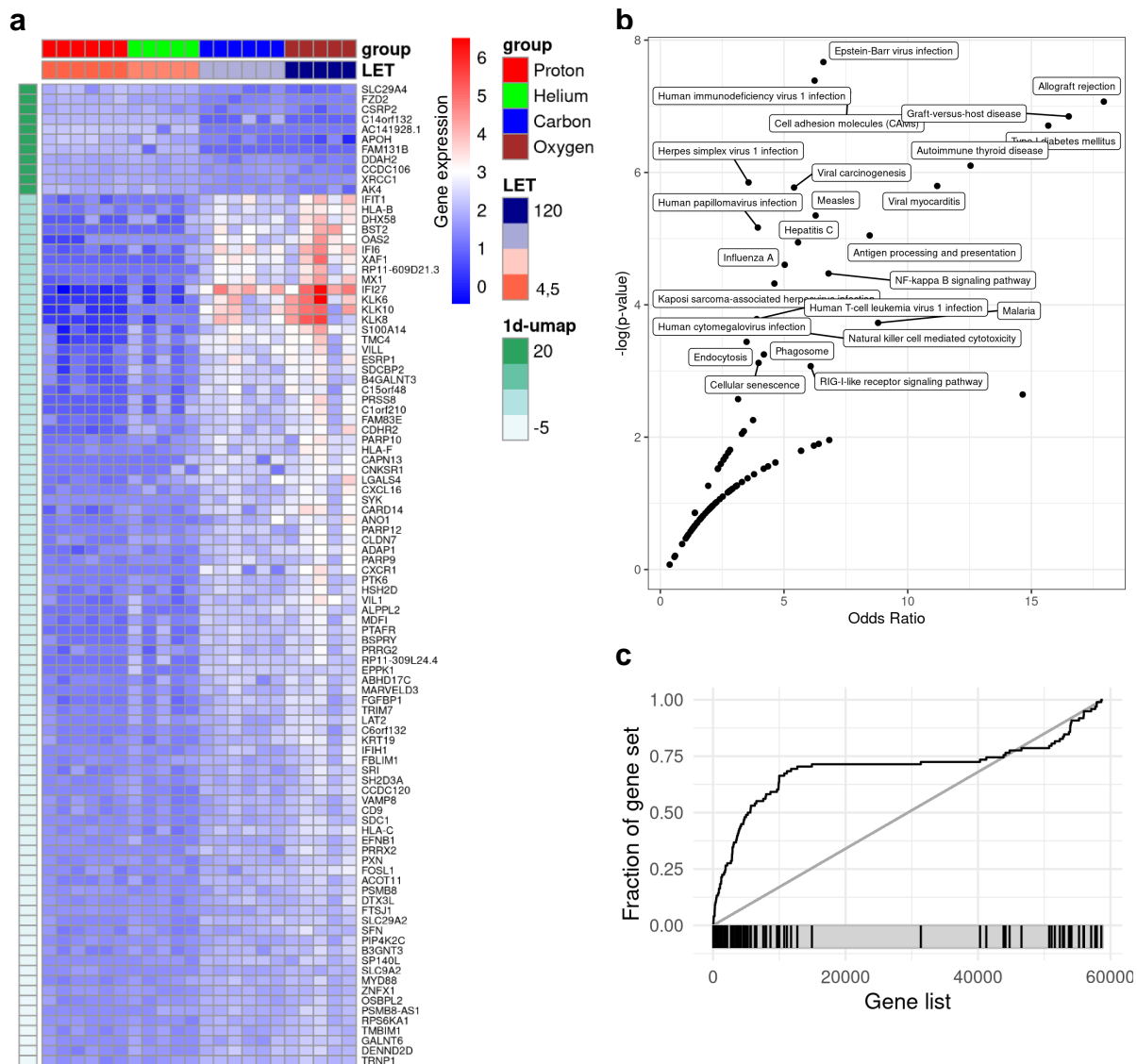


Figure 19. Gene expression association with LET in FaDu and A549 models. a) A549 ~LET heatmap: $n=98$ genes, $p_{Bonf} < 0.05$, linear model analysis, ordered by 1d umap (Euclidean distance). b) KEGG pathway enrichment in A549 model ($n=98$ genes), no p-value adjustment. Gradual LET dependent increase of genes associated immune signaling processes (HLAs, interferon response, MX1, etc.) matches well with enrichment of pathways found to be related to immune response e.g. viral infection, autoimmune and transplantation immunology (d) Enrichment analysis of $n=98$ geneset in FaDu model (linear model analysis for LET dependent differences, $p < 0.001$).

More relaxed selection criteria ($p < 0.05$) identified 303 genes commonly associated with LET in FaDu and A549 models (Table 7) and was visualized as volcano plot (Figure 20). The labeling of samples in x-axis indicates degree of regulation depending on LET (positive or negative association with LET, black or blue labels, respectively), coefficient indicates the degree of regulation (mean difference between groups).

In FaDu model (Figure 20 a), transcription factors Signal transducer and activator of transcription 1 (STAT1) and Signal transducer and activator of transcription 3 (STAT3), both of which have oncogenic or oncosuppressive roles (Verhoeven et al., 2020; Yu et al., 2009), were upregulated in samples irradiated with high LET, as well as enzyme Adenosine deaminase RNA specific (ADAR) that has a role in immune silencing in tumors (Bhate et al., 2019).

In A549, model (Figure 20 b), STAT1 was also upregulated in high LET samples, as well as proapoptotic tumor suppressor XIAP Associated Factor 1 (XAF1) (Zhu et al., 2014).

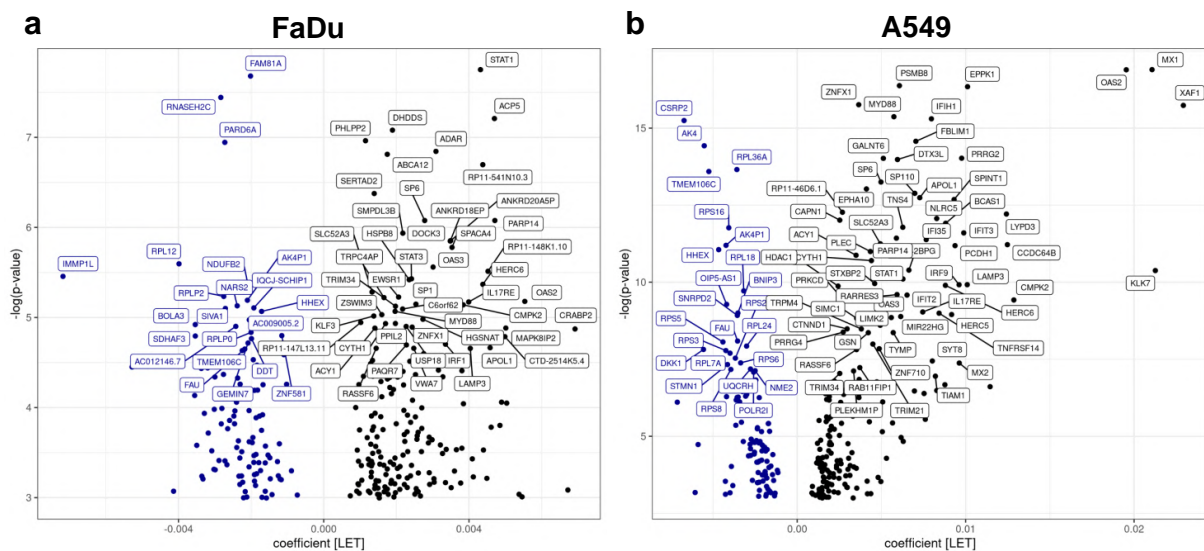


Figure 20. Genes commonly associated with LET in FaDu and A549 models. a,b) Genes regulated in FaDu and A549 and models respectively (non-adjusted $p < 0.05$, $n = 303$). FaDu: Genes with $p < 0.01$ are labeled, A549: Genes with $p < 0.001$ are labeled.

3.10 Guide RNA abundance analyses

The data in paragraphs 3.11 – 3.16 represents gRNA abundance and its relation with treatments and the analysis is described in detail in Materials and Methods in section 2.2.15. Briefly, genes were first aggregated per sample, following aggregation per treatment. Due to the high selection pressure and consequently low number of guides which were detected in carbon and oxygen ion treated tumors and since one of the main aspects of the analysis was to compare the differences between high and low LET irradiation effects, genes that were detected in any carbon and oxygen ion treated

samples were used for further analyses. This resulted in 1331 genes in FaDu model, 18686 genes in A549 model and 1328 intersect genes. Imputation of missing data was performed to replace missing reads of the genes that were detected in carbon and oxygen treated groups but not in the other groups. Imputed data matrices (calculated using the data of genes aggregated per sample) were used to visualize differences between control and irradiated tumors, and associations with LET.

3.11 UMAP representation of gRNA data in FaDu and A549

In order to assess similarities between irradiation qualities on gRNA level, UMAP representation of rank transformed gene level aggregated guide data was computed (Figure 21). Control and photon irradiated samples showed a separation in FaDu model but clustered mostly together in A549 model (Figure 21 a,c). In LET samples, helium and photon clustered together and the two high LET (carbon and oxygen ions) samples clustered together (Figure 21 b,d). Thus, a LET dependent organization could be detected in both models on gRNA level. Of note, the positioning of the photon samples might be related to the higher cumulative prescribed dose (39Gy) compared to particle irradiation (24Gy).

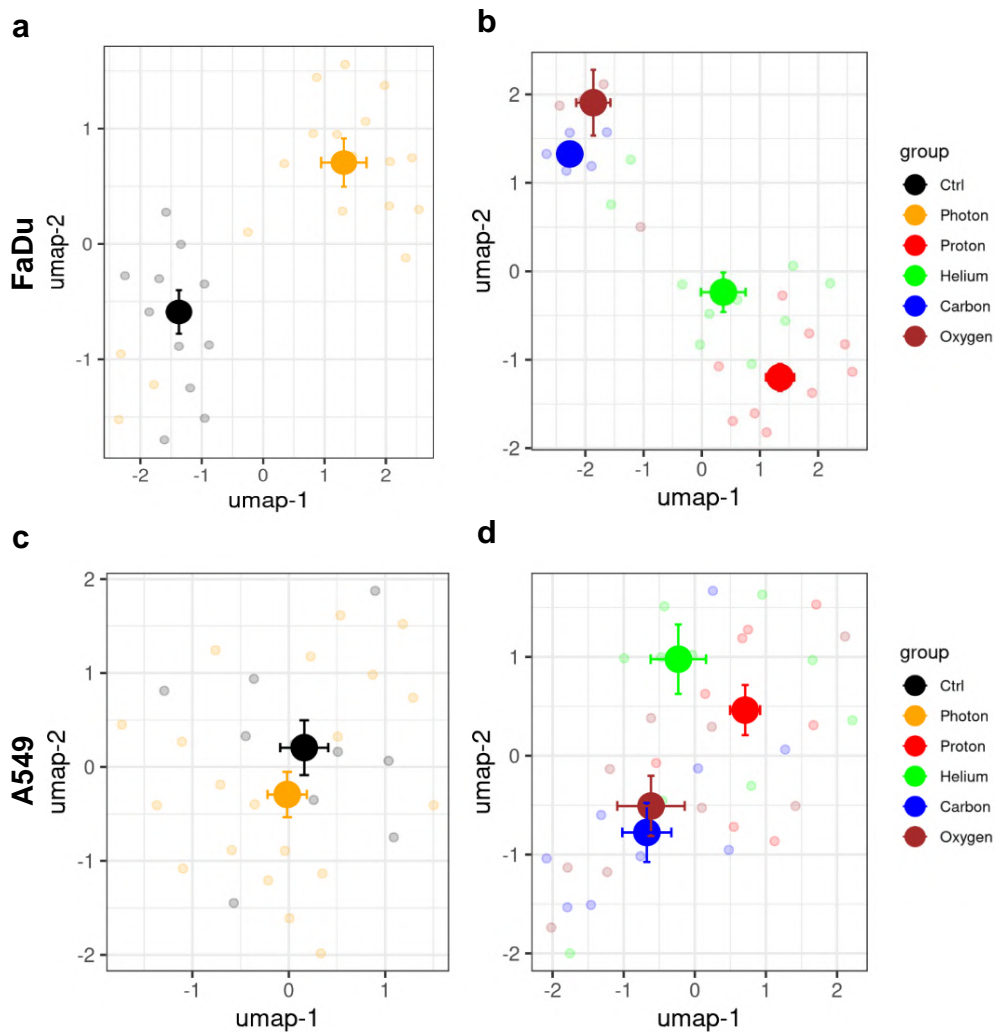


Figure 21. UMAP representation of rank transformed gene aggregated (maximum value) guide data. a,b) Comparison of radiation qualities in FaDu model. c,d) Comparison of radiation qualities in A549 model. Thick dots visualize treatments median and SE for treatment. Data were imputed with the mice R package.

3.12 Genes with higher gRNA abundance in photon irradiated vs. control FaDu tumors

Differently abundant genes between control and photon treatments in FaDu model were analyzed. Top 5% most abundant gRNA after photon irradiation, showing a larger difference between groups (effect size), are depicted and labeled (Figure 22 a). Imputed ranks (n=100) for selected genes are shown (direct ranks), genes with higher gRNA abundance are ranked higher.

TGF- β signaling pathway growth factor Bone Morphogenetic Protein 8a (BMP8A) and histone demethylase Lysine Demethylase 5C (KDM5C) are representatively shown (Figure 22 a lower panel). These genes were more frequently detected on gRNA level in photon treated tumors in comparison to untreated control tumors, reminiscent of the expansion of gRNA harboring clones in photon treated tumors.

KEGG pathway analysis (Figure 22 b) identified a number of cell signaling pathways (MAPK and p53 signaling pathways), DNA base excision repair pathway, ATP-binding cassette transporters (ABC transporters) and Folate biosynthesis.

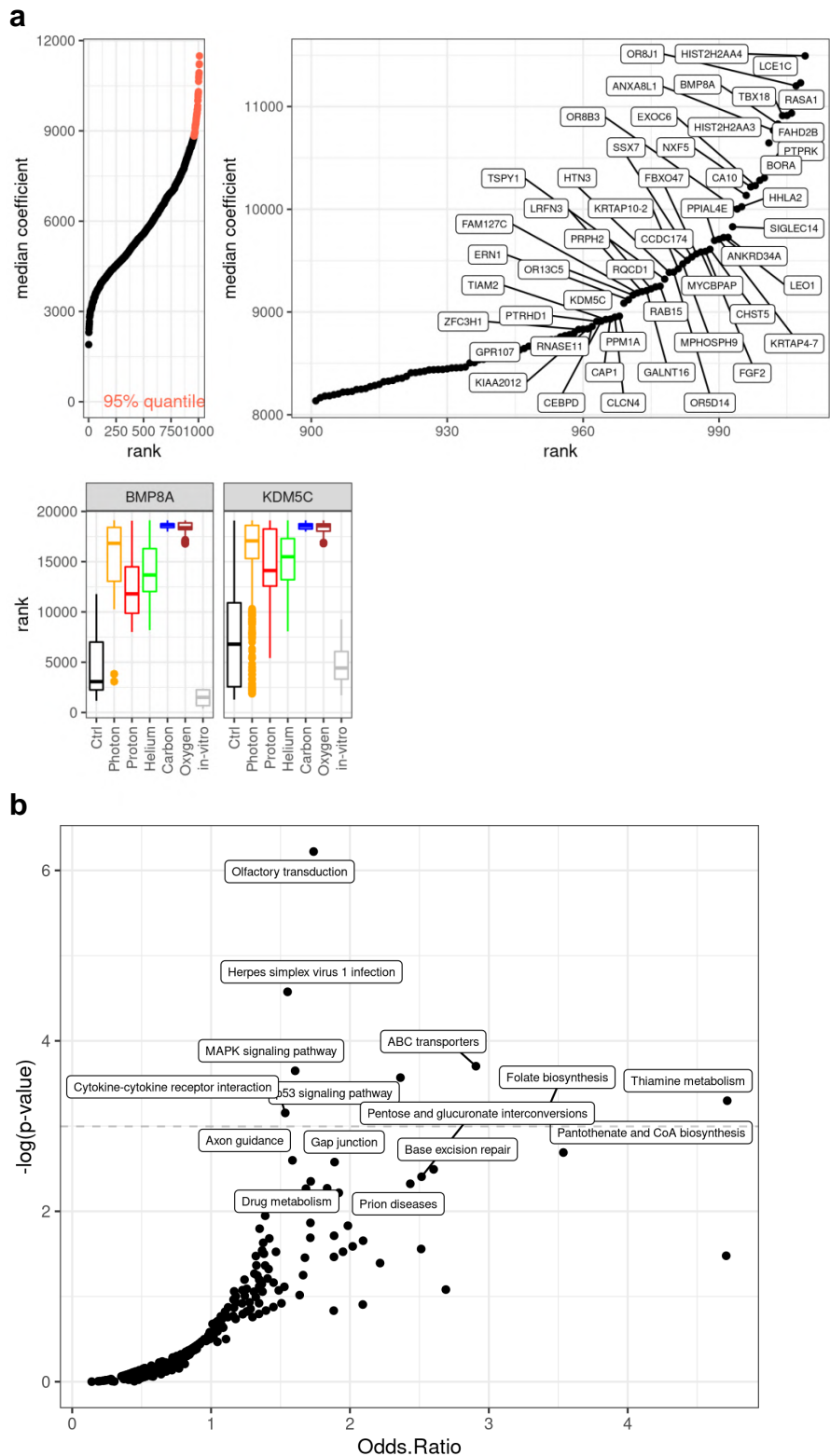


Figure 22. Increased gRNA abundance in photon treatments vs control FaDu tumors. a) Linear model analysis derived effects between control and photon treated rank transformed data with FDR < 0.05, median aggregated and sorted for n=100 imputed datasets. Top 5% genes are colored (left) and labeled. The two key comparative groups (bold), additional groups are shown to illustrate relative enrichment being specific to photon treatment, *in-vivo* condition or also observed irrespective to radiation quality utilized. b) KEGG pathway analysis of all

identified genes in A (n=1009), non-adjusted pathway enrichment p-value. Dashed line: $p=0.05$, terms with $p<0.1$ are labeled.

3.13 Genes with higher gRNA abundance in photon irradiated vs. control A549 tumors

The analysis described in previous section was applied to A549 model. Top 5% ranked gRNA targeted genes such as Mitochondrial malate dehydrogenase 2 (MDH2), Matrix metalloproteinase-19 (MMP19) and an extracellular matrix protein Tenascin C (TNC), which are highly expressed in most solid tumors and plays a role in tumor angiogenesis and metastasis (Kwa et al., 2019). All the gRNA mentioned were more frequently detected in photon treated tumors in comparison to untreated control tumors (Figure 23 a).

KEGG pathway analysis (Figure 23 b) results revealed some pathways which were related to cancers like melanoma, hepatocellular carcinoma and endometrial cancer, p53, VEGF signaling pathways and citrate cycle (TCA).

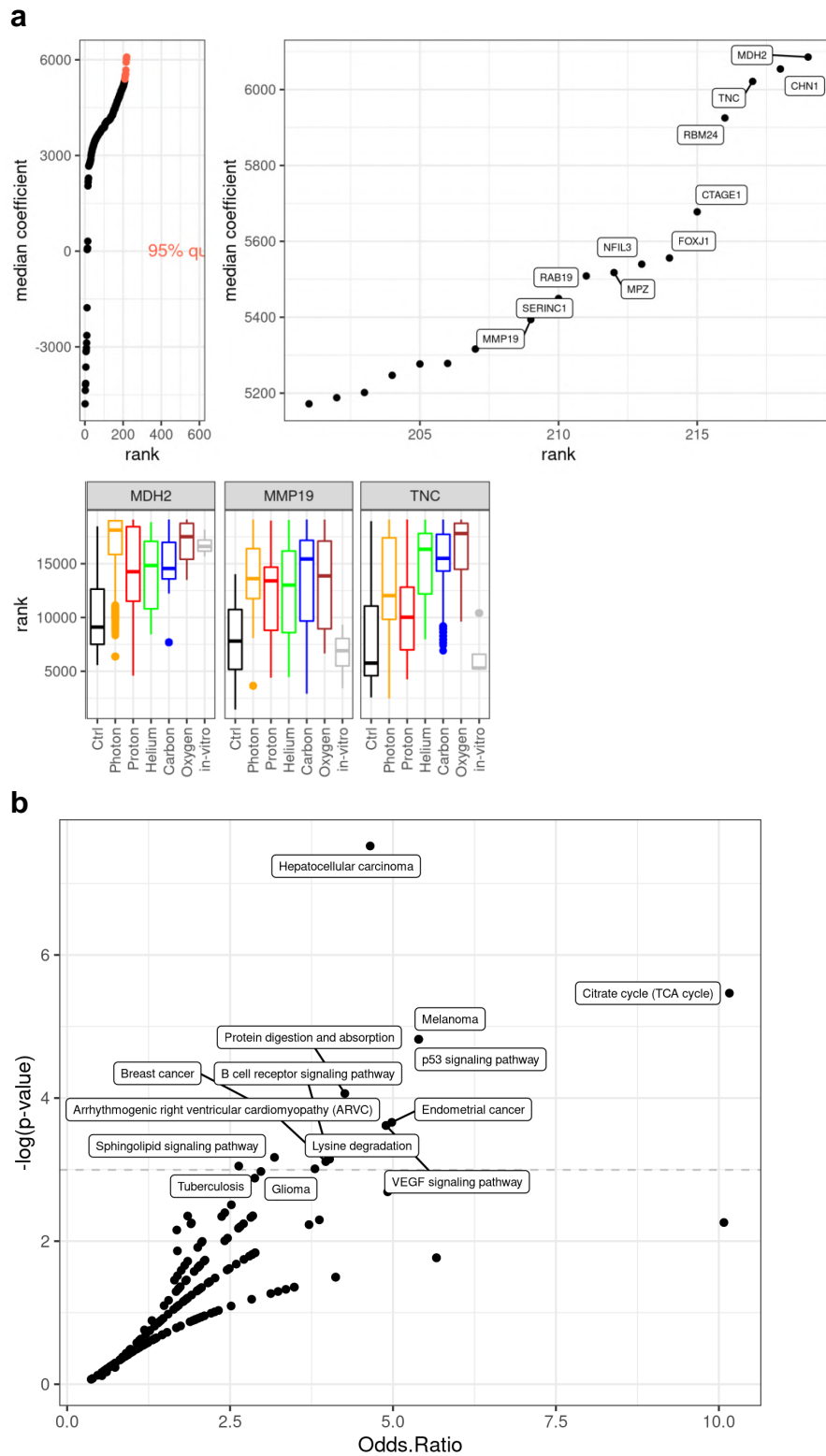


Figure 23. Genes showing relative guide abundance differences between control and photon treatments in A549 model. a) Linear model analysis, non-adjusted p-value < 0.05. Imputation of missing data (n=100). b) KEGG pathway analysis, non-adjusted p-value, dashed line: p=0.05.

3.14 Genes showing relative guide abundance association with LET in FaDu model

After comparing guide abundance differences between control and photon irradiated tumors, guide abundance association with LET was analyzed to identify differences between ionizing high and low LET radiation qualities. Top 5% of genes associated with LET are shown in Figure 24 a.

Some of the highlighted genes (Figure 24 a lower panel) included BMP8A, angiogenic factor Fibroblast growth Factor 2 (FGF2) and tumor suppressor TSC Complex Subunit 1 (TSC1). Interestingly, BMP8A was also detected in photon irradiated samples.

KEGG pathway analysis (Figure 24 b) with identified pathways that are involved in fundamental cellular processes (phospholipase D signaling pathway, Glycosphingolipid biosynthesis) and intercellular communication (Gap junction) and p53 signaling pathway.

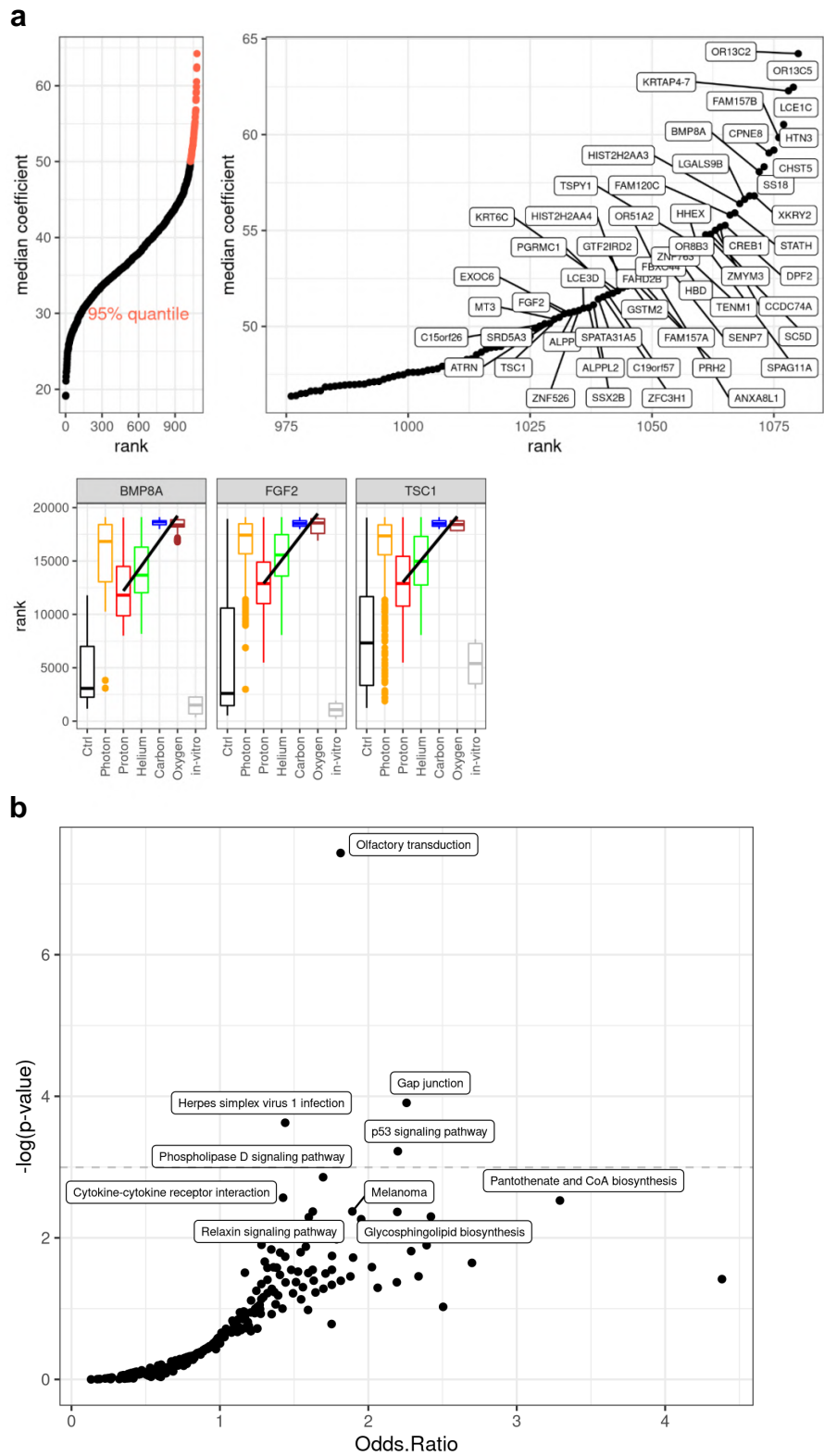


Figure 24. Genes showing relative guide abundance association with LET in FaDu model. a) Linear model analysis, FDR < 0.05. Imputation of missing data (n=100). b) KEGG pathway analysis (non-adjusted p-value). Dashed line: $p=0.05$, terms with $p<0.1$ are labeled.

3.15 Genes showing relative guide abundance association with LET in A549 model

As described in section 3.10, 1328 reference genes in A549 model were analyzed to show guide abundance association with LET. Top associated genes with LET are shown in Figure 25 a.

With $p < 0.05$ value, apoptosis regulating genes BCL2 Associated Agonist of Cell Death (BAD) and BCL2 Interacting Protein 3 (BNIP3) genes were among the significant genes (Figure 25 a lower panel). For more restricted selection of genes, the p value was increased to < 0.001 (Figure 25 b), and interestingly, TGF- β family genes, TGF- β Receptor 1 (TGFB1) and 2 (TGFB2) were detected. AT-rich Interaction Domain 2 (ARID2), another highlighted gene, is a putative tumor suppressor in lung cancer (Moreno et al., 2021).

KEGG pathway analysis (Figure 26) identified differently regulated pathways like as ErbB, MAPK, NF- κ B, Ras, cellular senescence and p53 signaling pathway.

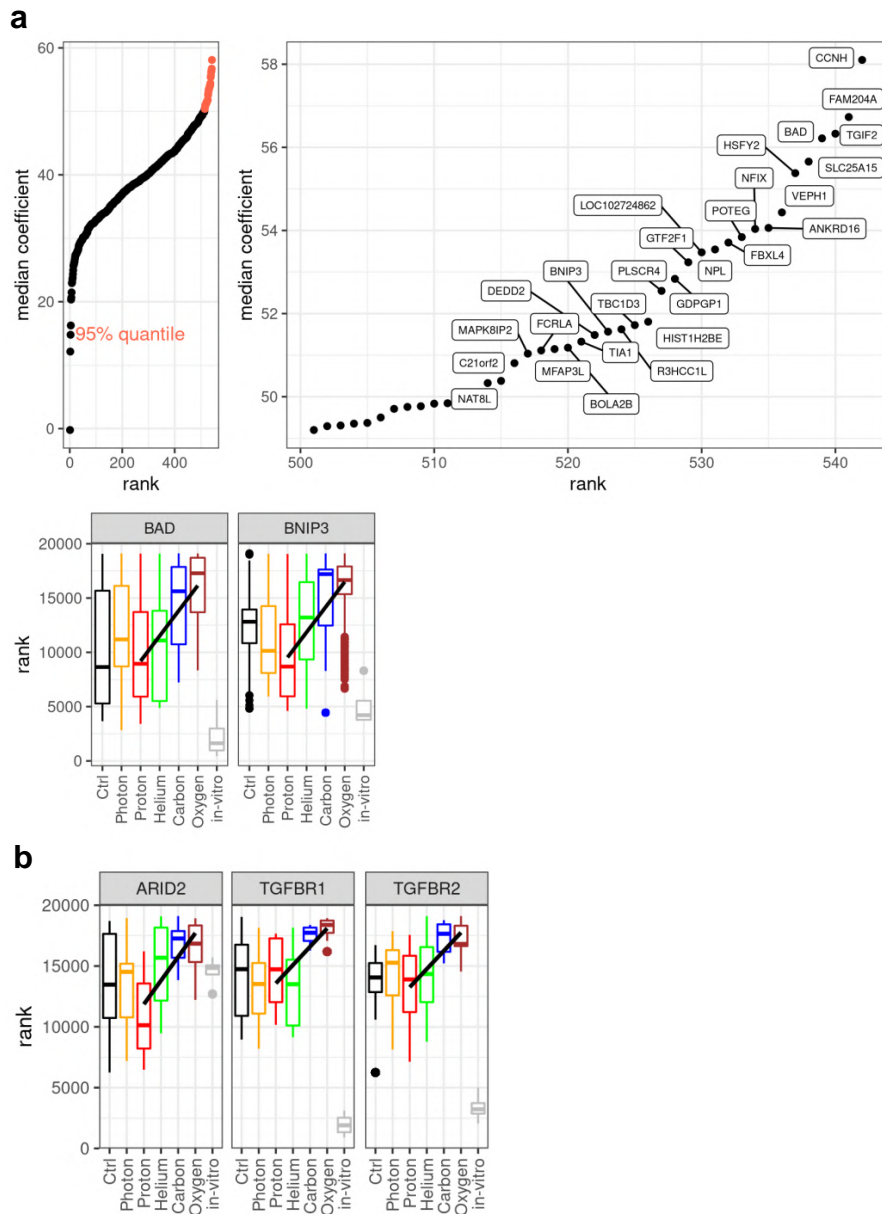


Figure 25. Genes showing relative guide abundance association with LET in A549 model. a, b) Linear model analysis, non-adjusted p-value < 0.05 and < 0.001, respectively. Imputation of missing data (n=100).

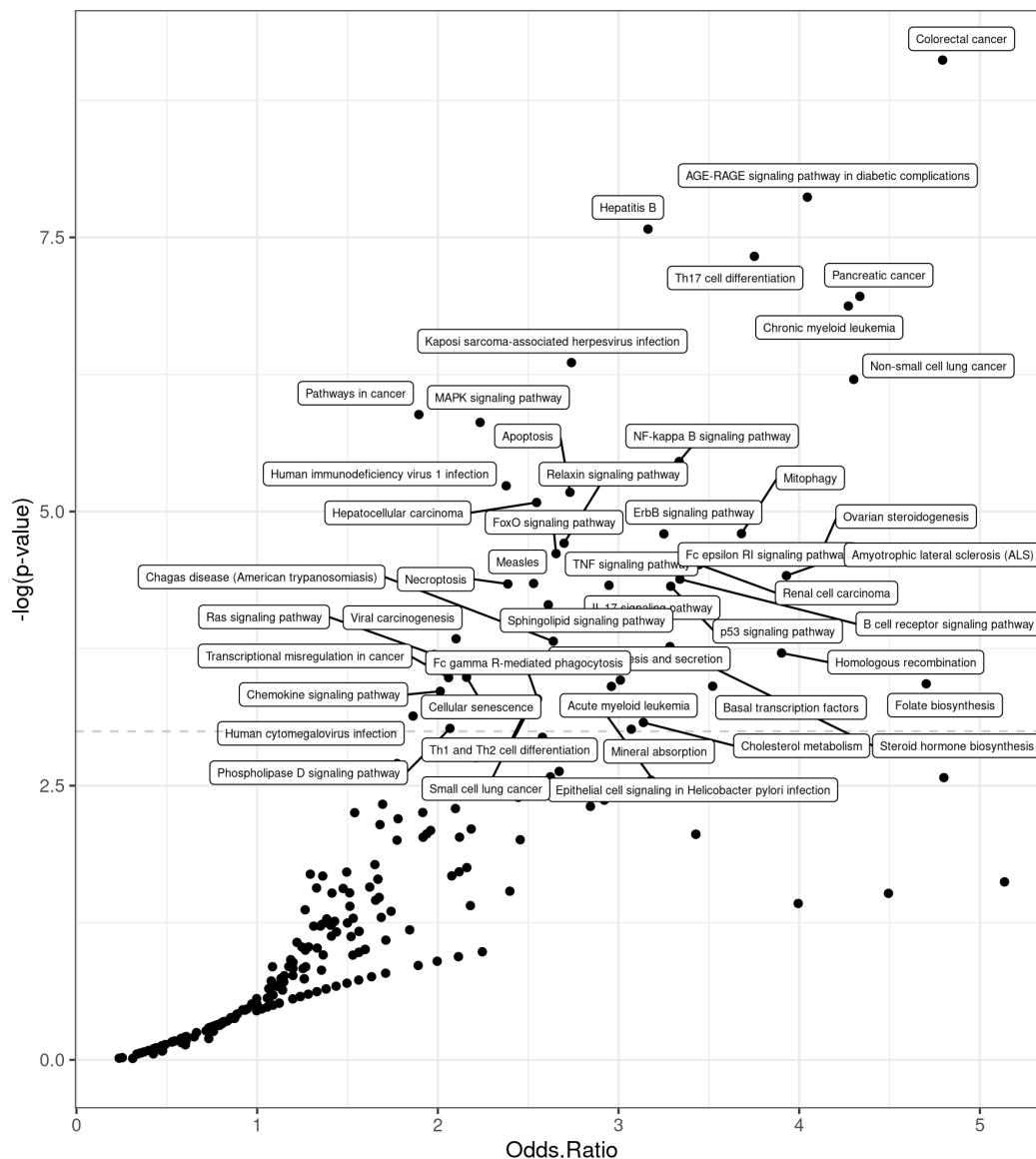


Figure 26. Genes showing relative guide abundance association with LET in A549 model. KEGG pathway analysis (non-adjusted p-value).

3.16 Guide abundance differences between control and treated tumors and regulation on gene expression level

In previous sections, gene expression data by RNAseq (Sections 3.7 - 3.9) and gRNA abundance data (Sections 3.11 - 3.15) in tumors after different radiation treatments was analyzed. In the following section, both results were combined in order to verify the correlation between RNA expression and guide abundance levels. The genes that intersect in FaDu and A549 models are presented in Table 8 and Table 9, respectively.

Highlighted genes for FaDu model include DNA- and RNA-binding protein Far upstream element binding protein 1 (FUBP1) and Tumor necrosis factor receptor associated protein 1 (TRAP1), both of which have been described to have either oncogenic or oncosuppressive roles (Debaize & Troadec, 2019; Matassa et al., 2018), tumor suppressor Hematopoietically expressed homeobox (HHEX), WD repeat domain 5 (WDR5), which recruits an oncoprotein MYC to chromatin (Thomas et al., 2019) and Serine/Arginine-Rich Splicing Factor Kinase 1 (SRPK1), which is implicated in various oncogenic signaling pathways (Nikas et al., 2019). RUNX1 was downregulated in FaDu model and CACNA2D3 was downregulated in A549 model after photon radiation (see Chapter 3.8).

Table 8. Regulated genes in FaDu model

ACADM	AGO2	ALKBH2	ALPP	ANXA10	ATE1	ATP5F1
C10orf2	C11orf86	C3orf62	CARM1	CCDC169	CD55	CDK16
CDK5RAP2	DGKE	DLST	DNAH14	DPF2	DUSP2	EPCAM
EPHA6	ESPL1	FAHD2B	FAM175B	FAM213A	FUBP1	GCLM
HHEX	ITGAX	KAT2A	LYPD1	METTL15	MKLN1	MPHOSPH9
MUTYH	PCOLCE	PGAM5	PNMA6A	PNN	RABEP1	RAPGEF5
RCE1	RPIA	RQCD1	RRP8	RUNX1	SEC24C	SLFN11
SRPK1	SYT12	TRAP1	TTL	USP11	WDR5	ZNF473

Table 9. Regulated genes of A549 model

ACOT2	AMH	C16orf45	CACNA2D3	FAM58A	GJA1	NASP
PIR	PSIP1	RASSF9	TIMP4	WBP1	ZNF573	

4. Discussion

CRISPR/Cas9 screens are a versatile tool to study genetic alterations, often performed as loss-of-function screens. Several genome-wide libraries are available, differing in their guide RNA composition (number of targeted genes and number of guides per gene), which allow assessment of complex genetic perturbations. Increasingly, *in-vivo* CRISPR/Cas9 screens are performed (Doench, 2018; Ghosh et al., 2019; Shi et al., 2022; Winters et al., 2018) as they reflect better the complex interactions between tumor and its microenvironment i.e., oxygen gradient, tumor microvessel interface, communication with stroma cells like carcinoma associated fibroblasts (CAFs) and innate immune cells among others. Compared to human tumors, human tumor cell lines represent a lower intratumoral genetic heterogeneity. Therefore, addition of functional loss of one gene per cell using the CRISPR/Cas9 gene editing technology offers a novel venue to assess engineered genetic heterogeneity and its impact against defined *in-vivo* selection pressures. In addition to standard radiotherapy, the *in-vivo* selection pressures induced by a broad spectrum of novel radiation qualities were studied in this thesis. Despite using the immunocompromised nude mouse host microenvironment innate immune cells as well as natural killer cells are present in these prototypic xenograft models. Therefore, not the full but a partial spectrum of radiation induced tumor immune response e.g. effects on innate immune cells like tumor associated macrophages (TAM, incl. M1/2 polarization) could be addressed in these models.

Particle irradiation confers novel treatment modalities with specific biophysical properties. A highly precise and dose deposition makes it a versatile tool for treatment in the direct vicinity of high-risk organs by achieving a steep dose gradient and sparing adjacent healthy tissue (Rackwitz & Debus, 2019). Available particle irradiation modalities with increasing LET at Heidelberg Ion Beam Therapy Center (HIT), utilized in this study – are proton, helium, carbon and oxygen particles.

Biological effects of particle treatment differ from conventional photon therapy, e.g., direct interaction of heavy charged particles with DNA backbone leading to complex clustered and unreparable damage is elicited also under lack of oxygen presence in hypoxic tumor regions (Tinganelli et al., 2015). In contrast, DNA-damage and cell killing

by conventional photon irradiation is highly dependent on the presence of oxygen (OER effect). It has been shown that irradiation with carbon particles induces favorable alterations in glioma model by influencing the niche toward an antiangiogenic and less immunosuppressive state and eradicating tumor stem cells (Chiblak et al., 2019), and the first clinical data show benefits of carbon irradiation in high grade glioma (Eberle et al., 2020). Nevertheless, despite rapidly growing use of accelerated charged particles in cancer treatment worldwide, tumors can still inevitably recur after irradiation, even if therapy efficacy might be improved as compared to conventional photon radiotherapy. Regardless of the various efforts to overcome radioresistance, the mechanisms behind it are still not fully understood (Konings et al., 2020).

In this thesis, whole-genome CRISPR/Cas9 screens in preclinical *in-vivo* cancer models were performed to study the following questions:

1. How does CRISPR library composition change between *in-vitro* and *in-vivo* conditions considering tumor microenvironment selection pressure?
2. What is the effect of long term fractionated standard photon irradiation and particle therapy consisting of proton, helium, carbon, and oxygen ions *in-vivo*?
3. How does CRISPR library complexity change as the function of standard photon irradiation and particle therapy *in-vivo*?
4. Which genes and pathways promote radio-sensitivity and resistance to photon and particle therapy?
5. What is the transcriptional response in relapsed tumors after photon and particle therapy in xenograft models?

Experiments were performed in nude (NMRI) mouse; this mouse has an autosomal recessive mutation in the Forkhead box N1 (Foxn1) gene, leading to partial or total thymic aplasia, resulting in immunodeficiency. This leads to impaired adaptive immune responses, depending on functional T-cells that are also required for B-cell maturation (Milicevic et al., 2005).

In this thesis, A549, human non-small cell lung adenocarcinoma (NSCLC) and FaDu (head and neck squamous cell carcinoma) were used for experiments. NSCLC Adenocarcinoma frequently exhibits mutations in TP53 (46%), KRAS (33%), KEAP1 and STK11 (17%), EGFR (11%) and CDKN2A (4%) (Cancer Genome Atlas Research, 2014). A549 cells are TP53 wildtype (Tate et al., 2019), exhibit a KRAS gain of function missense mutation (c.34G>A), CDKN2A (p16) copy number deletion, STK11 (Q37*) loss of function, KEAP1 (G333C) alteration and SMARCA4 (H736Y) loss of function [cellmodelpassports.sanger.ac.uk]. Thus, transferability of findings in A549 to Adeno-NSCLC patient data might be impaired w.r.t. frequently occurring TP53 status. Also absent in A549 are EGFR driver mutations leading to oncogene addiction and distinct treatment in clinics with tyrosine-kinase inhibitors.

HNSCC tumors tremendously differ between HPV status w.r.t prognoses, giving rise to molecular stratified treatment recommendations (Tawk et al., 2021). Most frequently mutated genes comprise TP53 (71%), FAT1 (23%), CDKN2A (22%), almost exclusively in HPV- tumors, and PIK3CA (21%), NOTCH1 (19%), and KMT2D (18%) (Cancer Genome Atlas, 2015). FaDu cells are HPV negative (Gottgens et al., 2021) show alterations in CDKN2A and FAT1 (loss of function) and TP53 (R248L) [cellmodelpassports.sanger.ac.uk].

In the experiments described in this thesis, cells were implanted subcutaneously to easily monitor tumor growth. The site of implantation, however, can influence tumor growth (orthotopic vs. heterotopic), as a number of factors i.e., angiogenesis, immunological, available space for expansion etc. may differ between the respective organ-specific conditions. It has been shown that –depending on the treatment and tumor model – specific therapeutic effects might be altered (Lehmann et al., 2017; Sharma et al., 2014).

On the described backgrounds (A549, FaDu), GeCKO A and Brunello libraries were studied to assess global library specific effects, as multiple generations and improvements of genome wide libraries have been reported (Sanson et al., 2018). GeCKO A library consist of over 60,000 unique guide RNAs for gene knockout in human genome. For each gene, 3 single guides were used, and the library contains 1000 control guides that do not target the genome. The library also targets 1,864

miRNAs using 4 guides per miRNA. The Brunello CRISPR knockout pooled library targets 19,114 genes using over 70,000 gRNAs with 4 gRNAs per gene and 1000 control gRNAs designed not to target in the genome. Thus, both libraries are designed to yield a high degree of redundancy for single genes.

4.1 Changes in library complexity

4.1.1 Library representation decreases between *in-vitro* and *in-vivo* conditions

First, we assessed the impact of microenvironmental selection pressure on library composition. In our experiments, we observed a tremendous drop of CRISPR library complexity *in-vivo* vs *in-vitro*. *In-vitro* samples showed high representation of gRNAs present in the library (>90%), whereas *in-vivo*, up to half of these guides were not detected anymore. This supports the notion of a more complex interaction *in-vivo*, with strong selection mechanisms.

We further observed a considerable difference in gRNA distributions between *in-vivo* and *in-vitro*. Despite the reduced complexity (which also complicated data analysis, see below), *in-vivo* gRNA abundance distribution was highly skewed. A high fraction of guides was detected less abundantly as compared to *in-vitro* (*in-vitro* between 100 and 1000 reads: 70-80% of guides > 0 reads vs 25-50%; *in-vivo* between 10 and 100 reads: 30-50% of guides > 0 reads vs 20%), but the fraction of guides with high read counts (>1000) was higher *in-vivo* (~10% of guides > 0 reads vs <1%). This indicates a clonal expansion of (possibly few) guides *in-vivo*, in line with the concept of a clonal evolution in cancers (Greaves & Maley, 2012; Körber & Höfer, 2019; Williams et al., 2019) and competitive selection pressure. Single cell sequencing technology has also indicated that tumors are constituted of several clones, which compete during tumor growth (Patel et al., 2014). Interestingly, guide distributions were qualitatively comparable between A549 and FaDu cells, hinting towards selection mechanisms *in-vivo* like angiogenic growth, stroma modulation etc. which are less dependent on the respective cell's molecular background.

4.1.2 Library complexity decreases over time

To further elucidate selection processes *in-vivo*, we tested if complexity in tumors - mirroring intratumoral heterogeneity – is altered over time in untreated animals. Indeed, we observed a decrease in tumor complexity in animals with longer survival times, independent of the molecular background of the cell line and the evaluated library (GeCKO and Brunello). These results were similar to data reported by Chen et al. in which early primary tumors retained less than half (32% - 49%) of the gRNAs found in the transplanted cell populations while only a small fraction (less than 8%) of gRNAs were detected in the late-stage primary tumor samples of the corresponding tumors (Chen et al., 2015).

This finding shows that tumors with high intratumoral heterogeneity (higher complexity) grow faster which results in shorter survival, without being able to give rise to few predominant clones. The observation that high intratumoral heterogeneity is linked to poorer outcome has also been made in genome sequencing inferred tumor complexity in patients (Zhang et al., 2014). These tumors are not controlled by the animals' innate immune system. On the other hand, if the harsh *in-vivo* constraints lack or slow vascularization, presence of innate immune cells (NK, TAMs) is able to control the tumors initially, only fewer fit clones will expand, which finally constitute the majority of the tumor. These clones have thus the ability to among others evade the immune system “on the long run”, for an extended period of time.

4.1.3 Tumor growth kinetics correlates with library complexity and radiation treatment

We observed that tumor irradiation leads to longer survival and slower tumor growth after both photon and particle treatment in both A549 and FaDu models. Overall survival after irradiation with high LET (carbon and oxygen ions) increased significantly in comparison with proton and helium ion treated mice. High LET treatment leads even to a tumor shrinkage in FaDu cells, in contrast to A549 tumors, where tumor sizes were stabilized and tumor growth was delayed. In FaDu, median survival was not reached for oxygen and carbon, in A549, median survival was not reached only for oxygen. I observed that irradiation also strongly reduces library complexity, photon and proton irradiation showing a comparable decrease (compared to control), helium and

carbon/oxygen show even further gradual decrease, thus demonstrating a strong LET dependency. Thus, w.r.t. efficacy of tumor cell killing, high LET treatment seems favorable – a finding, which has been reported for glioma models (preclinical) (Chiblak et al., 2019) and recurrent high grade glioma (retrospective clinical study) (Knoll et al., 2019) as well.

Moreover, experimental as well as encouraging clinical results support advantages of radiotherapy with high-LET carbon ions over standard photon irradiation for HNSCC (Ding et al., 2022; Eekers et al., 2016; Held et al., 2022; Held et al., 2019; Mizoe et al., 2012; Takahashi et al., 2022) and NSCLC (Chun et al., 2017; Liang et al., 2022; Ono et al., 2020) patients.

4.2 Transcriptome profiling and gene expression differences after irradiation

Next, we assessed if recurrent tumors show a specific transcriptome signature, as this could help to better interpret the underlying molecular mechanisms for recurrence and resistance. UMAP analysis clearly separated control from photon samples and showed that high-LET samples are similar in their transcriptome. Detailed examination of differences in gene expression revealed that in both A549 and FaDu models, genes were expressed differentially between groups and models. The amount of differentially expressed genes was higher in A549 model than in FaDu model. A number of detected genes which were expressed differentially have been shown to be either diagnostically useful and/or expressed in specific cancers.

4.2.1 Gene expression differences in FaDu model

Genes differentially expressed in photon irradiated FaDu tumors include genes involved in immune modulation, such as Peptidoglycan Recognition Protein 4 (PGLYRP4), S100 Calcium Binding Protein A12 (S100A12), C-X-C motif chemokine ligand 14 (CXCL14), Purinergic Receptor P2X 7 (P2RX7) and Interleukin 32 (IL32). In line with upregulation of these genes after photon irradiation, PGLYRP4 and S100A12 have been also found to be upregulated in patient HNSCC tumor tissues compared to normal tissues (Han et al., 2021; Sun et al., 2020). S100A12 was associated with improved clinical outcome (Funk et al., 2015). CXCL14 is a homeostatic chemokine

that can stimulate the chemotaxis of immune cells and suppress angiogenesis. In HPV-positive HNSCC cells, CXCL14 can upregulate the expression of MHC-I which inhibits the growth of tumors (Westrich et al., 2019) and the expression level of CXCL14 in HNSCC can be utilized to screen for patients that respond to cetuximab therapy (Kondo et al., 2016). High CXCL14 levels in HNSCC patients also predict longer overall and disease-free survival (Li et al., 2020). P2RX7 has been proposed to positively modulate antitumor immune response in HNSCC and its activation combined with α PD-1 immune checkpoint inhibitor leads to tumor regression and elevation of immunological memory response (Douguet et al., 2021). IL32 has been implicated in pro- and anti-tumor effects, potentially arising from functionally different isoforms, by modulation of the tumor microenvironment (Yan et al., 2018). However, also clearly unfavorable alterations following photon irradiation were observed, i.e., pro-angiogenic alterations (overexpression of SERPINB11, decreased expression of SEMA3B).

Upregulated genes in high LET samples revealed several interesting results. Signal transducer and activator of transcription 1 and 3 (STAT1 and STAT3, respectively), belong to STAT transcription factor family that can regulate diverse processes, such as cellular immunity, proliferation, apoptosis, angiogenesis, and differentiation (Verhoeven et al., 2020). Moreover, STAT1 and STAT3 can induce PD-L1 and therefore be potential biomarkers for α PD-L1 immunotherapy response (Nakayama et al., 2019). Activated STAT1 has been mainly described as having a tumor suppressor role in cancer cells (Koromilas & Sexl, 2013) and STAT1 knockout mice develop mammary carcinomas (Chan et al., 2012). STAT3, on the other hand, is predominantly described as tumor growth and immune evasion promoter (Yu et al., 2009) with elevated activity in more than 70% of human cancers (Roeser et al., 2015). Consequently, STAT3 inhibitor is an attractive target for cancer therapy, and although none of the inhibitors are in the market yet, there are several STAT3 inhibitors in preclinical development and a few of them in clinical trials (Dong et al., 2021).

An enzyme that promotes immune silencing and tumor viability, Adenosine deaminase RNA specific (ADAR), was also upregulated in high LET recurrent FaDu samples. ADAR is a proposed novel target for cancer immunotherapy as recent studies show that loss of ADAR1 sensitizes tumor cells to immunotherapy and overcome resistance to PD-1 checkpoint blockade that is caused by antigen presentation inactivation by

tumor cells (Bhate et al., 2019; Ishizuka et al., 2019). Therefore, high LET induced ADAR upregulation may provide an interesting target for combinatorial radio-immune therapy.

4.2.2 Gene expression differences in A549 model

Among upregulated genes in A549 photon treated tumors there were several genes (FUT6, LUM, MACC1 and PKIB) which expression roles have been confirmed in tumor growth, proliferation, invasion and/or metastasis.

Fucosyltransferase 6 (FUT6) gene, member of the fucosylation pathway, has altered expression in NSCLC and upregulation has been shown to promote cell invasion and metastasis (Park et al., 2020). Elevated expression of Lumican (LUM) in lung cancer cells promotes bone metastasis (Hsiao et al., 2020). Yang et al. indicated that LUM could affect cadherin-mediated invasion of A549 cells (Yang et al., 2018). Increased LUM expression in re-grown tumors could therefore help the survival of cells and confer resistance against treatment. Metastasis-associated in colon cancer-1 (MACC1) is a prognostic and predictive metastasis biomarker in several cancer entities (Lisec et al., 2021) and its overexpression also predicts metastases and poor prognosis for NSCLC (Wang et al., 2014). PKIB (cAMP-dependent protein kinase inhibitor- β) is another gene that was shown to be upregulated in HNCLC and promotes cell proliferation, invasion, and migration in A549 cells (Dou et al., 2016).

Downregulated genes in photon irradiation treated A549 model included putative tumor suppressor and apoptosis related gene CACNA2D3 (Calcium voltage-gated channel auxiliary subunit alpha2delta3) and an apoptotic activator Bcl2 modifying factor (BMF). CACNA2D3 has been proposed to act as a tumor suppressor in NSCLC (Tai et al., 2006) with more recent roles in chemosensitivity enhancement to cisplatin by triggering Ca²⁺ mediated apoptosis and blocking the PI3K/AKT pathways (Nie et al., 2019). BMF is a pro-apoptotic regulator and functions as an apoptotic activator in cellular stresses (Pinon et al., 2008).

Interestingly, upregulated genes in high LET samples included STAT1, which was also upregulated in high LET FaDu model samples (see section 4.2.1). Another upregulated gene was XIAP Associated Factor 1 (XAF1), which is expressed at low levels in cancer

cell lines, and on the contrary to our results, inhibits angiogenesis and induces apoptosis when overexpressed (Zhu et al., 2014).

4.3 KEGG pathway analysis

KEGG pathway analysis which was performed in both models for genes reveal different DNA repair pathways, such as p53 signaling, nucleotide excision repair, base excision repair as well as immune pathways, such as antigen processing and presentation, Graft-vs-host disease, and Allograft rejection pathways. Detected pathways which were related to immune system showed that even though there is no complete immune response in used models but remained parts of acquired immunity like as B cells and innate immunity could play an important role in tumors behavior in both models and can change the fate of tumors in irradiated mice.

Different immune cell populations are important for the immune response after irradiation; some of them are natural killer cells and dendritic cells. Relation between immune system activation with irradiation could be explained by the fact that exposure of tumor cells with irradiation increase peptide pool also release of danger associated molecular patterns (DAMPs) and could activate receptors like as toll like receptors (TLRs) (Roses et al., 2008). The downstream signaling pathways lead to the production of inflammatory cytokines which could explain partial role of immune system in irradiated cells.

4.4 gRNA analysis

Analysis of gRNAs turned out to be challenging. The above mentioned low complexity resulted in detection of mostly only few guides per gene in each sample. That representation problem of libraries *in-vivo* is known, which is usually solved by pooling multiple tumors. We therefore made to following assumptions for analysis: all samples can be considered to be a sub-part of a “synthetic” tumor (clonal architecture of tumors) and a single “hit” (detection of guide) was considered sufficient to impair function of the respective gene. We therefore first aggregated guides on gene level, by considering only the maximum observed value (maximum expansion of a clone with this genetic alteration). This is different to established analysis methods (Model-based Analysis of Genome-wide CRISPR/Cas9 Knockout – MaGECK (Li et al., 2014), where aggregation

on gene level occurs only after evaluation of single genes. To weight down highly abundant clones, we then rank transformed obtained gene values (as proposed in methods for analysis of RNAi screens (Birmingham et al., 2009), and as high LET treatment led to a tremendous decrease in observed complexity, we only considered genes detected in any of the high LET treated samples for evaluation of LET effects (positive selection).

4.4.1 gRNA abundance differences in FaDu model

Highly abundant gRNAs (leading to loss of function of the gene) in FaDu model included Bone Morphogenetic Protein 8a (BMP8A) and histone demethylase Lysine demethylase 5C (KDM5C) in photon treated tumors compared to untreated tumors. BMP8A is a TGF- β signaling pathway gene and is mainly described in embryonic development with recent reports describing its role in promoting cancer cell survival and drug resistance (Yu et al., 2020). KDM5C is a cancer-associated epigenetic regulator as it can remove methyl marks from Histone H3 lysine K4 (H3K4), thereby either activating or repressing transcription. KDM5C is a putative tumor suppressor, and its loss has been correlated with increased genomic instability and identified in several types of cancers (Ohguchi & Ohguchi, 2022; Plch et al., 2019).

Interestingly, gRNA abundance in association with LET also revealed BMP8A as one of the top genes. Fibroblast growth Factor 2 (FGF2) and TSC Complex Subunit 1 (TSC1) also had high gRNA counts in LET treated tumors. Aberrant FGFR signaling has been widely described in tumorigenesis and resistance to therapy, which has led to development of therapies targeting the FGFR pathway (Babina & Turner, 2017). TSC1, a member of pro-survival PI3K/AKT/MTOR signaling pathway, is a tumor suppressor that is downregulated in several human cancers. Downregulation of TSC1 can lead to increased proliferation, migration and angiogenesis (Mallela & Kumar, 2021).

4.4.2 gRNA abundance differences in A549 model

gRNA analysis revealed several interesting results in A549 model. In photon treated tumors, more frequently detected gRNAs included Mitochondrial malate dehydrogenase 2 (MDH2), Matrix metalloproteinase-19 (MMP19) and Tenascin C

(TNC). MDH2 is a mitochondrial gene that has been found to be highly expressed in NSCLC, suggesting it as a biomarker for early detection of NSCLC (Ma et al., 2021). Therefore, an enrichment for A549 clones with MDH2 loss under photon selection pressure further underscore the relevance of this protein in tumor biology and therapy resistance.

MMP19 stimulates proliferation and cell migration and is similarly found to be overexpressed in NSCLC and proposed as a biomarker for severity and outcome of the disease (Yu et al., 2014). TNC facilitates tumor tissue remodeling and is highly expressed by cancer-associated fibroblasts (CAFs) and upregulated in most solid tumors (Kwa et al., 2019).

Genes which guide abundance was associated with LET were BCL2 Associated Agonist of Cell Death (BAD), BCL2 Interacting Protein 3 (BNIP3), AT-rich Interaction Domain 2 (ARID2) and TGF- β Receptor 1 (TGFR1) and 2 (TGFR2). BAD is a pro-apoptotic sensitizer and its overexpression in A549 cells was reported to inhibit cell growth and promote apoptosis (Huang et al., 2012). BNIP3 is a mitochondrial pro-apoptotic mediator that is activated by hypoxia that is overexpressed in up to 80% of lung cancer cases and in about 57% of patients with NSCLC (Karpathiou et al., 2013), and it correlates with poor prognosis in early stages (Gorbunova et al., 2020). ARID2 is a chromatin remodeler which loss has been found in 20% of lung cancers with its deficiency leading to increased proliferation and metastasis while also sensitizing cells to DNA damaging agents (Moreno et al., 2021).

TGF- β pathway plays crucial roles in carcinogenesis and metastasis. While suppressing inflammation and regulating wound healing during homeostasis, it can promote malignancy during tumor evolution. Loss of TGF- β related pathways in tumor is a mechanism by which tumor cells become resistant to tumor suppressing effect of TGF- β , and enhanced TGF- β expression can thereby induce negative effects in the tumor microenvironment - epithelial to mesenchymal transition, immunosuppression, and stroma remodeling. In pancreatic cancer, one of the early events is loss of SMAD4, which desensitizes tumor cells to TGF- β tumor suppressive effects and enables TGF- β to negatively modulate the stroma (Barcellos-Hoff, 2022; Lan et al., 2021). Inhibiting

TGF- β triggers potent antitumor responses in preclinical model systems by enabling to restore cancer immunity (Tauriello et al., 2022).

4.5 Correlation between RNA expression and gRNA abundance genes

Combining gene expression data by RNAseq and gRNA abundance data revealed many overlapping genes in FaDu model and less in A549 model. Interesting results in FaDu model include Far upstream element binding protein 1 (FUBP1), Hematopoietically expressed homeobox (HHEX), Serine/Arginine-Rich splicing factor Kinase 1 (SPRK1), Tumor necrosis factor receptor associated protein 1 (TRAP1) and WD repeat domain 5 (WDR5). FUBP1 is a transcription activator or repressor which, when overexpressed, can downregulate MYC oncogene. FUBP1 loss is associated with tumor suppressive role (Debaize & Troadec, 2019). HHEX is considered to be a transcriptional repressor and similarly to FUBP1, has been also shown suppress MYC activity when overexpressed (Marfil et al., 2015). In addition, HHEX was reported to be downregulated in patient HNSCC tumor tissues compared to normal tissues (Sun et al., 2020). SPRK1 is regulating alternative splicing that has been implicated in oncogenic signaling pathways and is overexpressed in various cancer types, correlating with worse outcome. SPRK1 downregulation has shown to be tumor-suppressive in preclinical models (Nikas et al., 2019). TRAP1 is involved in regulating metabolism in cancer cells and its expression is elevated in several cancers that correlates with drug resistance while being downregulated in others, also correlating with resistance and poor prognosis (Matassa et al., 2018). WDR5 interacts with MYC, promoting its recruitment onto chromatin and controls subsequent gene expression. Blocking the MYC-WDR5 interaction causes existing tumors to regress, suggesting targeting this interaction as a potential anticancer therapeutic strategy (Thomas et al., 2019). Data also revealed RUNX1, which was downregulated in FaDu model and CACNA2D3, which was downregulated in A549 model after photon radiation (see Chapter 4.2.1 and 4.2.2 respectively).

5. Summary

This thesis combines the use of novel radiation qualities with *in-vivo* functional genetic screens in prototypic head and neck squamous cell carcinoma (HNSCC, FaDu) and non-small cell lung cancer (NSCLC, A549) preclinical xenograft models. Using whole-genome FaDu and A549 CRISPR/Cas9 libraries, *in-vivo* tumor response to conventional photon radiotherapy as well as a series of particles with gradually enhanced ionization density (LET), i.e., proton, helium, carbon- and oxygen ion irradiation were investigated. Two genome wide - GeCKO A and Brunello – gRNA libraries were integrated in Cas9 expressing FaDu and A549 cells. Transcriptome and guide representation studies using next-generation sequencing (NGS) and quantitative analysis provided insights into the tumor evolutionary landscape and genes/pathways contributing to tumor fitness under different *in-vivo* and therapeutic selection pressures.

A pronounced reduction of library complexity was detected *in-vivo* vs *in-vitro*, regardless of tumor model and library. Additional reduction was observed in irradiated samples. Clonal tumor evolution could be recapitulated, as outgrown tumors showed an expansion of few clones constituting the majority of the tumors. Tumor growth rate was negatively linked to library complexity – a potential surrogate for intratumoral heterogeneity – strengthening the previously described association between high intratumoral complexity and increased tumor aggressiveness.

High-LET irradiation showed improved capacity for cell killing, with either tumor regression (in FaDu model) or enhanced growth delay (in A549 model). Irradiation type specific transcriptome fingerprints revealed both favorable- and non-favorable changes, comprising modulation of the tumor microenvironment (TGF- β), inflammation and senescence, pro- and anti-angiogenic alterations, DNA damage repair, hypoxia and antigen presentation. Main factors influencing transcriptome profiles differences within particles were LET (high vs. low LET groups).

On guide level, radio-resistance seems to be mediated by loss of TGF- β signaling components (BMP8A), chromatin remodeling (KDM5C) and metabolic pathways

(MDH2). LET dependency analyses also identified TGF- β signaling as key component, cell-death mediations (BAD, BNIP3) and tumor suppressors (ARID2).

Common pattern of upregulation across both tumors and libraries was a gradual LET dependent increase of genes associated immune signaling processes (HLAs, interferon response, MX1, etc.) which correlated well with enrichment of pathways found to be related to immune response. Together, this work provides novel insights into the molecular fitness landscape of tumors under conventional photon irradiation and ion beam therapy.

6. Zusammenfassung

In dieser Arbeit werden neuartige Strahlenqualitäten mit funktionellen genetischen *in-vivo*-Screens in prototypischen Kopf- und Halsplattenepithelkarzinomen (HNSCC, FaDu) und nicht-kleinzelligem Lungenkrebs (NSCLC, A549) in präklinischen Xenotransplantationsmodellen evaluiert. Unter Verwendung von genomweiten FaDu- und A549-CRISPR/Cas9-Bibliotheken wurde die *in-vivo*-Tumorantwort auf eine konventionelle Photonen-Strahlentherapie sowie auf eine Bestrahlung mit einer Reihe von Partikeln mit zunehmender Ionisationsdichte (LET), d.h. Protonen-, Helium-, Kohlenstoff- und Sauerstoffionen, untersucht. Zwei genomweite gRNA-Bibliotheken - GeCKO A und Brunello - wurden in Cas9-exprimierende FaDu- und A549-Zellen angewandt. Next-Generation-Sequencing (NGS) Analysen der gRNA Verteilung und der Genexpression erlaubten Einblicke in molekulare Vorgänge der Tumorentwicklung sowie die Identifikation von Genen und Signalwegen, die unter *in-vivo* und unter therapeutischem Selektionsdruck förderlich für das Tumorwachstum sind.

Unabhängig von Tumormodell und gRNA-Bibliothek wurde *in-vivo* eine deutliche Reduktion der gRNA basierten Komplexität gegenüber *in-vitro* festgestellt. Eine zusätzliche Verminderung wurde in bestrahlten Proben beobachtet. Eine klonale Tumor-Evolution wurde – im Sinne einer Expansion weniger Klone – beobachtet, wobei wenige Klone einen Großteil des Tumors ausmachten. Die Tumorwachstumsrate stand in einem negativen Zusammenhang mit der gemessenen Komplexität der gRNA Bibliothek - einem potenziellen Surrogat für die intratumorale Heterogenität -, was den zuvor beschriebenen Zusammenhang zwischen hoher intratumoraler Komplexität und erhöhter Tumoraggressivität untermauert.

Die Bestrahlung mit Partikeln mit hoher LET führte zu einer effizienteren Tumorkontrolle, beobachtbar als Tumorregression (im FaDu-Modell) bzw. als verstärkte Wachstumsverzögerung (im A549-Modell). Bestrahlungstyp-spezifische Transkriptom-Signaturen zeigten sowohl günstige als auch ungünstige Veränderungen, die eine Modulation der Tumormikroumgebung (TGF- β), Entzündung und Seneszenz, pro- und antiangiogene Veränderungen, DNA-Schadensreparatur, Hypoxie und Antigenpräsentation beinhalten. Die Hauptfaktoren, die die Unterschiede

in den Transkriptomprofilen innerhalb der Partikel beeinflussten, waren der LET (hohe vs. niedrige LET-Gruppen).

Auf Ebene der gRNAs scheint die Strahlenresistenz durch den Verlust von TGF- β -Signalkomponenten (BMP8A), Chromatin-Remodeling (KDM5C) und Stoffwechselwegen (MDH2) vermittelt zu werden. Analysen der LET-Abhängigkeit identifizierten auch die TGF- β -Signalübertragung als Schlüsselkomponente, die Vermittlung des Zelltods (BAD, BNIP3) und Tumorsuppressoren (ARID2).

Ein gemeinsames Muster übergreifend über die analysierten Tumormodelle und Bibliotheken war ein gradueller, LET-abhängiger Anstieg von Genen, die mit Immunsignalprozessen in Verbindung stehen (HLAs, Interferonantwort, MX1 usw.), und mit der Anreicherung von Signalwegen korrelieren, die mit der Immunantwort in Verbindung stehen. Zusammenfassend bietet diese Arbeit neue Einblicke in die molekularen Faktoren, die das Tumorstadium unter konventioneller Photonen- und Ionenstrahltherapie beeinflussen.

7. References

- Abdollahi, A., & Folkman, J. (2010). Evading tumor evasion: current concepts and perspectives of anti-angiogenic cancer therapy. *Drug Resist Updat*, 13(1-2), 16-28. <https://doi.org/10.1016/j.drug.2009.12.001>
- Adamson, B., Norman, T. M., Jost, M., Cho, M. Y., Nunez, J. K., Chen, Y., Villalta, J. E., Gilbert, L. A., Horlbeck, M. A., Hein, M. Y., Pak, R. A., Gray, A. N., Gross, C. A., Dixit, A., Parnas, O., Regev, A., & Weissman, J. S. (2016). A Multiplexed Single-Cell CRISPR Screening Platform Enables Systematic Dissection of the Unfolded Protein Response. *Cell*, 167(7), 1867-1882 e1821. <https://doi.org/10.1016/j.cell.2016.11.048>
- Adelstein, D. J., Li, Y., Adams, G. L., Wagner, H., Jr., Kish, J. A., Ensley, J. F., Schuller, D. E., & Forastiere, A. A. (2003). An intergroup phase III comparison of standard radiation therapy and two schedules of concurrent chemoradiotherapy in patients with unresectable squamous cell head and neck cancer. *J Clin Oncol*, 21(1), 92-98. <https://doi.org/10.1200/JCO.2003.01.008>
- Adli, M. (2018). The CRISPR tool kit for genome editing and beyond. *Nat Commun*, 9(1), 1911. <https://doi.org/10.1038/s41467-018-04252-2>
- Alsaifi, E., Begg, K., Amelio, I., Raulf, N., Lucarelli, P., Sauter, T., & Tavassoli, M. (2019). Clinical update on head and neck cancer: molecular biology and ongoing challenges. *Cell Death Dis*, 10(8), 540. <https://doi.org/10.1038/s41419-019-1769-9>
- Anders, C., Niewoehner, O., Duerst, A., & Jinek, M. (2014). Structural basis of PAM-dependent target DNA recognition by the Cas9 endonuclease. *Nature*, 513(7519), 569-573. <https://doi.org/10.1038/nature13579>
- Ang, K. K., Harris, J., Wheeler, R., Weber, R., Rosenthal, D. I., Nguyen-Tan, P. F., Westra, W. H., Chung, C. H., Jordan, R. C., Lu, C., Kim, H., Axelrod, R., Silverman, C. C., Redmond, K. P., & Gillison, M. L. (2010). Human papillomavirus and survival of patients with oropharyngeal cancer. *N Engl J Med*, 363(1), 24-35. <https://doi.org/10.1056/NEJMoa0912217>
- Antonovic, L., Lindblom, E., Dasu, A., Bassler, N., Furusawa, Y., & Toma-Dasu, I. (2014). Clinical oxygen enhancement ratio of tumors in carbon ion radiotherapy: the influence of local oxygenation changes. *J Radiat Res*, 55(5), 902-911. <https://doi.org/10.1093/jrr/rru020>
- Baas, P., Belderbos, J. S., & van den Heuvel, M. (2011). Chemoradiation therapy in nonsmall cell lung cancer. *Curr Opin Oncol*, 23(2), 140-149. <https://doi.org/10.1097/CCO.0b013e328341eed6>
- Babina, I. S., & Turner, N. C. (2017). Advances and challenges in targeting FGFR signalling in cancer. *Nat Rev Cancer*, 17(5), 318-332. <https://doi.org/10.1038/nrc.2017.8>
- Balis, J. U., Bumgarner, S. D., Paciga, J. E., Paterson, J. F., & Shelley, S. A. (1984). Synthesis of lung surfactant-associated glycoproteins by A549 cells: description of an in vitro model for human type II cell dysfunction. *Exp Lung Res*, 6(3-4), 197-213. <https://doi.org/10.3109/01902148409109248>
- Barcellos-Hoff, M. H. (2022). The radiobiology of TGFbeta. *Semin Cancer Biol*, 86(Pt 3), 857-867. <https://doi.org/10.1016/j.semcancer.2022.02.001>
- Barta, J. A., Powell, C. A., & Wisnivesky, J. P. (2019). Global Epidemiology of Lung Cancer. *Ann Glob Health*, 85(1). <https://doi.org/10.5334/aogh.2419>
- Baskar, R., Lee, K. A., Yeo, R., & Yeoh, K. W. (2012). Cancer and radiation therapy: current advances and future directions. *Int J Med Sci*, 9(3), 193-199. <https://doi.org/10.7150/ijms.3635>
- Bendinger, A. L., Welzel, T., Huang, L., Babushkina, I., Peschke, P., Debus, J., Glowa, C., Karger, C. P., & Saager, M. (2021). DCE-MRI detected vascular permeability changes in the rat spinal cord do not explain shorter latency times for paresis after carbon ions relative to photons. *Radiother Oncol*, 165, 126-134. <https://doi.org/10.1016/j.radonc.2021.09.035>
- Bernier, J., Cooper, J. S., Pajak, T. F., van Glabbeke, M., Bourhis, J., Forastiere, A., Ozsahin, E. M., Jacobs, J. R., Jassem, J., Ang, K. K., & Lefebvre, J. L. (2005). Defining risk levels in locally

- advanced head and neck cancers: a comparative analysis of concurrent postoperative radiation plus chemotherapy trials of the EORTC (#22931) and RTOG (# 9501). *Head Neck*, 27(10), 843-850. <https://doi.org/10.1002/hed.20279>
- Bhate, A., Sun, T., & Li, J. B. (2019). ADAR1: A New Target for Immuno-oncology Therapy. *Mol Cell*, 73(5), 866-868. <https://doi.org/10.1016/j.molcel.2019.02.021>
- Birmingham, A., Selfors, L. M., Forster, T., Wrobel, D., Kennedy, C. J., Shanks, E., Santoyo-Lopez, J., Dunican, D. J., Long, A., Kelleher, D., Smith, Q., Beijersbergen, R. L., Ghazal, P., & Shamu, C. E. (2009). Statistical methods for analysis of high-throughput RNA interference screens. *Nat Methods*, 6(8), 569-575. <https://doi.org/10.1038/nmeth.1351>
- Bol, V., & Gregoire, V. (2014). Biological basis for increased sensitivity to radiation therapy in HPV-positive head and neck cancers. *Biomed Res Int*, 2014, 696028. <https://doi.org/10.1155/2014/696028>
- Braakhuis, B. J., Tabor, M. P., Kummer, J. A., Leemans, C. R., & Brakenhoff, R. H. (2003). A genetic explanation of Slaughter's concept of field cancerization: evidence and clinical implications. *Cancer Res*, 63(8), 1727-1730. <https://www.ncbi.nlm.nih.gov/pubmed/12702551>
- Braun, C. J., Bruno, P. M., Horlbeck, M. A., Gilbert, L. A., Weissman, J. S., & Hemann, M. T. (2016). Versatile in vivo regulation of tumor phenotypes by dCas9-mediated transcriptional perturbation. *Proc Natl Acad Sci U S A*, 113(27), E3892-3900. <https://doi.org/10.1073/pnas.1600582113>
- Bray, F., Ferlay, J., Soerjomataram, I., Siegel, R. L., Torre, L. A., & Jemal, A. (2018). Global cancer statistics 2018: GLOBOCAN estimates of incidence and mortality worldwide for 36 cancers in 185 countries. *CA Cancer J Clin*, 68(6), 394-424. <https://doi.org/10.3322/caac.21492>
- Brennan, S., Baird, A. M., O'Regan, E., & Sheils, O. (2021). The Role of Human Papilloma Virus in Dictating Outcomes in Head and Neck Squamous Cell Carcinoma. *Front Mol Biosci*, 8, 677900. <https://doi.org/10.3389/fmolb.2021.677900>
- Burdett, S., Pignon, J. P., Tierney, J., Tribodet, H., Stewart, L., Le Pechoux, C., Auperin, A., Le Chevalier, T., Stephens, R. J., Arriagada, R., Higgins, J. P., Johnson, D. H., Van Meerbeeck, J., Parmar, M. K., Souhami, R. L., Bergman, B., Douillard, J. Y., Dunant, A., Endo, C., Girling, D., Kato, H., Keller, S. M., Kimura, H., Knuutila, A., Kodama, K., Komaki, R., Kris, M. G., Lad, T., Mineo, T., Piantadosi, S., Rosell, R., Scagliotti, G., Seymour, L. K., Shepherd, F. A., Sylvester, R., Tada, H., Tanaka, F., Torri, V., Waller, D., Liang, Y., & Non-Small Cell Lung Cancer Collaborative, G. (2015). Adjuvant chemotherapy for resected early-stage non-small cell lung cancer. *Cochrane Database Syst Rev*(3), CD011430. <https://doi.org/10.1002/14651858.CD011430>
- Califano, J., van der Riet, P., Westra, W., Nawroz, H., Clayman, G., Piantadosi, S., Corio, R., Lee, D., Greenberg, B., Koch, W., & Sidransky, D. (1996). Genetic progression model for head and neck cancer: implications for field cancerization. *Cancer Res*, 56(11), 2488-2492. <https://www.ncbi.nlm.nih.gov/pubmed/8653682>
- Cancer Genome Atlas, N. (2015). Comprehensive genomic characterization of head and neck squamous cell carcinomas. *Nature*, 517(7536), 576-582. <https://doi.org/10.1038/nature14129>
- Cancer Genome Atlas Research, N. (2014). Comprehensive molecular profiling of lung adenocarcinoma. *Nature*, 511(7511), 543-550. <https://doi.org/10.1038/nature13385>
- Chan, S. R., Vermi, W., Luo, J., Lucini, L., Rickert, C., Fowler, A. M., Lonardi, S., Arthur, C., Young, L. J., Levy, D. E., Welch, M. J., Cardiff, R. D., & Schreiber, R. D. (2012). STAT1-deficient mice spontaneously develop estrogen receptor alpha-positive luminal mammary carcinomas. *Breast Cancer Res*, 14(1), R16. <https://doi.org/10.1186/bcr3100>
- Chang, J. Y. (2015). Stereotactic ablative radiotherapy: aim for a cure of cancer. *Ann Transl Med*, 3(1), 12. <https://doi.org/10.3978/j.issn.2305-5839.2014.11.17>
- Chapman, J. R., Taylor, M. R., & Boulton, S. J. (2012). Playing the end game: DNA double-strand break repair pathway choice. *Mol Cell*, 47(4), 497-510. <https://doi.org/10.1016/j.molcel.2012.07.029>

- Chen, S., Sanjana, N. E., Zheng, K., Shalem, O., Lee, K., Shi, X., Scott, D. A., Song, J., Pan, J. Q., Weissleder, R., Lee, H., Zhang, F., & Sharp, P. A. (2015). Genome-wide CRISPR screen in a mouse model of tumor growth and metastasis. *Cell*, *160*(6), 1246-1260. <https://doi.org/10.1016/j.cell.2015.02.038>
- Chiblak, S., Tang, Z., Lemke, D., Knoll, M., Dokic, I., Warta, R., Moustafa, M., Mier, W., Brons, S., Rapp, C., Muschal, S., Seidel, P., Bendszus, M., Adeberg, S., Wiestler, O. D., Haberkorn, U., Debus, J., Herold-Mende, C., Wick, W., & Abdollahi, A. (2019). Carbon irradiation overcomes glioma radioresistance by eradicating stem cells and forming an antiangiogenic and immunopermissive niche. *JCI Insight*, *4*(2). <https://doi.org/10.1172/jci.insight.123837>
- Chow, R. D., & Chen, S. (2018). Cancer CRISPR Screens In Vivo. *Trends Cancer*, *4*(5), 349-358. <https://doi.org/10.1016/j.trecan.2018.03.002>
- Christian, E., Adamietz, I. A., Willich, N., Schafer, U., Micke, O., German Working Group Palliative, R., & German Society for Radiation, O. (2008). Radiotherapy in oncological emergencies--final results of a patterns of care study in Germany, Austria and Switzerland. *Acta Oncol*, *47*(1), 81-89. <https://doi.org/10.1080/02841860701481554>
- Chun, S. G., Solberg, T. D., Grosshans, D. R., Nguyen, Q. N., Simone, C. B., 2nd, Mohan, R., Liao, Z., Hahn, S. M., Herman, J. M., & Frank, S. J. (2017). The Potential of Heavy-Ion Therapy to Improve Outcomes for Locally Advanced Non-Small Cell Lung Cancer. *Front Oncol*, *7*, 201. <https://doi.org/10.3389/fonc.2017.00201>
- Cowley, G. S., Weir, B. A., Vazquez, F., Tamayo, P., Scott, J. A., Rusin, S., East-Seletsky, A., Ali, L. D., Gerath, W. F., Pantel, S. E., Lizotte, P. H., Jiang, G., Hsiao, J., Tsherniak, A., Dwinell, E., Aoyama, S., Okamoto, M., Harrington, W., Gelfand, E., Green, T. M., Tomko, M. J., Gopal, S., Wong, T. C., Li, H., Howell, S., Stransky, N., Liefeld, T., Jang, D., Bistline, J., Hill Meyers, B., Armstrong, S. A., Anderson, K. C., Stegmaier, K., Reich, M., Pellman, D., Boehm, J. S., Mesirov, J. P., Golub, T. R., Root, D. E., & Hahn, W. C. (2014). Parallel genome-scale loss of function screens in 216 cancer cell lines for the identification of context-specific genetic dependencies. *Sci Data*, *1*, 140035. <https://doi.org/10.1038/sdata.2014.35>
- de Groot, P. M., Wu, C. C., Carter, B. W., & Munden, R. F. (2018). The epidemiology of lung cancer. *Transl Lung Cancer Res*, *7*(3), 220-233. <https://doi.org/10.21037/tlcr.2018.05.06>
- Debaize, L., & Troadec, M. B. (2019). The master regulator FUBP1: its emerging role in normal cell function and malignant development. *Cell Mol Life Sci*, *76*(2), 259-281. <https://doi.org/10.1007/s00018-018-2933-6>
- Delaney, G., Jacob, S., Featherstone, C., & Barton, M. (2005). The role of radiotherapy in cancer treatment: estimating optimal utilization from a review of evidence-based clinical guidelines. *Cancer*, *104*(6), 1129-1137. <https://doi.org/10.1002/cncr.21324>
- Deltcheva, E., Chylinski, K., Sharma, C. M., Gonzales, K., Chao, Y., Pirzada, Z. A., Eckert, M. R., Vogel, J., & Charpentier, E. (2011). CRISPR RNA maturation by trans-encoded small RNA and host factor RNase III. *Nature*, *471*(7340), 602-607. <https://doi.org/10.1038/nature09886>
- Ding, L., Sishc, B. J., Polsdofer, E., Yordy, J. S., Facoetti, A., Ciocca, M., Saha, D., Pompos, A., Davis, A. J., & Story, M. D. (2022). Evaluation of the Response of HNSCC Cell Lines to gamma-Rays and (12)C Ions: Can Radioresistant Tumors Be Identified and Selected for (12)C Ion Radiotherapy? *Front Oncol*, *12*, 812961. <https://doi.org/10.3389/fonc.2022.812961>
- Doench, J. G. (2018). Am I ready for CRISPR? A user's guide to genetic screens. *Nat Rev Genet*, *19*(2), 67-80. <https://doi.org/10.1038/nrg.2017.97>
- Doench, J. G., Fusi, N., Sullender, M., Hegde, M., Vaimberg, E. W., Donovan, K. F., Smith, I., Tothova, Z., Wilen, C., Orchard, R., Virgin, H. W., Listgarten, J., & Root, D. E. (2016). Optimized sgRNA design to maximize activity and minimize off-target effects of CRISPR-Cas9. *Nat Biotechnol*, *34*(2), 184-191. <https://doi.org/10.1038/nbt.3437>
- Dong, J., Cheng, X. D., Zhang, W. D., & Qin, J. J. (2021). Recent Update on Development of Small-Molecule STAT3 Inhibitors for Cancer Therapy: From Phosphorylation Inhibition to Protein Degradation. *J Med Chem*, *64*(13), 8884-8915. <https://doi.org/10.1021/acs.jmedchem.1c00629>

- Dou, P., Zhang, D., Cheng, Z., Zhou, G., & Zhang, L. (2016). PKIB promotes cell proliferation and the invasion-metastasis cascade through the PI3K/Akt pathway in NSCLC cells. *Exp Biol Med (Maywood)*, 241(17), 1911-1918. <https://doi.org/10.1177/1535370216655908>
- Doudna, J. A., & Charpentier, E. (2014). Genome editing. The new frontier of genome engineering with CRISPR-Cas9. *Science*, 346(6213), 1258096. <https://doi.org/10.1126/science.1258096>
- Douguet, L., Janho Dit Hreich, S., Benzaquen, J., Seguin, L., Juhel, T., Dezitter, X., Durantou, C., Ryffel, B., Kanellopoulos, J., Delarasse, C., Renault, N., Furman, C., Homerin, G., Feral, C., Cherfils-Vicini, J., Millet, R., Adriouch, S., Ghinet, A., Hofman, P., & Vouret-Craviari, V. (2021). A small-molecule P2RX7 activator promotes anti-tumor immune responses and sensitizes lung tumor to immunotherapy. *Nat Commun*, 12(1), 653. <https://doi.org/10.1038/s41467-021-20912-2>
- Drilon, A., Rekhtman, N., Ladanyi, M., & Paik, P. (2012). Squamous-cell carcinomas of the lung: emerging biology, controversies, and the promise of targeted therapy. *Lancet Oncol*, 13(10), e418-426. [https://doi.org/10.1016/S1470-2045\(12\)70291-7](https://doi.org/10.1016/S1470-2045(12)70291-7)
- Durante, M., & Debus, J. (2018). Heavy Charged Particles: Does Improved Precision and Higher Biological Effectiveness Translate to Better Outcome in Patients? *Seminars in Radiation Oncology*, 28(2), 160-167. <https://doi.org/https://doi.org/10.1016/j.semradonc.2017.11.004>
- Eberhard, D. A., Johnson, B. E., Amler, L. C., Goddard, A. D., Heldens, S. L., Herbst, R. S., Ince, W. L., Janne, P. A., Januario, T., Johnson, D. H., Klein, P., Miller, V. A., Ostland, M. A., Ramies, D. A., Sebisano, D., Stinson, J. A., Zhang, Y. R., Seshagiri, S., & Hillan, K. J. (2005). Mutations in the epidermal growth factor receptor and in KRAS are predictive and prognostic indicators in patients with non-small-cell lung cancer treated with chemotherapy alone and in combination with erlotinib. *J Clin Oncol*, 23(25), 5900-5909. <https://doi.org/10.1200/JCO.2005.02.857>
- Eberle, F., Lautenschlager, S., Engenhart-Cabillic, R., Jensen, A. D., Carl, B., Stein, M., Debus, J., & Hauswald, H. (2020). Carbon Ion Beam Reirradiation in Recurrent High-Grade Glioma. *Cancer Manag Res*, 12, 633-639. <https://doi.org/10.2147/CMAR.S217824>
- Eekers, D. B. P., Roelofs, E., Jelen, U., Kirk, M., Granzier, M., Ammazalorso, F., Ahn, P. H., Janssens, G., Hoebers, F. J. P., Friedmann, T., Solberg, T., Walsh, S., Troost, E. G. C., Kaanders, J., & Lambin, P. (2016). Benefit of particle therapy in re-irradiation of head and neck patients. Results of a multicentric in silico ROCOCO trial. *Radiother Oncol*, 121(3), 387-394. <https://doi.org/10.1016/j.radonc.2016.08.020>
- Eisbruch, A., Schwartz, M., Rasch, C., Vineberg, K., Damen, E., Van As, C. J., Marsh, R., Pameijer, F. A., & Balm, A. J. (2004). Dysphagia and aspiration after chemoradiotherapy for head-and-neck cancer: which anatomic structures are affected and can they be spared by IMRT? *Int J Radiat Oncol Biol Phys*, 60(5), 1425-1439. <https://doi.org/10.1016/j.ijrobp.2004.05.050>
- Feng, X., Zheng, Z., Wang, Y., Song, G., Wang, L., Zhang, Z., Zhao, J., Wang, Q., & Lun, L. (2021). Elevated RUNX1 is a prognostic biomarker for human head and neck squamous cell carcinoma. *Exp Biol Med (Maywood)*, 246(5), 538-546. <https://doi.org/10.1177/1535370220969663>
- Ferris, R. L., Blumenschein, G., Jr., Fayette, J., Guigay, J., Colevas, A. D., Licitra, L., Harrington, K., Kasper, S., Vokes, E. E., Even, C., Worden, F., Saba, N. F., Iglesias Docampo, L. C., Haddad, R., Rordorf, T., Kiyota, N., Tahara, M., Monga, M., Lynch, M., Geese, W. J., Kopit, J., Shaw, J. W., & Gillison, M. L. (2016). Nivolumab for Recurrent Squamous-Cell Carcinoma of the Head and Neck. *N Engl J Med*, 375(19), 1856-1867. <https://doi.org/10.1056/NEJMoa1602252>
- Funk, S., Mark, R., Bayo, P., Flechtenmacher, C., Grabe, N., Angel, P., Plinkert, P. K., & Hess, J. (2015). High S100A8 and S100A12 protein expression is a favorable prognostic factor for survival of oropharyngeal squamous cell carcinoma. *Int J Cancer*, 136(9), 2037-2046. <https://doi.org/10.1002/ijc.29262>
- Ganti, A. K., Klein, A. B., Cotarla, I., Seal, B., & Chou, E. (2021). Update of Incidence, Prevalence, Survival, and Initial Treatment in Patients With Non-Small Cell Lung Cancer in the US. *JAMA Oncol*, 7(12), 1824-1832. <https://doi.org/10.1001/jamaoncol.2021.4932>

- Garden, A. S., Harris, J., Trotti, A., Jones, C. U., Carrascosa, L., Cheng, J. D., Spencer, S. S., Forastiere, A., Weber, R. S., & Ang, K. K. (2008). Long-term results of concomitant boost radiation plus concurrent cisplatin for advanced head and neck carcinomas: a phase II trial of the radiation therapy oncology group (RTOG 99-14). *Int J Radiat Oncol Biol Phys*, *71*(5), 1351-1355. <https://doi.org/10.1016/j.ijrobp.2008.04.006>
- Ghosh, D., Venkataramani, P., Nandi, S., & Bhattacharjee, S. (2019). CRISPR-Cas9 a boon or bane: the bumpy road ahead to cancer therapeutics. *Cancer Cell Int*, *19*, 12. <https://doi.org/10.1186/s12935-019-0726-0>
- Giard, D. J., Aaronson, S. A., Todaro, G. J., Arnstein, P., Kersey, J. H., Dosik, H., & Parks, W. P. (1973). In vitro cultivation of human tumors: establishment of cell lines derived from a series of solid tumors. *J Natl Cancer Inst*, *51*(5), 1417-1423. <https://doi.org/10.1093/jnci/51.5.1417>
- Goldstraw, P., Chansky, K., Crowley, J., Rami-Porta, R., Asamura, H., Eberhardt, W. E., Nicholson, A. G., Groome, P., Mitchell, A., Bolejack, V., International Association for the Study of Lung Cancer, S., Prognostic Factors Committee, A. B., Participating, I., International Association for the Study of Lung Cancer, S., Prognostic Factors Committee Advisory, B., & Participating, I. (2016). The IASLC Lung Cancer Staging Project: Proposals for Revision of the TNM Stage Groupings in the Forthcoming (Eighth) Edition of the TNM Classification for Lung Cancer. *J Thorac Oncol*, *11*(1), 39-51. <https://doi.org/10.1016/j.jtho.2015.09.009>
- Gorbunova, A. S., Yapyntseva, M. A., Denisenko, T. V., & Zhivotovsky, B. (2020). BNIP3 in Lung Cancer: To Kill or Rescue? *Cancers (Basel)*, *12*(11). <https://doi.org/10.3390/cancers12113390>
- Gottgens, E. L., Ansems, M., Leenders, W. P. J., Bussink, J., & Span, P. N. (2021). Genotyping and Characterization of HPV Status, Hypoxia, and Radiosensitivity in 22 Head and Neck Cancer Cell Lines. *Cancers (Basel)*, *13*(5). <https://doi.org/10.3390/cancers13051069>
- Greaves, M., & Maley, C. C. (2012). Clonal evolution in cancer. *Nature*, *481*(7381), 306-313. <https://doi.org/10.1038/nature10762>
- Griffin, R., & Ramirez, R. A. (2017). Molecular Targets in Non-Small Cell Lung Cancer. *Ochsner J*, *17*(4), 388-392. <https://www.ncbi.nlm.nih.gov/pubmed/29230123>
- Grimm, S. (2004). The art and design of genetic screens: mammalian culture cells. *Nat Rev Genet*, *5*(3), 179-189. <https://doi.org/10.1038/nrg1291>
- Han, K., Jeng, E. E., Hess, G. T., Morgens, D. W., Li, A., & Bassik, M. C. (2017). Synergistic drug combinations for cancer identified in a CRISPR screen for pairwise genetic interactions. *Nat Biotechnol*, *35*(5), 463-474. <https://doi.org/10.1038/nbt.3834>
- Han, Z., Yang, B., Wang, Y., Zeng, X., & Tian, Z. (2021). Identification of Expression Patterns and Potential Prognostic Significance of m(5)C-Related Regulators in Head and Neck Squamous Cell Carcinoma. *Front Oncol*, *11*, 592107. <https://doi.org/10.3389/fonc.2021.592107>
- Hanahan, D., & Folkman, J. (1996). Patterns and emerging mechanisms of the angiogenic switch during tumorigenesis. *Cell*, *86*(3), 353-364. [https://doi.org/10.1016/s0092-8674\(00\)80108-7](https://doi.org/10.1016/s0092-8674(00)80108-7)
- Hanahan, D., & Weinberg, R. A. (2011). Hallmarks of cancer: the next generation. *Cell*, *144*(5), 646-674. <https://doi.org/10.1016/j.cell.2011.02.013>
- Hart, T., Chandrashekhar, M., Aregger, M., Steinhart, Z., Brown, K. R., MacLeod, G., Mis, M., Zimmermann, M., Fradet-Turcotte, A., Sun, S., Mero, P., Dirks, P., Sidhu, S., Roth, F. P., Rissland, O. S., Durocher, D., Angers, S., & Moffat, J. (2015). High-Resolution CRISPR Screens Reveal Fitness Genes and Genotype-Specific Cancer Liabilities. *Cell*, *163*(6), 1515-1526. <https://doi.org/10.1016/j.cell.2015.11.015>
- Hart, T., Tong, A. H. Y., Chan, K., Van Leeuwen, J., Seetharaman, A., Aregger, M., Chandrashekhar, M., Hustedt, N., Seth, S., Noonan, A., Habsid, A., Sizova, O., Nedyalkova, L., Climie, R., Tworzynski, L., Lawson, K., Sartori, M. A., Alibeh, S., Tieu, D., Masud, S., Mero, P., Weiss, A., Brown, K. R., Usaj, M., Billmann, M., Rahman, M., Conzanzo, M., Myers, C. L., Andrews, B. J., Boone, C., Durocher, D., & Moffat, J. (2017). Evaluation and Design of Genome-Wide CRISPR/SpCas9 Knockout Screens. *G3 (Bethesda)*, *7*(8), 2719-2727. <https://doi.org/10.1534/g3.117.041277>

- Hay, A., Migliacci, J., Karassawa Zanoni, D., Boyle, J. O., Singh, B., Wong, R. J., Patel, S. G., & Ganly, I. (2017). Complications following transoral robotic surgery (TORS): A detailed institutional review of complications. *Oral Oncol*, *67*, 160-166. <https://doi.org/10.1016/j.oraloncology.2017.02.022>
- Held, T., Tessonier, T., Franke, H., Regnery, S., Bauer, L., Weusthof, K., Harrabi, S., Herfarth, K., Mairani, A., Debus, J., & Adeberg, S. (2022). Ways to unravel the clinical potential of carbon ions for head and neck cancer reirradiation: dosimetric comparison and local failure pattern analysis as part of the prospective randomized CARE trial. *Radiat Oncol*, *17*(1), 121. <https://doi.org/10.1186/s13014-022-02093-4>
- Held, T., Windisch, P., Akbaba, S., Lang, K., El Shafie, R., Bernhardt, D., Plinkert, P., Kargus, S., Rieken, S., Herfarth, K., Debus, J., & Adeberg, S. (2019). Carbon Ion Reirradiation for Recurrent Head and Neck Cancer: A Single-Institutional Experience. *Int J Radiat Oncol Biol Phys*, *105*(4), 803-811. <https://doi.org/10.1016/j.ijrobp.2019.07.021>
- Herbst, R. S., Morgensztern, D., & Boshoff, C. (2018). The biology and management of non-small cell lung cancer. *Nature*, *553*(7689), 446-454. <https://doi.org/10.1038/nature25183>
- Hessel, F., Petersen, C., Zips, D., Krause, M., Pfitzmann, D., Thames, H. D., & Baumann, M. (2003). Impact of increased cell loss on the repopulation rate during fractionated irradiation in human FaDu squamous cell carcinoma growing in nude mice. *International Journal of Radiation Biology*, *79*(7), 479-486. <https://doi.org/10.1080/0955300031000107871>
- Hsiao, K. C., Chu, P. Y., Chang, G. C., & Liu, K. J. (2020). Elevated Expression of Lumican in Lung Cancer Cells Promotes Bone Metastasis through an Autocrine Regulatory Mechanism. *Cancers (Basel)*, *12*(1). <https://doi.org/10.3390/cancers12010233>
- Hsu, F., De Caluwe, A., Anderson, D., Nichol, A., Toriumi, T., & Ho, C. (2017). Patterns of spread and prognostic implications of lung cancer metastasis in an era of driver mutations. *Curr Oncol*, *24*(4), 228-233. <https://doi.org/10.3747/co.24.3496>
- Hsu, P. D., Lander, E. S., & Zhang, F. (2014). Development and applications of CRISPR-Cas9 for genome engineering. *Cell*, *157*(6), 1262-1278. <https://doi.org/10.1016/j.cell.2014.05.010>
- Huang, A., Garraway, L. A., Ashworth, A., & Weber, B. (2020). Synthetic lethality as an engine for cancer drug target discovery. *Nat Rev Drug Discov*, *19*(1), 23-38. <https://doi.org/10.1038/s41573-019-0046-z>
- Huang, N., Zhu, J., Liu, D., Li, Y. L., Chen, B. J., He, Y. Q., Liu, K., Mo, X. M., & Li, W. M. (2012). Overexpression of Bcl-2-associated death inhibits A549 cell growth in vitro and in vivo. *Cancer Biother Radiopharm*, *27*(2), 164-168. <https://doi.org/10.1089/cbr.2011.1018>
- Ishizuka, J. J., Manguso, R. T., Cheruiyot, C. K., Bi, K., Panda, A., Iracheta-Vellve, A., Miller, B. C., Du, P., Yates, K. B., Dubrot, J., Buchumenski, I., Comstock, D. E., Brown, F. D., Ayer, A., Kohnle, I. C., Pope, H. W., Zimmer, M. D., Sen, D. R., Lane-Reticker, S. K., Robitschek, E. J., Griffin, G. K., Collins, N. B., Long, A. H., Doench, J. G., Kozono, D., Levanon, E. Y., & Haining, W. N. (2019). Loss of ADAR1 in tumours overcomes resistance to immune checkpoint blockade. *Nature*, *565*(7737), 43-48. <https://doi.org/10.1038/s41586-018-0768-9>
- Jakel, O., Schulz-Ertner, D., Karger, C. P., Nikoghosyan, A., & Debus, J. (2003). Heavy ion therapy: status and perspectives. *Technol Cancer Res Treat*, *2*(5), 377-387. <https://doi.org/10.1177/153303460300200503>
- Jansen, R., Embden, J. D., Gaastra, W., & Schouls, L. M. (2002). Identification of genes that are associated with DNA repeats in prokaryotes. *Mol Microbiol*, *43*(6), 1565-1575. <https://doi.org/10.1046/j.1365-2958.2002.02839.x>
- Jinek, M., Chylinski, K., Fonfara, I., Hauer, M., Doudna, J. A., & Charpentier, E. (2012). A programmable dual-RNA-guided DNA endonuclease in adaptive bacterial immunity. *Science*, *337*(6096), 816-821. <https://doi.org/10.1126/science.1225829>
- Jinek, M., East, A., Cheng, A., Lin, S., Ma, E., & Doudna, J. (2013). RNA-programmed genome editing in human cells. *Elife*, *2*, e00471. <https://doi.org/10.7554/eLife.00471>

- Johnson, D. E., Burtneß, B., Leemans, C. R., Lui, V. W. Y., Bauman, J. E., & Grandis, J. R. (2020). Head and neck squamous cell carcinoma. *Nat Rev Dis Primers*, 6(1), 92. <https://doi.org/10.1038/s41572-020-00224-3>
- Jordan, E. J., Kim, H. R., Arcila, M. E., Barron, D., Chakravarty, D., Gao, J., Chang, M. T., Ni, A., Kundra, R., Jonsson, P., Jayakumaran, G., Gao, S. P., Johnsen, H. C., Hanrahan, A. J., Zehir, A., Rekhman, N., Ginsberg, M. S., Li, B. T., Yu, H. A., Paik, P. K., Drilon, A., Hellmann, M. D., Reales, D. N., Benayed, R., Rusch, V. W., Kris, M. G., Chaft, J. E., Baselga, J., Taylor, B. S., Schultz, N., Rudin, C. M., Hyman, D. M., Berger, M. F., Solit, D. B., Ladanyi, M., & Riely, G. J. (2017). Prospective Comprehensive Molecular Characterization of Lung Adenocarcinomas for Efficient Patient Matching to Approved and Emerging Therapies. *Cancer Discov*, 7(6), 596-609. <https://doi.org/10.1158/2159-8290.CD-16-1337>
- Kallini, J. R., Hamed, N., & Khachemoune, A. (2015). Squamous cell carcinoma of the skin: epidemiology, classification, management, and novel trends. *Int J Dermatol*, 54(2), 130-140. <https://doi.org/10.1111/ijd.12553>
- Karger, C. P., & Peschke, P. (2017). RBE and related modeling in carbon-ion therapy. *Phys Med Biol*, 63(1), 01TR02. <https://doi.org/10.1088/1361-6560/aa9102>
- Karpathiou, G., Sivridis, E., Koukourakis, M., Mikroulis, D., Bouros, D., Froudarakis, M., Bougioukas, G., Maltezos, E., & Giatromanolaki, A. (2013). Autophagy and Bcl-2/BNIP3 death regulatory pathway in non-small cell lung carcinomas. *APMIS*, 121(7), 592-604. <https://doi.org/10.1111/apm.12026>
- Katigbak, A., Cencic, R., Robert, F., Senecha, P., Scuoppo, C., & Pelletier, J. (2016). A CRISPR/Cas9 Functional Screen Identifies Rare Tumor Suppressors. *Sci Rep*, 6, 38968. <https://doi.org/10.1038/srep38968>
- Katti, A., Diaz, B. J., Caragine, C. M., Sanjana, N. E., & Dow, L. E. (2022). CRISPR in cancer biology and therapy. *Nat Rev Cancer*, 22(5), 259-279. <https://doi.org/10.1038/s41568-022-00441-w>
- Kim, C. H. (2013). Druggable targets of squamous cell lung cancer. *Tuberc Respir Dis (Seoul)*, 75(6), 231-235. <https://doi.org/10.4046/trd.2013.75.6.231>
- Knoll, M., Waltenberger, M., Bougatf, N., Bernhardt, D., Adeberg, S., Budach, V., Baumann, M., Stuschke, M., Fokas, E., Grosu, A., Zips, D., Belka, C., Combs, S. E., von Deimling, A., Bendszus, M., Wick, W., Unterberg, A., Rieken, S., Debus, J., & Abdollahi, A. (2019). Efficacy of re-irradiation with carbon ions (RiCi) in patients with recurrent high-grade glioma (rHGG) compared to the standard re-irradiation with photons (RiP): The reference multicenter cohort of the German Cancer Consortium Radiation Oncology Group (DKTK-ROG). *Journal of Clinical Oncology*, 37(15_suppl), 2057-2057. https://doi.org/10.1200/JCO.2019.37.15_suppl.2057
- Kondo, T., Ozawa, S., Ikoma, T., Yang, X. Y., Kanamori, K., Suzuki, K., Iwabuchi, H., Maehata, Y., Miyamoto, C., Taguchi, T., Kiyono, T., Kubota, E., & Hata, R. I. (2016). Expression of the chemokine CXCL14 and cetuximab-dependent tumour suppression in head and neck squamous cell carcinoma. *Oncogenesis*, 5(7), e240. <https://doi.org/10.1038/oncsis.2016.43>
- Konings, K., Vandevoorde, C., Baselet, B., Baatout, S., & Moreels, M. (2020). Combination Therapy With Charged Particles and Molecular Targeting: A Promising Avenue to Overcome Radioresistance. *Front Oncol*, 10, 128. <https://doi.org/10.3389/fonc.2020.00128>
- Körber, V., & Höfer, T. (2019). Inferring growth and genetic evolution of tumors from genome sequences. *Current Opinion in Systems Biology*, 16, 1-9. <https://doi.org/https://doi.org/10.1016/j.coisb.2019.10.015>
- Koromilas, A. E., & Sexl, V. (2013). The tumor suppressor function of STAT1 in breast cancer. *JAKSTAT*, 2(2), e23353. <https://doi.org/10.4161/jkst.23353>
- Kozubek, S., & Krasavin, E. A. (1984). Cell sensitivity to irradiation and DNA repair processes. II. The cell sensitivity to ionizing radiation of different LETs. *Neoplasma*, 31(6), 685-695. <https://www.ncbi.nlm.nih.gov/pubmed/6395028>

- Kuhn, M., Santinha, A. J., & Platt, R. J. (2021). Moving from in vitro to in vivo CRISPR screens. *Gene and Genome Editing*, 2, 100008. <https://doi.org/https://doi.org/10.1016/j.ggedit.2021.100008>
- Kwa, M. Q., Herum, K. M., & Brakebusch, C. (2019). Cancer-associated fibroblasts: how do they contribute to metastasis? *Clin Exp Metastasis*, 36(2), 71-86. <https://doi.org/10.1007/s10585-019-09959-0>
- Lan, Y., Moustafa, M., Knoll, M., Xu, C., Furkel, J., Lazorchak, A., Yeung, T. L., Hasheminasab, S. M., Jenkins, M. H., Meister, S., Yu, H., Schlegel, J., Marelli, B., Tang, Z., Qin, G., Klein, C., Qi, J., Zhou, C., Locke, G., Kronic, D., Derner, M. G., Schwager, C., Fontana, R. E., Kriegsmann, K., Jiang, F., Rein, K., Kriegsmann, M., Debus, J., Lo, K. M., & Abdollahi, A. (2021). Simultaneous targeting of TGF-beta/PD-L1 synergizes with radiotherapy by reprogramming the tumor microenvironment to overcome immune evasion. *Cancer Cell*, 39(10), 1388-1403 e1310. <https://doi.org/10.1016/j.ccell.2021.08.008>
- Langendijk, J. A., Doornaert, P., Verdonck-de Leeuw, I. M., Leemans, C. R., Aaronson, N. K., & Slotman, B. J. (2008). Impact of late treatment-related toxicity on quality of life among patients with head and neck cancer treated with radiotherapy. *J Clin Oncol*, 26(22), 3770-3776. <https://doi.org/10.1200/JCO.2007.14.6647>
- Lehmann, B., Biburger, M., Bruckner, C., Ipsen-Escobedo, A., Gordan, S., Lehmann, C., Voehringer, D., Winkler, T., Schaft, N., Dudziak, D., Sirbu, H., Weber, G. F., & Nimmerjahn, F. (2017). Tumor location determines tissue-specific recruitment of tumor-associated macrophages and antibody-dependent immunotherapy response. *Sci Immunol*, 2(7). <https://doi.org/10.1126/sciimmunol.aah6413>
- Li, W., Xu, H., Xiao, T., Cong, L., Love, M. I., Zhang, F., Irizarry, R. A., Liu, J. S., Brown, M., & Liu, X. S. (2014). MAGECK enables robust identification of essential genes from genome-scale CRISPR/Cas9 knockout screens. *Genome Biol*, 15(12), 554. <https://doi.org/10.1186/s13059-014-0554-4>
- Li, Y., Wu, T., Gong, S., Zhou, H., Yu, L., Liang, M., Shi, R., Wu, Z., Zhang, J., & Li, S. (2020). Analysis of the Prognosis and Therapeutic Value of the CXC Chemokine Family in Head and Neck Squamous Cell Carcinoma. *Front Oncol*, 10, 570736. <https://doi.org/10.3389/fonc.2020.570736>
- Liang, S., Zhou, G., & Hu, W. (2022). Research Progress of Heavy Ion Radiotherapy for Non-Small-Cell Lung Cancer. *Int J Mol Sci*, 23(4). <https://doi.org/10.3390/ijms23042316>
- Lieber, M. R. (2010). The mechanism of double-strand DNA break repair by the nonhomologous DNA end-joining pathway. *Annu Rev Biochem*, 79, 181-211. <https://doi.org/10.1146/annurev.biochem.052308.093131>
- Lisec, J., Kobelt, D., Walther, W., Mokrizkij, M., Grotzinger, C., Jaeger, C., Baum, K., Simon, M., Wolf, J., Beindorff, N., Brenner, W., & Stein, U. (2021). Systematic Identification of MACC1-Driven Metabolic Networks in Colorectal Cancer. *Cancers (Basel)*, 13(5). <https://doi.org/10.3390/cancers13050978>
- Love, M. I., Huber, W., & Anders, S. (2014). Moderated estimation of fold change and dispersion for RNA-seq data with DESeq2. *Genome Biol*, 15(12), 550. <https://doi.org/10.1186/s13059-014-0550-8>
- Ma, Y. C., Tian, P. F., Chen, Z. P., Yue, D. S., Liu, C. C., Li, C. G., Chen, C., Zhang, H., Liu, H. L., Zhang, Z. F., Chen, L., Zhang, B., & Wang, C. L. (2021). Urinary malate dehydrogenase 2 is a new biomarker for early detection of non-small-cell lung cancer. *Cancer Sci*, 112(6), 2349-2360. <https://doi.org/10.1111/cas.14845>
- Machtay, M., Moughan, J., Trotti, A., Garden, A. S., Weber, R. S., Cooper, J. S., Forastiere, A., & Ang, K. K. (2008). Factors associated with severe late toxicity after concurrent chemoradiation for locally advanced head and neck cancer: an RTOG analysis. *J Clin Oncol*, 26(21), 3582-3589. <https://doi.org/10.1200/JCO.2007.14.8841>
- Mallela, K., & Kumar, A. (2021). Role of TSC1 in physiology and diseases. *Mol Cell Biochem*, 476(6), 2269-2282. <https://doi.org/10.1007/s11010-021-04088-3>

- Marfil, V., Blazquez, M., Serrano, F., Castell, J. V., & Bort, R. (2015). Growth-promoting and tumorigenic activity of c-Myc is suppressed by Hhex. *Oncogene*, *34*(23), 3011-3022. <https://doi.org/10.1038/onc.2014.240>
- Matassa, D. S., Agliarulo, I., Avolio, R., Landriscina, M., & Esposito, F. (2018). TRAP1 Regulation of Cancer Metabolism: Dual Role as Oncogene or Tumor Suppressor. *Genes (Basel)*, *9*(4). <https://doi.org/10.3390/genes9040195>
- McVey, M., & Lee, S. E. (2008). MMEJ repair of double-strand breaks (director's cut): deleted sequences and alternative endings. *Trends Genet*, *24*(11), 529-538. <https://doi.org/10.1016/j.tig.2008.08.007>
- Milicevic, N. M., Nohroudi, K., Milicevic, Z., Hedrich, H. J., & Westermann, J. (2005). T cells are required for the peripheral phase of B-cell maturation. *Immunology*, *116*(3), 308-317. <https://doi.org/10.1111/j.1365-2567.2005.02226.x>
- Miller, T. E., Liao, B. B., Wallace, L. C., Morton, A. R., Xie, Q., Dixit, D., Factor, D. C., Kim, L. J. Y., Morrow, J. J., Wu, Q., Mack, S. C., Hubert, C. G., Gillespie, S. M., Flavahan, W. A., Hoffmann, T., Thummalapalli, R., Hemann, M. T., Paddison, P. J., Horbinski, C. M., Zuber, J., Scacheri, P. C., Bernstein, B. E., Tesar, P. J., & Rich, J. N. (2017). Transcription elongation factors represent in vivo cancer dependencies in glioblastoma. *Nature*, *547*(7663), 355-359. <https://doi.org/10.1038/nature23000>
- Mirghani, H., & Blanchard, P. (2018). Treatment de-escalation for HPV-driven oropharyngeal cancer: Where do we stand? *Clin Transl Radiat Oncol*, *8*, 4-11. <https://doi.org/10.1016/j.ctro.2017.10.005>
- Mizoe, J. E., Hasegawa, A., Jingu, K., Takagi, R., Bessyo, H., Morikawa, T., Tonoki, M., Tsuji, H., Kamada, T., Tsujii, H., Okamoto, Y., & Organizing Committee for the Working Group for Head Neck, C. (2012). Results of carbon ion radiotherapy for head and neck cancer. *Radiother Oncol*, *103*(1), 32-37. <https://doi.org/10.1016/j.radonc.2011.12.013>
- Mohamad, O., Sishc, B. J., Saha, J., Pompos, A., Rahimi, A., Story, M. D., Davis, A. J., & Kim, D. W. N. (2017). Carbon Ion Radiotherapy: A Review of Clinical Experiences and Preclinical Research, with an Emphasis on DNA Damage/Repair. *Cancers (Basel)*, *9*(6). <https://doi.org/10.3390/cancers9060066>
- Moreno, T., Monterde, B., Gonzalez-Silva, L., Betancor-Fernandez, I., Revilla, C., Agraz-Doblas, A., Freire, J., Isidro, P., Quevedo, L., Blanco, R., Montes-Moreno, S., Cereceda, L., Astudillo, A., Casar, B., Crespo, P., Morales Torres, C., Scaffidi, P., Gomez-Roman, J., Salido, E., & Varela, I. (2021). ARID2 deficiency promotes tumor progression and is associated with higher sensitivity to chemotherapy in lung cancer. *Oncogene*, *40*(16), 2923-2935. <https://doi.org/10.1038/s41388-021-01748-y>
- Nakayama, Y., Mimura, K., Tamaki, T., Shiraishi, K., Kua, L. F., Koh, V., Ohmori, M., Kimura, A., Inoue, S., Okayama, H., Suzuki, Y., Nakazawa, T., Ichikawa, D., & Kono, K. (2019). PhosphoSTAT1 expression as a potential biomarker for antiPD1/antiPDL1 immunotherapy for breast cancer. *Int J Oncol*, *54*(6), 2030-2038. <https://doi.org/10.3892/ijo.2019.4779>
- Nichols, A. C., Yoo, J., Palma, D. A., Fung, K., Franklin, J. H., Koropatnick, J., Mymryk, J. S., Batada, N. N., & Barrett, J. W. (2012). Frequent mutations in TP53 and CDKN2A found by next-generation sequencing of head and neck cancer cell lines. *Arch Otolaryngol Head Neck Surg*, *138*(8), 732-739. <https://doi.org/10.1001/archoto.2012.1558>
- Nie, C., Qin, X., Li, X., Tian, B., Zhao, Y., Jin, Y., Li, Y., Wang, Q., Zeng, D., Hong, A., & Chen, X. (2019). CACNA2D3 Enhances the Chemosensitivity of Esophageal Squamous Cell Carcinoma to Cisplatin via Inducing Ca(2+)-Mediated Apoptosis and Suppressing PI3K/Akt Pathways. *Front Oncol*, *9*, 185. <https://doi.org/10.3389/fonc.2019.00185>
- Nikas, I. P., Themistocleous, S. C., Paschou, S. A., Tsamis, K. I., & Ryu, H. S. (2019). Serine-Arginine Protein Kinase 1 (SRPK1) as a Prognostic Factor and Potential Therapeutic Target in Cancer: Current Evidence and Future Perspectives. *Cells*, *9*(1). <https://doi.org/10.3390/cells9010019>
- Ohguchi, Y., & Ohguchi, H. (2022). Diverse Functions of KDM5 in Cancer: Transcriptional Repressor or Activator? *Cancers (Basel)*, *14*(13). <https://doi.org/10.3390/cancers14133270>

- Ono, T., Yamamoto, N., Nomoto, A., Nakajima, M., Isozaki, Y., Kasuya, G., Ishikawa, H., Nemoto, K., & Tsuji, H. (2020). Long Term Results of Single-Fraction Carbon-Ion Radiotherapy for Non-small Cell Lung Cancer. *Cancers (Basel)*, 13(1). <https://doi.org/10.3390/cancers13010112>
- Park, S., Lim, J. M., Chun, J. N., Lee, S., Kim, T. M., Kim, D. W., Kim, S. Y., Bae, D. J., Bae, S. M., So, I., Kim, H. G., Choi, J. Y., & Jeon, J. H. (2020). Altered expression of fucosylation pathway genes is associated with poor prognosis and tumor metastasis in nonsmall cell lung cancer. *Int J Oncol*, 56(2), 559-567. <https://doi.org/10.3892/ijo.2019.4953>
- Patel, A. P., Tirosh, I., Trombetta, J. J., Shalek, A. K., Gillespie, S. M., Wakimoto, H., Cahill, D. P., Nahed, B. V., Curry, W. T., Martuza, R. L., Louis, D. N., Rozenblatt-Rosen, O., Suva, M. L., Regev, A., & Bernstein, B. E. (2014). Single-cell RNA-seq highlights intratumoral heterogeneity in primary glioblastoma. *Science*, 344(6190), 1396-1401. <https://doi.org/10.1126/science.1254257>
- Patel, S. J., Sanjana, N. E., Kishton, R. J., Eidizadeh, A., Vodnala, S. K., Cam, M., Gartner, J. J., Jia, L., Steinberg, S. M., Yamamoto, T. N., Merchant, A. S., Mehta, G. U., Chichura, A., Shalem, O., Tran, E., Eil, R., Sukumar, M., Guijarro, E. P., Day, C. P., Robbins, P., Feldman, S., Merlino, G., Zhang, F., & Restifo, N. P. (2017). Identification of essential genes for cancer immunotherapy. *Nature*, 548(7669), 537-542. <https://doi.org/10.1038/nature23477>
- Pignon, J. P., le Maitre, A., Maillard, E., Bourhis, J., & Group, M.-N. C. (2009). Meta-analysis of chemotherapy in head and neck cancer (MACH-NC): an update on 93 randomised trials and 17,346 patients. *Radiother Oncol*, 92(1), 4-14. <https://doi.org/10.1016/j.radonc.2009.04.014>
- Pinon, J. D., Labi, V., Egle, A., & Villunger, A. (2008). Bim and Bmf in tissue homeostasis and malignant disease. *Oncogene*, 27 Suppl 1, S41-52. <https://doi.org/10.1038/onc.2009.42>
- Platt, R. J., Chen, S., Zhou, Y., Yim, M. J., Swiech, L., Kempton, H. R., Dahlman, J. E., Parnas, O., Eisenhaure, T. M., Jovanovic, M., Graham, D. B., Jhunjhunwala, S., Heidenreich, M., Xavier, R. J., Langer, R., Anderson, D. G., Hacohen, N., Regev, A., Feng, G., Sharp, P. A., & Zhang, F. (2014). CRISPR-Cas9 knockin mice for genome editing and cancer modeling. *Cell*, 159(2), 440-455. <https://doi.org/10.1016/j.cell.2014.09.014>
- Plch, J., Hrabeta, J., & Eckschlager, T. (2019). KDM5 demethylases and their role in cancer cell chemoresistance. *Int J Cancer*, 144(2), 221-231. <https://doi.org/10.1002/ijc.31881>
- Prior, I. A., Lewis, P. D., & Mattos, C. (2012). A comprehensive survey of Ras mutations in cancer. *Cancer Res*, 72(10), 2457-2467. <https://doi.org/10.1158/0008-5472.CAN-11-2612>
- Przybyla, L., & Gilbert, L. A. (2022). A new era in functional genomics screens. *Nat Rev Genet*, 23(2), 89-103. <https://doi.org/10.1038/s41576-021-00409-w>
- Quail, D. F., & Joyce, J. A. (2013). Microenvironmental regulation of tumor progression and metastasis. *Nat Med*, 19(11), 1423-1437. <https://doi.org/10.1038/nm.3394>
- Rackwitz, T., & Debus, J. (2019). Clinical applications of proton and carbon ion therapy. *Semin Oncol*, 46(3), 226-232. <https://doi.org/10.1053/j.seminoncol.2019.07.005>
- Rangan, S. R. (1972). A new human cell line (FaDu) from a hypopharyngeal carcinoma. *Cancer*, 29(1), 117-121. [https://doi.org/10.1002/1097-0142\(197201\)29:1<117::aid-cncr2820290119>3.0.co;2-r](https://doi.org/10.1002/1097-0142(197201)29:1<117::aid-cncr2820290119>3.0.co;2-r)
- Rettig, E. M., & D'Souza, G. (2015). Epidemiology of head and neck cancer. *Surg Oncol Clin N Am*, 24(3), 379-396. <https://doi.org/10.1016/j.soc.2015.03.001>
- Ringborg, U., Bergqvist, D., Brorsson, B., Cavallin-Stahl, E., Ceberg, J., Einhorn, N., Frodin, J. E., Jarhult, J., Lamnevik, G., Lindholm, C., Littbrand, B., Norlund, A., Nylen, U., Rosen, M., Svensson, H., & Moller, T. R. (2003). The Swedish Council on Technology Assessment in Health Care (SBU) systematic overview of radiotherapy for cancer including a prospective survey of radiotherapy practice in Sweden 2001--summary and conclusions. *Acta Oncol*, 42(5-6), 357-365. <https://doi.org/10.1080/02841860310010826>
- Rockwell, S., Dobrucki, I. T., Kim, E. Y., Marrison, S. T., & Vu, V. T. (2009). Hypoxia and radiation therapy: past history, ongoing research, and future promise. *Curr Mol Med*, 9(4), 442-458. <https://doi.org/10.2174/156652409788167087>

- Roeser, J. C., Leach, S. D., & McAllister, F. (2015). Emerging strategies for cancer immunoprevention. *Oncogene*, 34(50), 6029-6039. <https://doi.org/10.1038/onc.2015.98>
- Rosenthal, D. I., Mendoza, T. R., Fuller, C. D., Hutcheson, K. A., Wang, X. S., Hanna, E. Y., Lu, C., Garden, A. S., Morrison, W. H., Cleeland, C. S., & Gunn, G. B. (2014). Patterns of symptom burden during radiotherapy or concurrent chemoradiotherapy for head and neck cancer: a prospective analysis using the University of Texas MD Anderson Cancer Center Symptom Inventory-Head and Neck Module. *Cancer*, 120(13), 1975-1984. <https://doi.org/10.1002/cncr.28672>
- Roses, R. E., Xu, M., Koski, G. K., & Czerniecki, B. J. (2008). Radiation therapy and Toll-like receptor signaling: implications for the treatment of cancer. *Oncogene*, 27(2), 200-207. <https://doi.org/10.1038/sj.onc.1210909>
- San Filippo, J., Sung, P., & Klein, H. (2008). Mechanism of eukaryotic homologous recombination. *Annu Rev Biochem*, 77, 229-257. <https://doi.org/10.1146/annurev.biochem.77.061306.125255>
- Sander, J. D., & Joung, J. K. (2014). CRISPR-Cas systems for editing, regulating and targeting genomes. *Nat Biotechnol*, 32(4), 347-355. <https://doi.org/10.1038/nbt.2842>
- Sanjana, N. E., Shalem, O., & Zhang, F. (2014). Improved vectors and genome-wide libraries for CRISPR screening. *Nat Methods*, 11(8), 783-784. <https://doi.org/10.1038/nmeth.3047>
- Sanjana, N. E., Wright, J., Zheng, K., Shalem, O., Fontanillas, P., Joung, J., Cheng, C., Regev, A., & Zhang, F. (2016). High-resolution interrogation of functional elements in the noncoding genome. *Science*, 353(6307), 1545-1549. <https://doi.org/10.1126/science.aaf7613>
- Sanson, K. R., Hanna, R. E., Hegde, M., Donovan, K. F., Strand, C., Sullender, M. E., Vaimberg, E. W., Goodale, A., Root, D. E., Piccioni, F., & Doench, J. G. (2018). Optimized libraries for CRISPR-Cas9 genetic screens with multiple modalities. *Nat Commun*, 9(1), 5416. <https://doi.org/10.1038/s41467-018-07901-8>
- Schaub, L., Harrabi, S. B., & Debus, J. (2020). Particle therapy in the future of precision therapy. *Br J Radiol*, 93(1114), 20200183. <https://doi.org/10.1259/bjr.20200183>
- Shalem, O., Sanjana, N. E., Hartenian, E., Shi, X., Scott, D. A., Mikkelsen, T., Heckl, D., Ebert, B. L., Root, D. E., Doench, J. G., & Zhang, F. (2014). Genome-scale CRISPR-Cas9 knockout screening in human cells. *Science*, 343(6166), 84-87. <https://doi.org/10.1126/science.1247005>
- Sharma, R., Buitrago, S., Pitoniak, R., Gibbs, J. F., Curtin, L., Seshadri, M., Repasky, E. A., & Hylander, B. L. (2014). Influence of the implantation site on the sensitivity of patient pancreatic tumor xenografts to Apo2L/TRAIL therapy. *Pancreas*, 43(2), 298-305. <https://doi.org/10.1097/MPA.0000000000000099>
- Shi, H., Doench, J. G., & Chi, H. (2022). CRISPR screens for functional interrogation of immunity. *Nat Rev Immunol*. <https://doi.org/10.1038/s41577-022-00802-4>
- Shirvani, S. M., Jiang, J., Chang, J. Y., Welsh, J., Likhacheva, A., Buchholz, T. A., Swisher, S. G., & Smith, B. D. (2014). Lobectomy, sublobar resection, and stereotactic ablative radiotherapy for early-stage non-small cell lung cancers in the elderly. *JAMA Surg*, 149(12), 1244-1253. <https://doi.org/10.1001/jamasurg.2014.556>
- Siegel, R. L., Miller, K. D., & Jemal, A. (2018). Cancer statistics, 2018. *CA Cancer J Clin*, 68(1), 7-30. <https://doi.org/10.3322/caac.21442>
- Skoulidis, F., & Heymach, J. V. (2019). Co-occurring genomic alterations in non-small-cell lung cancer biology and therapy. *Nat Rev Cancer*, 19(9), 495-509. <https://doi.org/10.1038/s41568-019-0179-8>
- Sorek, R., Lawrence, C. M., & Wiedenheft, B. (2013). CRISPR-mediated adaptive immune systems in bacteria and archaea. *Annu Rev Biochem*, 82, 237-266. <https://doi.org/10.1146/annurev-biochem-072911-172315>
- Sorensen, B. S., Pawelke, J., Bauer, J., Burnet, N. G., Dasu, A., Hoyer, M., Karger, C. P., Krause, M., Schwarz, M., Underwood, T. S. A., Wagenaar, D., Whitfield, G. A., & Luhr, A. (2021). Does the uncertainty in relative biological effectiveness affect patient treatment in proton therapy? *Radiother Oncol*, 163, 177-184. <https://doi.org/10.1016/j.radonc.2021.08.016>

- Soria, J. C., Ohe, Y., Vansteenkiste, J., Reungwetwattana, T., Chewaskulyong, B., Lee, K. H., Dechaphunkul, A., Imamura, F., Nogami, N., Kurata, T., Okamoto, I., Zhou, C., Cho, B. C., Cheng, Y., Cho, E. K., Voon, P. J., Planchard, D., Su, W. C., Gray, J. E., Lee, S. M., Hodge, R., Marotti, M., Rukazenkov, Y., Ramalingam, S. S., & Investigators, F. (2018). Osimertinib in Untreated EGFR-Mutated Advanced Non-Small-Cell Lung Cancer. *N Engl J Med*, *378*(2), 113-125. <https://doi.org/10.1056/NEJMoa1713137>
- Sternberg, S. H., Redding, S., Jinek, M., Greene, E. C., & Doudna, J. A. (2014). DNA interrogation by the CRISPR RNA-guided endonuclease Cas9. *Nature*, *507*(7490), 62-67. <https://doi.org/10.1038/nature13011>
- Stracker, T. H., & Petrini, J. H. (2011). The MRE11 complex: starting from the ends. *Nat Rev Mol Cell Biol*, *12*(2), 90-103. <https://doi.org/10.1038/nrm3047>
- Sun, Y., Zhang, Q., Yao, L., Wang, S., & Zhang, Z. (2020). Comprehensive analysis reveals novel gene signature in head and neck squamous cell carcinoma: predicting is associated with poor prognosis in patients. *Transl Cancer Res*, *9*(10), 5882-5892. <https://doi.org/10.21037/tcr-20-805>
- Tai, A. L., Mak, W., Ng, P. K., Chua, D. T., Ng, M. Y., Fu, L., Chu, K. K., Fang, Y., Qiang Song, Y., Chen, M., Zhang, M., Sham, P. C., & Guan, X. Y. (2006). High-throughput loss-of-heterozygosity study of chromosome 3p in lung cancer using single-nucleotide polymorphism markers. *Cancer Res*, *66*(8), 4133-4138. <https://doi.org/10.1158/0008-5472.CAN-05-2775>
- Takahashi, D., Demizu, Y., Koto, M., Kubo, N., Suefuji, H., Ikawa, H., Ohno, T., Shioyama, Y., Okimoto, T., Tsuji, H., & Japan Carbon-Ion Radiation Oncology Study, G. (2022). Multicenter study of re-irradiation using carbon-ions for head and neck malignancies after photon radiotherapy. *Cancer Med*, *11*(19), 3593-3601. <https://doi.org/10.1002/cam4.4741>
- Tate, J. G., Bamford, S., Jubb, H. C., Sondka, Z., Beare, D. M., Bindal, N., Boutselakis, H., Cole, C. G., Creatore, C., Dawson, E., Fish, P., Harsha, B., Hathaway, C., Jupe, S. C., Kok, C. Y., Noble, K., Ponting, L., Ramshaw, C. C., Rye, C. E., Speedy, H. E., Stefancsik, R., Thompson, S. L., Wang, S., Ward, S., Campbell, P. J., & Forbes, S. A. (2019). COSMIC: the Catalogue Of Somatic Mutations In Cancer. *Nucleic Acids Res*, *47*(D1), D941-D947. <https://doi.org/10.1093/nar/gky1015>
- Tauriello, D. V. F., Sancho, E., & Batlle, E. (2022). Overcoming TGFbeta-mediated immune evasion in cancer. *Nat Rev Cancer*, *22*(1), 25-44. <https://doi.org/10.1038/s41568-021-00413-6>
- Tawk, B., Debus, J., & Abdollahi, A. (2021). Evolution of a Paradigm Switch in Diagnosis and Treatment of HPV-Driven Head and Neck Cancer-Striking the Balance Between Toxicity and Cure. *Front Pharmacol*, *12*, 753387. <https://doi.org/10.3389/fphar.2021.753387>
- Tawk, B., Wirkner, U., Schwager, C., Rein, K., Zaoui, K., Federspil, P. A., Adeberg, S., Linge, A., Ganswindt, U., Hess, J., Unger, K., Tinhofer, I., Budach, V., Lohaus, F., Krause, M., Guberina, M., Stuschke, M., Balermipas, P., Rodel, C., Grosu, A. L., Schafer, H., Zips, D., Combs, S. E., Pigorsch, S., Zitzelsberger, H., Baumeister, P., Kirchner, T., Bewerunge-Hudler, M., Weichert, W., Hess, J., Herpel, E., Belka, C., Baumann, M., Debus, J., Abdollahi, A., & Dtkk, R. O. G. (2022). Tumor DNA-methylome derived epigenetic fingerprint identifies HPV-negative head and neck patients at risk for locoregional recurrence after postoperative radiochemotherapy. *Int J Cancer*, *150*(4), 603-616. <https://doi.org/10.1002/ijc.33842>
- Thames, H. D., Bentzen, S. M., Turesson, I., Overgaard, M., & Van den Bogaert, W. (1990). Time-dose factors in radiotherapy: a review of the human data. *Radiother Oncol*, *19*(3), 219-235. [https://doi.org/10.1016/0167-8140\(90\)90149-q](https://doi.org/10.1016/0167-8140(90)90149-q)
- Thomas, L. R., Adams, C. M., Wang, J., Weissmiller, A. M., Creighton, J., Lorey, S. L., Liu, Q., Fesik, S. W., Eischen, C. M., & Tansey, W. P. (2019). Interaction of the oncoprotein transcription factor MYC with its chromatin cofactor WDR5 is essential for tumor maintenance. *Proc Natl Acad Sci U S A*, *116*(50), 25260-25268. <https://doi.org/10.1073/pnas.1910391116>
- Tinganelli, W., Durante, M., Hirayama, R., Kramer, M., Maier, A., Kraft-Weyrather, W., Furusawa, Y., Friedrich, T., & Scifoni, E. (2015). Kill-painting of hypoxic tumours in charged particle therapy. *Sci Rep*, *5*, 17016. <https://doi.org/10.1038/srep17016>

- van Buuren, S., & Groothuis-Oudshoorn, K. (2011). mice: Multivariate Imputation by Chained Equations in R. *Journal of Statistical Software*, 45(3), 1 - 67. <https://doi.org/10.18637/jss.v045.i03>
- Verhoeven, Y., Tilborghs, S., Jacobs, J., De Waele, J., Quatannens, D., Deben, C., Prenen, H., Pauwels, P., Trinh, X. B., Wouters, A., Smits, E. L. J., Lardon, F., & van Dam, P. A. (2020). The potential and controversy of targeting STAT family members in cancer. *Semin Cancer Biol*, 60, 41-56. <https://doi.org/10.1016/j.semcancer.2019.10.002>
- Wang, Z., Li, Z., Wu, C., Wang, Y., Xia, Y., Chen, L., Zhu, Q., & Chen, Y. (2014). MACC1 overexpression predicts a poor prognosis for non-small cell lung cancer. *Med Oncol*, 31(1), 790. <https://doi.org/10.1007/s12032-013-0790-6>
- Weber, U., & Kraft, G. (2009). Comparison of carbon ions versus protons. *Cancer J*, 15(4), 325-332. <https://doi.org/10.1097/PPO.0b013e3181b01935>
- Weiner 3rd J, Domaszewska T. 2016. tmod: an R package for general and multivariate enrichment analysis. PeerJ Preprints 4:e2420v1 <https://doi.org/10.7287/peerj.preprints.2420v1>
- Westrich, J. A., Vermeer, D. W., Silva, A., Bonney, S., Berger, J. N., Cicchini, L., Greer, R. O., Song, J. I., Raben, D., Slansky, J. E., Lee, J. H., Spanos, W. C., & Pyeon, D. (2019). CXCL14 suppresses human papillomavirus-associated head and neck cancer through antigen-specific CD8(+) T-cell responses by upregulating MHC-I expression. *Oncogene*, 38(46), 7166-7180. <https://doi.org/10.1038/s41388-019-0911-6>
- Williams, M. J., Sottoriva, A., & Graham, T. A. (2019). Measuring Clonal Evolution in Cancer with Genomics. *Annu Rev Genomics Hum Genet*, 20, 309-329. <https://doi.org/10.1146/annurev-genom-083117-021712>
- Winters, I. P., Murray, C. W., & Winslow, M. M. (2018). Towards quantitative and multiplexed in vivo functional cancer genomics. *Nat Rev Genet*, 19(12), 741-755. <https://doi.org/10.1038/s41576-018-0053-7>
- Woodard, G. A., Jones, K. D., & Jablons, D. M. (2016). Lung Cancer Staging and Prognosis. *Cancer Treat Res*, 170, 47-75. https://doi.org/10.1007/978-3-319-40389-2_3
- Wu, Y. L., Tsuboi, M., He, J., John, T., Grohe, C., Majem, M., Goldman, J. W., Laktionov, K., Kim, S. W., Kato, T., Vu, H. V., Lu, S., Lee, K. Y., Akewanlop, C., Yu, C. J., de Marinis, F., Bonanno, L., Domine, M., Shepherd, F. A., Zeng, L., Hodge, R., Atasoy, A., Rukazenzov, Y., Herbst, R. S., & Investigators, A. (2020). Osimertinib in Resected EGFR-Mutated Non-Small-Cell Lung Cancer. *N Engl J Med*, 383(18), 1711-1723. <https://doi.org/10.1056/NEJMoa2027071>
- Wu, Z., Yang, H., & Colosi, P. (2010). Effect of genome size on AAV vector packaging. *Mol Ther*, 18(1), 80-86. <https://doi.org/10.1038/mt.2009.255>
- Xue, W., Chen, S., Yin, H., Tammela, T., Papagiannakopoulos, T., Joshi, N. S., Cai, W., Yang, G., Bronson, R., Crowley, D. G., Zhang, F., Anderson, D. G., Sharp, P. A., & Jacks, T. (2014). CRISPR-mediated direct mutation of cancer genes in the mouse liver. *Nature*, 514(7522), 380-384. <https://doi.org/10.1038/nature13589>
- Yamamoto-Hino, M., & Goto, S. (2013). In Vivo RNAi-Based Screens: Studies in Model Organisms. *Genes (Basel)*, 4(4), 646-665. <https://doi.org/10.3390/genes4040646>
- Yan, H., He, D., Huang, X., Zhang, E., Chen, Q., Xu, R., Liu, X., Zi, F., & Cai, Z. (2018). Role of interleukin-32 in cancer biology. *Oncol Lett*, 16(1), 41-47. <https://doi.org/10.3892/ol.2018.8649>
- Yang, C. T., Li, J. M., Chu, W. K., & Chow, S. E. (2018). Downregulation of lumican accelerates lung cancer cell invasion through p120 catenin. *Cell Death Dis*, 9(4), 414. <https://doi.org/10.1038/s41419-017-0212-3>
- Yau, E. H., Kummetha, I. R., Lichinchi, G., Tang, R., Zhang, Y., & Rana, T. M. (2017). Genome-Wide CRISPR Screen for Essential Cell Growth Mediators in Mutant KRAS Colorectal Cancers. *Cancer Res*, 77(22), 6330-6339. <https://doi.org/10.1158/0008-5472.CAN-17-2043>
- Yu, G., Herazo-Maya, J. D., Nukui, T., Romkes, M., Parwani, A., Juan-Guardela, B. M., Robertson, J., Gauldie, J., Siegfried, J. M., Kaminski, N., & Kass, D. J. (2014). Matrix metalloproteinase-19 promotes metastatic behavior in vitro and is associated with increased mortality in non-small

- cell lung cancer. *Am J Respir Crit Care Med*, 190(7), 780-790.
<https://doi.org/10.1164/rccm.201310-1903OC>
- Yu, H., Pardoll, D., & Jove, R. (2009). STATs in cancer inflammation and immunity: a leading role for STAT3. *Nat Rev Cancer*, 9(11), 798-809. <https://doi.org/10.1038/nrc2734>
- Yu, Y. P., Cai, L. C., Wang, X. Y., Cheng, S. Y., Zhang, D. M., Jian, W. G., Wang, T. D., Yang, J. K., Yang, K. B., & Zhang, C. (2020). BMP8A promotes survival and drug resistance via Nrf2/TRIM24 signaling pathway in clear cell renal cell carcinoma. *Cancer Sci*, 111(5), 1555-1566.
<https://doi.org/10.1111/cas.14376>
- Zhang, J., Fujimoto, J., Zhang, J., Wedge, D. C., Song, X., Zhang, J., Seth, S., Chow, C. W., Cao, Y., Gumbs, C., Gold, K. A., Kalhor, N., Little, L., Mahadeshwar, H., Moran, C., Protopopov, A., Sun, H., Tang, J., Wu, X., Ye, Y., William, W. N., Lee, J. J., Heymach, J. V., Hong, W. K., Swisher, S., Wistuba, II, & Futreal, P. A. (2014). Intratumor heterogeneity in localized lung adenocarcinomas delineated by multiregion sequencing. *Science*, 346(6206), 256-259.
<https://doi.org/10.1126/science.1256930>
- Zhang, J., Si, J., Gan, L., Zhou, R., Guo, M., & Zhang, H. (2021). Harnessing the targeting potential of differential radiobiological effects of photon versus particle radiation for cancer treatment. *J Cell Physiol*, 236(3), 1695-1711. <https://doi.org/10.1002/jcp.29960>
- Zhang, J. P., Li, X. L., Li, G. H., Chen, W., Arakaki, C., Botimer, G. D., Baylink, D., Zhang, L., Wen, W., Fu, Y. W., Xu, J., Chun, N., Yuan, W., Cheng, T., & Zhang, X. B. (2017). Efficient precise knockin with a double cut HDR donor after CRISPR/Cas9-mediated double-stranded DNA cleavage. *Genome Biol*, 18(1), 35. <https://doi.org/10.1186/s13059-017-1164-8>
- Zhou, C., Jones, B., Moustafa, M., Yang, B., Brons, S., Cao, L., Dai, Y., Schwager, C., Chen, M., Jaekel, O., Chen, L., Debus, J., & Abdollahi, A. (2019). Determining RBE for development of lung fibrosis induced by fractionated irradiation with carbon ions utilizing fibrosis index and high-LET BED model. *Clin Transl Radiat Oncol*, 14, 25-32.
<https://doi.org/10.1016/j.ctro.2018.10.005>
- Zhu, L. M., Shi, D. M., Dai, Q., Cheng, X. J., Yao, W. Y., Sun, P. H., Ding, Y., Qiao, M. M., Wu, Y. L., Jiang, S. H., & Tu, S. P. (2014). Tumor suppressor XAF1 induces apoptosis, inhibits angiogenesis and inhibits tumor growth in hepatocellular carcinoma. *Oncotarget*, 5(14), 5403-5415.
<https://doi.org/10.18632/oncotarget.2114>

Thesis related publications

[Differential transcriptome response to proton versus X-ray radiation reveals novel candidate targets for combinatorial PT therapy in lymphoma.](#)

Sertorio M, Nowrouzi A, **Akbarpour M**, Chetal K, Salomonis N, Brons S, Mascia A, Ionascu D, McCauley S, Kupneski T, Köthe A, Debus J, Perentesis JP, Abdollahi A, Zheng Y, Wells SI. *Radiother Oncol.* 2021 Feb;155:293-303. doi: 10.1016/j.radonc.2020.10.024. Epub 2020 Oct 20. PMID: 33096164

[Personalized Assessment of Normal Tissue Radiosensitivity via Transcriptome Response to Photon, Proton and Carbon Irradiation in Patient-Derived Human Intestinal Organoids.](#)

Nowrouzi A, Sertorio MG, **Akbarpour M**, Knoll M, Krunic D, Kuhar M, Schwager C, Brons S, Debus J, Wells SI, Wells JM, Abdollahi A. *Cancers (Basel).* 2020 Feb 18;12(2):469. doi: 10.3390/cancers12020469. PMID: 32085439

Acknowledgments

I would like to express my sincere gratitude to Prof. Dr. Dr. Amir Abdollahi for letting me be part of his lab and for his consistent support and guidance during my thesis. Further, I would like to thank Prof. Dr. Dr. Jürgen Debus and Prof. Dr. Christel Herold-Mende for the willingness to be my examiners and for their valuable attendance in my TAC meetings with intelligent advice and guidance.

I would like to express my endless thanks to Dr. Katrin Rein, Dr. Maximilian Knoll and Dr. Carmen Klein Bonilla for their review, corrections and critical comments during the preparation process of my thesis. Thanks for all the time you spare during our online meetings and talks. Katrin many thanks for graphical support that are pleasing to the eye.

I would like to thank Dr. Bouchra Tawk for reviewing my thesis and her valuable comments. I am grateful to Dr. Christian Schwager for quick responding to my questions and for scientific discussions. Special thanks to Mrs. Claudia Rittmüller for helping to find a solution to every problem with a smiling face.

Thanks to Dr. Ali Nowrouzi for supervising experiments and being my TAC member and for his comments during experimental parts of my thesis. Many thanks to Dr. Anne Mink for her help in the lab and in the mouse room.

Special thanks to Dr. Stephan Brons for his kindly help for irradiation planning and also Mrs. Mona Splinter and Mrs. Christiane Stahl-Arnsberger from Department of Medical Physics in Radiation Therapy (DKFZ) for their help during photon irradiation.

Finally, I would like to express my deep sense of gratitude to my wife Nargiz who always supported me by her generous love and patience and by standing by my side in all situations.

Eidesstattliche Versicherung

1. Bei der eingereichten Dissertation zu dem Thema

Evaluation of photon, proton, helium, and carbon ion irradiation in prototypic NSCLC and HNSCC preclinical xenograft models

handelt es sich um meine eigenständig erbrachte Leistung.

2. Ich habe nur die angegebenen Quellen und Hilfsmittel benutzt und mich keiner unzulässigen Hilfe Dritter bedient. Insbesondere habe ich wörtlich oder sinngemäß aus anderen Werken übernommene Inhalte als solche kenntlich gemacht.

3. Die Arbeit oder Teile davon habe ich bislang nicht an einer Hochschule des In- oder Auslands als Bestandteil einer Prüfungs- oder Qualifikationsleistung vorgelegt.

4. Die Richtigkeit der vorstehenden Erklärungen bestätige ich.

5. Die Bedeutung der eidesstattlichen Versicherung und die strafrechtlichen Folgen einer unrichtigen oder unvollständigen eidesstattlichen Versicherung sind mir bekannt. Ich versichere an Eides statt, dass ich nach bestem Wissen die reine Wahrheit erkläre und nichts verschwiegen habe.

Heidelberg

signature